Max Planck Institut für Kolloid und Grenzflächenforschung

Nucleation in Emulsion Polymerization

Steps towards a Non-micellar Nucleation Theory

Dissertation
zur Erlangung des akademischen Grades
"doctor rerum naturalium"
(Dr. rer. nat.)
in der Wissenschaftsdisziplin "Kolloidchemie"

eingereicht an der
Mathematisch-Naturwissenschaftlichen Fakultät
der Universität Potsdam

von
Pantea Nazaran

Potsdam, Januar 2008

Elektronisch veröffentlicht auf dem
Publikationsserver der Universität Potsdam:
http://opus.kobv.de/ubp/volltexte/2008/1752/
urn:nbn:de:kobv:517-opus-17521
[http://nbn-resolving.de/urn:nbn:de:kobv:517-opus-17521]

Abstract

For more than 70 years, understanding of the mechanism of particle nucleation in emulsion polymerization has been one of the most challenging issues in heterophase polymerization research.

Within this work a comprehensive experimental study of particle nucleation in emulsion polymerization of styrene at 70 °C and variety of conditions has been performed. To follow the onset of nucleation, on-line conductivity measurements were applied. This technique is highly sensitive to the mobility of conducting species and hence, it can be employed to follow aggregation processes leading to particle formation. On the other hand, by recording the optical transmission (turbidity) of the reaction mixture particle growth was followed. Complementary to the on-line investigations, off-line characterizations of the particle morphology and the molecular weight have been performed. The aim was to achieve a better insight in the processes taking place after starting the reaction via particle nucleation until formation of colloidally stable latex particles.

With this experimental protocol the initial period of styrene emulsion polymerization in the absence as well as in the presence of various surfactants (concentrations above and below the critical micellization concentration) and also in the presence of seed particles has been investigated. Ionic and non-ionic initiators (hydrophilic and hydrophobic types) have been applied to start the polymerizations.

Following the above algorithm, experimental evidence has been obtained showing the possibility of performing surfactant-free emulsion polymerization of styrene with oil-soluble initiators. The duration of the pre-nucleation period (that is the time between starting the polymerization and nucleation) can be precisely adjusted with the initiator hydrophobicity, the equilibration time of styrene in water, and the surfactant concentration. Spontaneous emulsification of monomer in water, as soon as both phases are brought into contact, is a key factor to explain the experimental results. The equilibration time of monomer in water as well as the type and concentration of other materials in water (surfactants, seed particles, etc.) control the formation rate and the size of the emulsified droplets and thus, have a strong influence on the particle nucleation and the particle morphology.

One of the main tasks was to investigate the effect of surfactant molecules and especially micelles on the nucleation mechanism. Experimental results revealed that in the presence of emulsifier micelles the conductivity pattern does not change essentially. This means that the presence of emulsifiers does not change the mechanism of particle formation qualitatively. However, surfactants assist in the nucleation process as they lower the activation free energy of particle formation. Contrary, seed particles influence particle nucleation, substantially. In the presence of seed particles above a critical volume fraction the formation of new particles can be suppressed. However, micelles and seed particles as absorbers exhibit a common behavior under conditions where monomer equilibration is not allowed.

Results prove that the nucleation mechanism comprises the initiation of water soluble oligomers in the aqueous phase followed by their aggregation. The process is heterogeneous in nature due to the presence of monomer droplets.

Table of Contents

1 Introduction

1.1 History and general description

Polymers dominate our world. From naturally occurring polymers necessary to sustain life, such as proteins, polynucleotides and polysaccharides, to man-made and commercialized macromolecules many important building blocks can be identified. [1] The observation of polymers and work devoted to their synthesis goes back to the beginning of the 19th century. Since then, the growth of polymer science and industry has been exorable. Major developments have been achieved in understanding and control of different types of polymerization processes. Each year numerous papers, patents and books appear dealing with various types and aspects of polymerization methods and polymer technology. [2]

Heterophase polymerization techniques might be considered as the "working horse" of industrial radical polymerization. Among the polymer synthesis methods, emulsion polymerization has developed into a widely used process for the production of synthetic latexes since its first introduction on an industrial scale during the early 20th century. Emulsion polymerization is a unique polymerization process in which a monomer or a mixture of monomers is polymerized in an aqueous medium to a colloidal dispersion of polymer particles, known as *latex*. Today, millions of tons of synthetic polymer latexes are prepared by emulsion polymerization for use as (a) commodity polymers in a wide variety of applications, such as synthetic rubber, high-impact polymers, latex foam, latex paints, paper coatings, carpet backing and adhesives, and (b) specialty applications such as diagnostic tests, drug delivery systems and chromatographic separations. [3] The major reason for this enormous extent of industrial applications lays on several distinct advantages of the emulsion polymerization process. First, the physical state of the colloidal system in the aqueous phase makes it easy to control the process. Thermal and viscosity problems are much less significant than in solution or bulk polymerization. Second, the synthesized latex can in many instances be used directly without further separations. Third and more importantly, emulsion polymerization process affords the means of increasing the

polymer molecular weight without decreasing the polymerization rate; thus, both high molecular weights and high reaction rates are simultaneously achievable.

Since the early days of emulsion polymers, understanding of the mechanism of polymerization process as well as the improvements to and refinements of the synthesis method have been of increasing interest aimed at achieving a better control of latex properties and polymer microstructure. This thesis will exclusively deal with "classical" emulsion polymerization, i.e. free-radical-initiated chain polymerization of partially water-soluble monomers to the final polymer colloids. The main ingredients for conducting such reactions are water, monomer and initiator. For the sake of colloidal stability a stabilizing agent (surfactant) might be added, otherwise, the initiator residues must provide the colloidal stability.

The center part of free-radical polymerization is the consumption of monomer by the propagation of a free-radical chain end, which in the simplest situation can be depicted by:

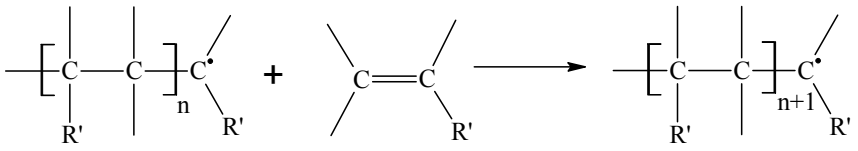

Equation 1

The overall polymerization process can be divided at least into three distinct stages: initiation, propagation and termination. In the first stage, an initiator, **I**, is decomposed to produce free-radicals, $\mathbf{R}^{\bullet}$, (equation 2), which react with the monomer, **M**, to initiate the polymerization (equation 3). [3, 4]

$$\mathrm{I} \xrightarrow{k_{\mathrm{d}}} 2\mathrm{R}^{\bullet} \qquad \textbf{Equation 2}$$

$$\mathrm{R}^{\bullet} + \mathrm{M} \xrightarrow{k_{\mathrm{i}}} \mathrm{RM}^{\bullet} \qquad \textbf{Equation 3}$$

The kinetics of these two reactions, in terms of the rate of appearance of free radicals determined by the rate constants, $\boldsymbol{k}_{\mathbf{d}}$ and $\boldsymbol{k}_{\mathbf{i}}$, and the concentrations of the reacting species follows equations 4 and 5, respectively.

$$R_{\mathrm{d}} = \frac{\mathrm{d}\left[\mathrm{R}^{\bullet}\right]}{\mathrm{d}t} = 2 \cdot f \cdot k_{\mathrm{d}} \cdot \left[\mathrm{I}\right] \qquad \textbf{Equation 4}$$

$$R_i = \frac{d[RM^\bullet]}{dt} = k_i \cdot [R^\bullet] \cdot [M]$$ **Equation 5**

where the factor ***f*** in equation 4 denotes the initiator efficiency. Because the rate of initiator decomposition (R_d) is much lower than the consumption rate (R_i), the former is the rate-determining step. Once a chain is started, it propagates (equation 6) at a rate determined by equation 7.

$$RM_n^\bullet + M \xrightarrow{k_p} RM_{n+1}^\bullet$$ **Equation 6**

$$R_p = \frac{d[RM_{n+1}^\bullet]}{dt} = k_p \cdot [RM_n^\bullet] \cdot [M]$$ **Equation 7**

where $\boldsymbol{k_p}$ is the propagation rate coefficient and the subscript ***n*** indicates the degree of polymerization.

Finally, in the last stage, the growth of polymer chains is terminated. Combination and disproportionation are the two most common termination reactions; both involve ending reactions between two growing polymer chains. In addition, reactions known as *chain transfer reactions* can take place between a growing radical and another molecule (normally a *transfer agent)*, yielding a "dead" polymer molecule and a new radical. Equations 8-10 show the corresponding kinetics for the termination and the transfer stage.

$$RM_n^\bullet + RM_p^\bullet \xrightarrow{k_{tc}} RM_n\text{-}M_pR \quad \text{(combination)}$$ **Equation 8**

$$RM_n^\bullet + RM_p^\bullet \xrightarrow{k_{td}} RM_n + RM_p \quad \text{(disproportionation)}$$ **Equation 9**

$$RM_n^\bullet + T\text{-}A \xrightarrow{k_{tr,TA}} RM_n^\bullet + A^\bullet \quad \text{(transfer to Transfer Agent)}$$ **Equation 10**

The rate at which monomer is consumed, or the polymer is produced (equation 7) is the most important quantity, known as the *rate of polymerization*. However, in order to use it as a predictive equation, it is necessary to define $\mathbf{[RM_{n+1}^\bullet]}$, or simply $\mathbf{[M^\bullet]}$, in terms of easily accessible quantities. Considering a balance between creation and loss of chain radicals, the rate of change of $\mathbf{[M^\bullet]}$ with time is given by equation 11. Here, several assumptions are taken into account. First, the chain transfer reactions

are followed by rapid re-initiation. Second, the rate coefficient for the termination reactions is given by the sum of combination and disproportionation termination reactions. Third, after the first few seconds of the polymerization, a value of **[M$^\bullet$]** is attained at which the rate of loss of radicals by termination exactly equals the rate of radical formation. The net rate of change of **[M$^\bullet$]** is then zero, and the reaction is said to be under *steady-state conditions*.

$$\left[\mathrm{M}^\bullet\right] = \left(\frac{R_\mathrm{i}}{2k_\mathrm{t}}\right)^{1/2} \qquad \textbf{Equation 11}$$

In above equation, rate of initiation is determined from equation 4. The result can be substituted into equation 7, to give a general expression for the rate of polymerization. [5]

$$R_\mathrm{p} = k_\mathrm{p}\left(\frac{f \cdot k_\mathrm{i}}{k_\mathrm{t}}\right)^{1/2} \cdot [\mathrm{M}] \cdot [\mathrm{I}]^{1/2} \qquad \textbf{Equation 12}$$

1.2 Basic issues; Nature of the problem

The above picture of polymerization mechanism is applicable to describe the overall rate of the polymerization and molar mass development of the latex particles. However, the most important feature of emulsion polymerization is neglected, which is its heterogeneity from beginning to the end. Upon mixing the monomer and water, a heterogeneous reaction medium is established in which, the monomer is present in form of dissolved molecules, clusters of a few molecules, nanodrops and large-size droplets. If surfactants are added into the mixture, they facilitate the formation of monomer drops coexisting at higher surfactant concentration with monomer swollen micelles (cf. Fig. 1).

In the absolute majority of cases, the polymerization starts with radical generation in the aqueous phase. The radicals have several possibilities to react: with monomer molecules dissolved, enter monomer aggregates or droplets, or micelles. Particle nucleation begins at this point. However, partitioning of the initiator radicals leads to the possibility that the polymerization continues in all phases, which instantly brings

us to one of the main issues in emulsion polymerization and the scope of this thesis: understanding the process by which latex particles are formed.

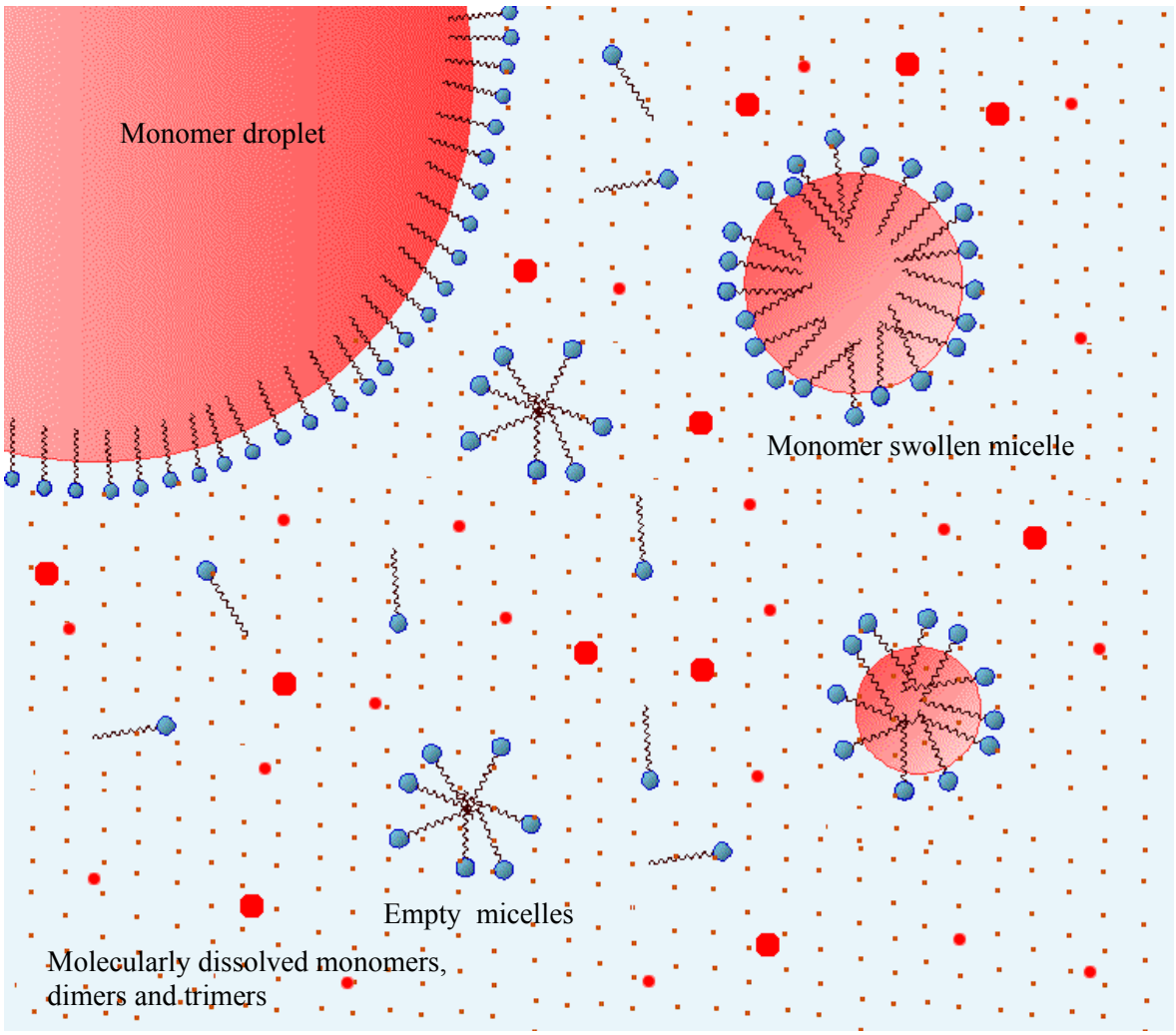

Figure 1 General picture of emulsion polymerization.

The kinetics of particle formation, like any other reaction, is determined by the available concentration of reacting species involved, i.e. the generated radicals and the monomer. The picture of emulsion polymerization (cf. Fig. 1) implies immediately that the number of dissolved monomer molecules is orders of magnitude higher than the number of micelles or monomer droplets. The latter is usually discarded as primary nucleation loci in the literature, as a consequence of their small contribution to the overall surface area. However, they play an important role as the monomer reservoir in the course of polymerization.

Despite the clear kinetic consideration that the possibility of a reaction between a radical and the monomer inside the micelles is by far smaller than the aqueous phase polymerization, in earlier theories of particle formation the radical consumption by

polymerization inside the aqueous phase has been neglected. This assumption is the core of the *Micellar Nucleation Theory*, originally proposed by Harkins [6] in 1947. Based on series of experimental investigations of the styrene emulsion polymerization process and the observation that the polymerization rate is much larger when micelles are present, he concluded that micelles are the principal loci of particle formation.

The original qualitative picture for the micellar mechanism of particle formation is quite simple. The primary free radicals formed by dissociation of the initiator in the aqueous phase enter the monomer-swollen surfactant micelles. Continuing the polymerization inside the micelles, monomer-swollen polymer particles are formed. The growing particles having larger interface are stabilized by adsorption of extra surfactants from un-entered micelles. Immediately after disappearance of the micelles, the nucleation ceases. After this stage, the newly-formed radicals are absorbed by the growing polymer particles. These polymer particles are then, the main loci of polymerization and they grow in size. The monomer concentration inside the polymer particles is kept constant by diffusion of monomer from the monomer reservoir (monomer droplets) through the aqueous phase into the polymer particles. At a certain conversion, the monomer reservoirs are consumed and disappear, resulting in a decreasing rate of polymerization.

Following the Harkins' original theory and the picture of ideal emulsion polymerization, Smith and Ewart [7] proposed a quantitative description of polymerization mechanism. They assumed that once a radical enters a micelle, it stays inside and polymerizes smoothly to from the polymer particle. Based on this assumption, they derived the famous relation for the number of polymer particles, N, depending on the concentration of micellar surfactants [S] and initiator [I] (equation 13):

$$N \propto [S_{micelles}]^{3/5} \cdot [I]^{2/5} \qquad \textbf{Equation 13}$$

However, Smith and Ewart excluded the possibility of nucleation in a locus other than the core of surfactant micelles. Consequently, this relation can not be applicable to an emulsifier-free polymerization as well as polymerization with surfactant concentration below the *Critical Micellization Concentration* (CMC). Moreover,

experimental data show that the exponent of **[S]** can cover a huge range from 0.615 [8] to 2.67 [9] for emulsion polymerizations of styrene with different types of surfactants.

The logical consequence of the general picture of emulsion polymerization (cf. Fig. 1), is that the radicals surrounded by a high number of monomer molecules propagate by reacting with monomer units. As monomer units are added, ordinarily the growing chain molecule becomes increasingly less water-soluble until it reaches a critical chain length, $\boldsymbol{j_{cr}}$, at which phase separation occurs, i.e. the chain comes out of the solution and forms a primary particle. Figure 2 shows the main picture of this mode, the *Self-aggregation Nucleation*.

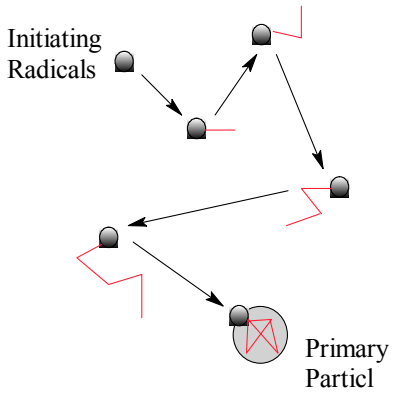

Figure 2 Schematic representation of the self-aggregation nucleation. [4] ▬ depicts a monomeric repeat unit.

The quantitative treatment of this theory requires a detailed description of the processes that oligomer radicals can undergo before they reach the critical length and collapse upon themselves. Fitch and Tsai [10-13] considered a kinetic approach for the nucleation stage. They proposed that the rate of appearance of primary particles would initially be equal to the rate of generation of free radicals, $\boldsymbol{R_i}$, since according to Fig. 2, every effective radical generated leads to the formation of a new particle. Later on, the oligoradicals may adsorb, reversibly, with the rate of $\boldsymbol{R_c}$ on the surface of primary particles before they reach the critical chain length. Moreover, aggregation of particles by flocculation with the overall rate of $\boldsymbol{R_f}$ must be considered. The particles do coalescence because they are softened by the presence of monomer, and in this way, they increase their surface charge density. All of these considerations lead to the famous Fitch-Tsai Equation (equation 14):

$$\left(\frac{dN}{dt}\right) = b \cdot R_i - R_c - R_f \qquad \textbf{Equation 14}$$

where ***b*** is a correction factor introduced to account for the reduction in the particle formation rate due to the side reactions of radicals in the aqueous phase prior to nucleation.

The Fitch-Tsai equation can be a useful tool in developing a qualitative understanding of the processes which govern the formation of particles in emulsion polymerization. Ugelstad and Hansen [9, 14, 15] made significant improvements on this picture, both theoretically and experimentally. They followed the kinetic approach to obtain the overall rate of particle formation by determining the rate of radical formation, the absolute capture rate and the rate of flocculation, individually.

The theory of single-chain nucleation does not consider thermodynamics of the phase formation. From the thermodynamic point of view, when a new interface is created, there is a corresponding interfacial energy required:

$$\Delta G_s = 4\pi r^2 \cdot \gamma_{PW} \qquad \textbf{Equation 15}$$

where γ_{PW} is the interfacial tension between polymer and water and ***r*** is the radius of incipient particle. For the nucleation process to be spontaneous, this energy must be supplied from some internal source, which in this case derives from the aggregation of the hydrophobic parts of the growing chain:

$$\Delta G_c = -\frac{4}{3}\pi r^3 \cdot g_v \qquad \textbf{Equation 16}$$

where g_v is the free energy of condensation per unit volume of the primary particle or nucleus. The overall free energy of a growing chain is then simply the sum of equations 15 and 16, as shown in equation 17.

$$\Delta G = \Delta G_s + \Delta G_c \qquad \textbf{Equation 17}$$

At very small sizes, $r < r^*$, (cf. Fig. 5) the first term in equation 17 dominates, preventing formation of a particle. But as the "embryo" grows there becomes enough energy of condensation to overcome the surface energy requirement. Thus, a stable "nucleus", or primary particle, can form. This is shown schematically in Fig. 3.

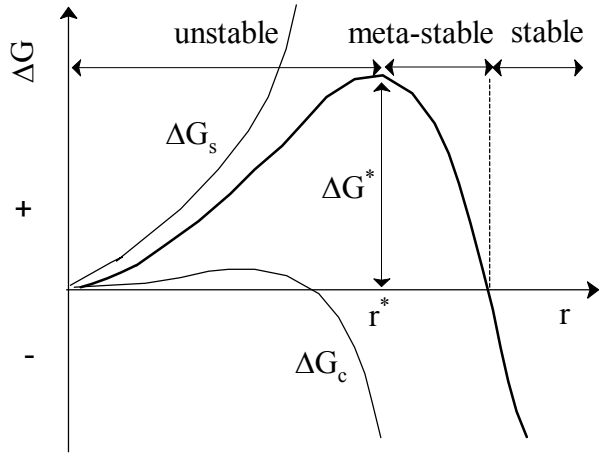

Figure 3 Energetics of aggregative nucleation. [16]

Following the study within this framework, particle formation by *Aggregative Nucleation Theory* has been proposed. [17-19] The theory assumes the coagulation of small oligoradicals to stable particles. Tauer et al. developed a new experimental tool to follow the onset of nucleation within several seconds. Based on the experimental results and the important remark that "a single molecule alone can not form cluster"; they showed that the well-known "Classical Nucleation Theory" can be applied to describe the process of particle formation. [4] Accordingly, the rate of formation of the new phase (here, the rate of nucleation, ***J***) is following the exponential dependency of equation 18.

$$J \propto A \cdot \exp\left(-\frac{\sigma^3 \cdot v^2}{\left(k_B T \cdot \ln S\right)^2} \right) \qquad \textbf{Equation 18}$$

where ***A*** is the pre-exponential factor, $\boldsymbol{\sigma}$ is the interfacial tension between nucleus and water, ***v*** is the molar volume of the nucleating species, $\boldsymbol{k_B T}$ is the thermal energy, and ***S*** is the supersaturation defined as the ratio of concentration to solubility of the nucleating species. In fact, a supersaturated solution contains nuclei in the range of "meta-stable" to "stable" criteria of Fig. 3. The nucleus with a size $r > r^*$ is stable, it can not dissolve anymore but continues to grow. Increasing the concentration of nucleating species or decreasing their solubility, which means increasing the supersaturation, increases the nucleation rate according to equation 18.

1.3 Scope and Objectives

Two major mechanisms of particle nucleation are summarized in Fig. 4. In conventional emulsion polymerization with surfactant concentration above the CMC, one might believe that both mechanisms, i.e. micellar and aggregative, operate simultaneously; however, with different extent.

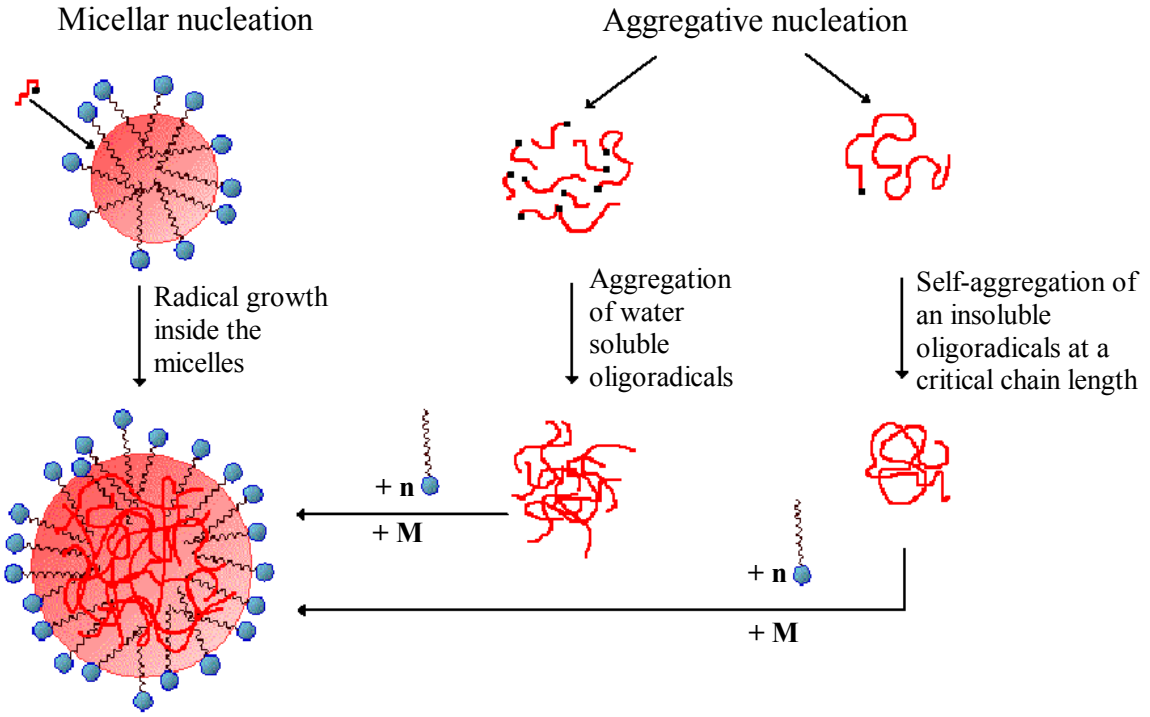

Figure 4 Particle formation in emulsion polymerization, micellar and aggregative nucleation mechanisms. [17]

For example, micellar nucleation is considered to be the primary nucleation mechanism for the monomers with relatively low water solubilities ($[M]_{aq}$ < 15 mmol dm^{-3}). Homogeneous nucleation, on the other hand, is considered to be the primary mechanism of particle formation for the monomers with relatively high water solubilities ($[M]_{aq}$ > 170 mmol dm^{-3}). [3, 20] Homogeneous nucleation is also proposed as the primary mechanism for the particle formation in systems where the surfactant concentration is below its CMC and in surfactant-free emulsion polymerization. [21-23]

Nevertheless, the controversy regarding the dominant mode of particle nucleation has existed since the development of the first ideas of emulsion polymerization.

Particle growth, on the other hand, is quite well understood which finds expression in the industrially widely used semibatch seeded emulsion polymerization. [24] The semibatch seeded emulsion polymerization is carried out in such a way that basically monomer or monomer emulsion is fed continuously into a reactor containing seed particles. If the seed concentration is high enough, particle formation and all uncertainties contributed with it can be avoided. The rate of polymerization is controlled so that no monomer accumulation in the reactor takes place. The monomer feeding rate corresponds almost to the rate of polymerization, which is determined by the heat exchange limit of the reactor.

Contrary, the nucleation mechanism in the presence of surfactants needs still clear experimental verifications. Trying to solve this issue, the scopes of the present thesis are:

- To follow the stage of nucleation in different polymerization systems; to investigate the role of each component through a detailed experimental study.
- To answer the question as to what degree each reaction locus, i.e. water phase, monomer droplets and micellar surfactants, is responsible for the nucleation.
- To re-examine the role of absorbing species (seed particles, micelles) in the reaction medium in particle nucleation.
- Finally, to combine the experimental results with the existing theories of nucleation, and develop a complete model for the particle formation in emulsion polymerization.

In the second chapter of this thesis, a short overview of the experimental design and measurements is provided. Detailed experimental information as well as the instrumentation are presented in the Appendix.

In the third chapter, starting with standard ingredients of an emulsion polymerization, the effect of each component is discussed. Main issues are: the state of monomer in water; the influence of water-solubility of monomer and initiator; and the role of new phase on the partitioning of monomer and initiator radicals. In the latter case,

surfactant micelles are compared with the seed particles of polystyrene. Only some examples of the obtained results are discussed in this chapter. A complete data set is available in “Categorized Library of Results”, in the appendix chapter.

From the overall results obtained, a complete model for the nucleation mechanism is proposed in the conclusion chapter. Furthermore, this chapter contains an outlook for future studies.

2 Experimental Section

An outstanding issue regarding the nucleation stage in emulsion polymerization is the need for reliable experimental data to support or to refuse a particular nucleation mechanism. One of the difficulties on this way is the high rate of nucleation, which requires a fast and sensitive method for on-line investigation. Another complexity is the existence of at least two reaction loci: the continuous phase and the dispersed phase.

Within this work, the stage of nucleation in different polymerization systems is followed. Particle nucleation in *ab-initio* batch emulsion polymerizations starts at extremely low solids contents typically much below 1 %. Thus, the experimental challenge to detect the onset and follow particle nucleation is substantial. It turned out [17-19] that conductivity is an extremely good tool to detect the onset of nucleation. Besides on-line investigations (section 2.1.1), complementary polymerizations were carried out in the glass reactor to provide samples for off-line characterizations (section 2.1.2).

2.1 Materials

Starting with "standard" surfactant-free emulsion polymerization, i.e. polymerization of styrene in water at 70 °C initiated with potassium peroxydisulfate, the nucleation behavior in different systems is investigated. The continuous phase is kept as water and the polymerization temperature as 70 °C throughout all the experiments. Furthermore, during on-line experiments the stirring rate is adjusted to 70 rpm; which is so slow that only the aqueous phase is homogenized without dispersing the monomer. Regarding the basic ingredients, the monomer is fixed as styrene. It will be shown that styrene is the best choice for this particular investigation method. Comparison experiments are carried out with a homologous series of monomers with different water solubilities. The initiators are selected from both ionic and non-ionic types with different hydrophobicities. The initiator concentration is in a range that allows a certain duration of the pre-nucleation period in order to detect clearly the onset of nucleation. The polymerizations are carried out in the absence as well as in

the presence of surfactants at various concentrations. To study the role of surfactant micelles as "absorbing" objects complementary polymerizations are carried out in the presence of polystyrene seed particles.

The general recipe for the polymerization in different cases is shown in table 1.

Table 1 General polymerization recipe. The second column shows the variable parameter; except this parameter, all the other conditions are set according to the standard run.

No.	Variable parameter	Ingredients		
		Continuous phase (g)	Monomer (g)	Initiator (g)
0	Standard Run	410 (Water)	3.3 (Styrene)	0.064 (KPS)
	Initiator type			
1	KPS	410	3.3	0.064
2	AIBN	400	3.7	0.076
3	V59	400	3.7	0.07
4	VA-86	410	3.3	0.072
5	PEGA	410	3.3	0.072
6	DAS	410	3.3	0.99
7	HDAS	410	3.3	0.99
	Monomer type			
8	Styrene	410	3.3	0.064
9	4-*tert*-Butylstyrene	410	4.98	0.064
10	Methyl methacrylate	410	3.17	0.064
11	Butyl methacrylate	410	4.3	0.064
12	Lauryl methacrylate	410	7.8	0.064
	Absorbing species			
13	Surfactants (micelles)	410	3.3	0.064
14	Polystyrene seed particles	410	3.3	0.064

2.2 On-line Investigations

The most important information regarding events leading eventually to nucleation are obtained from the on-line methods that are sensitive to reactions taking place in the continuous aqueous phase. Particle formation in emulsion polymerization is a very fast process. Therefore, an on-line measurement with high-speed data acquisition and a good data resolution is needed. As well, the technique employed should not influence the nucleation process and must be easy to perform. The methods measuring the turbidity and conductivity of the reaction medium fulfil these requirements.

The polymerizations are carried out in a specially constructed all-Teflon reactor, depicted in Fig. 6. The reactor has 500 mL reaction volume and is equipped with a stirrer working at 70 rpm, a combined probe for on-line measurement of the temperature and conductivity, and two optical windows for an on-line monitoring of optical transmission in the aqueous phase. Furthermore, the reactor lid contains an initiator injection tube and an additional opening, which allows for taking samples from the reaction mixture for further analysis. In some experiments, the reactor is equipped with an extra probe for quasi elastic light scattering to measure on-line the average particle size.

The standard polymerization procedure is as follows. First, water is degassed under vacuum and elevated temperature. It has been shown [18, 19] that the prevention of bubble formation during the reaction is crucial for reproducibility. The reactor is filled with 400 g of de-gassed water. Then, monomer is placed on top of the water confined in a glass funnel. The monomer funnel maintains a constant monomer-water interface of 31 cm^2 throughout the experiment (the remaining water – air interface is 80 cm^2). The stirrer speed is so slow that the monomer phase is not comminuted but only the water phase mixed thoroughly. At defined times after allowing the monomer to equilibrate in water, the polymerization is started by injection 10 mL of the initiator solution through the initiator injection tube into the aqueous phase. At the end of the polymerizations, the monomer phase is separated from the aqueous phase and the polymer formed in the latex phase is isolated.

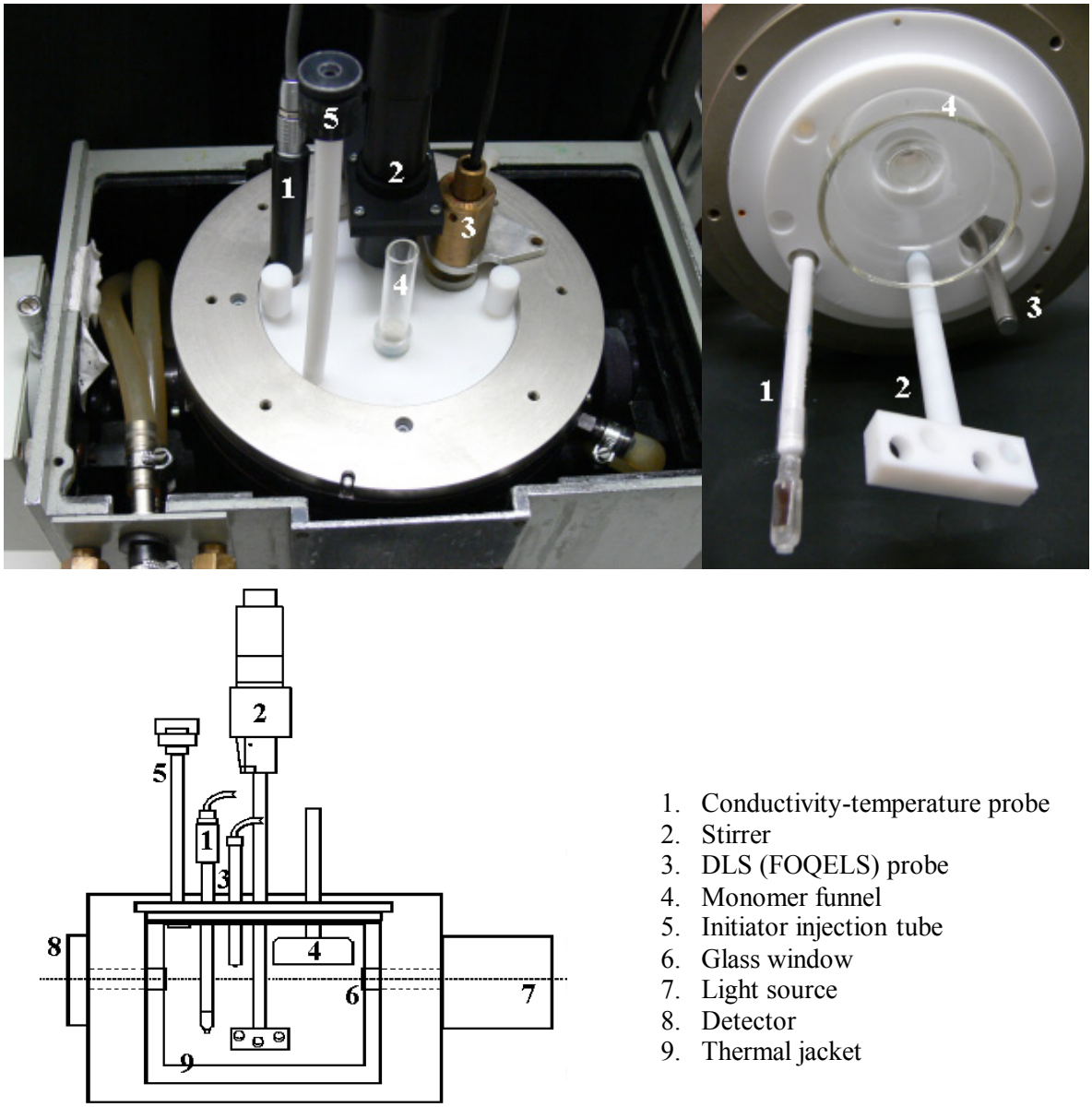

Figure 5 Teflon reactor applied for the nucleation experiments. Top: photos of the reactor and the probes. Down: Schematic representation with all the components.

A data acquisition module is written in PASCAL to collect values for temperature, electrical conductivity, and optical transmission every 6 seconds on a personal computer. [17] Furthermore, these quantities are displayed online on the PC screen as the time-dependent curves for reaction control, and for selecting interesting points to take samples. The reproducibility of the reported results is confirmed by at least three repeats.

2.2.1.1 On-line turbidity measurements

Characterization of latexes by turbidity measurements has been developed and applied in the research since a long time. [25-27] In a typical measurement, the light intensity after passing through the medium is compared with the incident light intensity. Then, the transmission, ***T***, and the turbidity, τ, can be calculated from equation 19. [28]

$$\frac{I}{I_0} = \frac{T}{100} = \exp(-\tau \cdot l) \qquad \textbf{Equation 19}$$

where ***I*** is the light intensity after passing through the polymerization mixture (at the detector), I_0 is the incident light intensity, and ***l*** is the optical path length, equal to 9.8 cm in the applied Teflon reactor. The spectrometer reports the transmission and the results as ***T*** versus time curve is displayed on the PC.

According to the Rayleigh theory, for small particles (relative to the wavelength of the incident light, $d < \lambda/20$) the turbidity is related to the concentration of scatters (***N***) and the particle scattering cross section (C_{sca}), as shown in equation 20.

$$\tau = N \cdot C_{sca} \qquad \textbf{Equation 20}$$

The particle scattering cross section is a function of the particle volume, V_P, the wavelength, λ, and , ***m***, the ratio of the refractive indices of the particles, n_P, and of the water, n_0, as described by equation 21.

$$C_{sca} = \frac{24\pi^2 \cdot V_P^2}{\lambda^4} \cdot \left(\frac{m^2 - 1}{m^2 + 2} \right)^2 \qquad \textbf{Equation 21}$$

For bigger particles, the Rayleigh theory is not applicable. Then, the ratio of turbidity to the concentration of scattering species, the so-called “specific turbidity”, can be determined according to Mie theory. [29-31] For a monodisperse system of nonabsorbing particles, assuming single point scattering, specific turbidity is related to the size of scattering particles, according to equation 22.

$$\left(\frac{\tau}{c_P} \right)_{c \to 0} = \frac{4\pi \cdot n_0}{\lambda \cdot \rho_P} \cdot f(\alpha, m) \qquad \textbf{Equation 22}$$

with: $\alpha = \frac{\pi \cdot d_P \cdot n_0}{\lambda}$, $m = \frac{n_P}{n_0}$

where C_P is the polymer concentration, d_P is the diameter of the particle, and ρ_P is the polymer density. $f(\alpha,m)$ is a numerical function and its value should be collected from the *Scattering Function Tables*, [31] but for small particles ($0 < \alpha \leq 1$) and low relative refraction indexes ($1 < m \leq 1.3$), it can be approximated by equation 23:

$$f(\alpha,m) = \left(\frac{m^2-1}{m^2+2}\right)^2 \cdot \left(\frac{\pi \cdot n_0 \cdot d_P}{\lambda}\right)^3 \qquad \textbf{Equation 23}$$

For the applied conditions the following values of the parameters in equation 23 are applicable: wavelength λ=546 nm, relative refraction index of polystyrene/water at 546 nm, (n_P/n_0) = 1.203 and $\alpha \leq 1$ is always true if the particle diameter is smaller than 130 nm. [18]

Applying equations 22-23 with experimental data for the specific turbidity or using the tables of scattering functions, it is possible to calculate the particle diameter, d_P. However, this can not be applied with the employed technique as the concentration of scattereous and hence, the specific turbidity are not known. If the particle diameter is known from another analytical method like dynamic light scattering or electron microscopy, the scattering tables can be used in the reverse sense to calculate the polymer concentration. [18] Knowing the particle size, the specific turbidity can be determined from the scattering tables. Comparing this value and the measured turbidity form transmission measurements, the polymer concentration is easily calculated. In the next step, knowing the polymer concentration, one can estimate the particle number according to equation 24.

$$N = \frac{c}{\rho_P \cdot \frac{\pi}{6} \cdot d_p^{\,3}} \qquad \textbf{Equation 24}$$

The above procedure is used, for instance, to follow the development of the particle number from the detection of the first particles up to later stages of the polymerization medium.

2.2.1.2 On-line conductivity measurements

Although turbidity measurement is a useful method for determination of the average particle sizes, its applicability is limited as a certain concentration of particles must be present. The necessary concentration is the larger the smaller the particles. In other words, the first variation in the measured transmission is reported when a large number of particles with a size of several nanometres is present. This means that the onset of nucleation can not precisely be identified by turbidity measurements.

On the other hand, experimental studies on the structure and interaction of the molecules in the continuous phase might be helpful to detect the early stages of the nucleation. The onset of nucleation is characterized as the time when phase separation occurs after the critical supersaturation of the species formed in the aqueous phase is reached. As the continuous phase is water, conductivity measurements might be applicable. Indeed, it turned out that conductivity measurement is an extremely useful tool to detect the onset of nucleation in surfactant-free polymerizations. [17, 18, 32-35]

Conductivity, **κ**, is the ability of a material to conduct electric current and depends on the concentration of ions present, and the conducting properties of each type of ions, defined by its molar (or, equivalent) conductivity, $\mathbf{\Lambda_m}$. [36]

$$\Lambda_{\mathrm{m}} = \frac{\kappa}{c_i} \qquad \textbf{Equation 25}$$

where c_i is the molar concentration of the conducting species. The molar conductivity varies with the concentration and the mobility of ions. In the limit of zero concentration, when the ions are effectively infinitely far apart and do not interact with one another, the *limiting molar conductivity*, $\mathbf{\Lambda^0_m}$ is defined, which can be expressed as the sum of contributions from individual ions (cf. equation 26). The relation between limiting conductivity and the molar conductivity depends on the ionic strength of the charged component. In any case, they can be converted to each other concerning a factor for the concentration and the degree of ionization in water.

$$\Lambda^0_{\mathrm{m}} = (u_+ \cdot \nu_+ \cdot z_+ + u_- \cdot \nu_- \cdot z_-) \cdot F \qquad \textbf{Equation 26}$$

where F is the Faraday constant, ν is the number, z is the charge and u is the mobility of ion. Subscripts + and - denote the values correspond to cations and anions,

respectively. The mobility of an ion shows how fast it is transported in an external electric field. For a sphere ion, the mobility is calculated from equation 27.

$$u = \frac{z_e}{6\pi \cdot \eta \cdot a_i}$$ **Equation 27**

where z_e is the electron charge, η is viscosity of the medium and a_i is the hydrodynamic radius of the ion. The overall conductivity is then determined by:

$$\kappa = \sum_i \nu_i \cdot z_i \cdot u_i \cdot F \cdot c_i$$ **Equation 28**

The experimental conductivity is determined by the concentration and mobility of charged species. For KPS as initiator the conductivity is dominated by the protons, as these ions posses the highest molar conductivity (Λ_m for H^+ measured at 25 °C is 349.6 m^2Smol^{-1} whereas for HSO_4^- is 50 m^2Smol^{-1} according to [37]).

The principle by which conductivity meter measures conductivity is simple: a pair of electrodes are immersed in the solution and a potential is applied across the circuit. The resistance that the solution adds to the circuit is converted to conductivity by a computer chip, and reported. The result is displayed on the PC as the conductivity versus time curve.

The instrument is extremely sensitive to follow every small variation in the ionic motion of aqueous phase during the reaction. This sensitivity makes the method perfectly valuable for the nucleation investigation. More details for the interpretation of the ionic changes in the conductivity during the polymerization are explained in section 3.1, for a concrete example.

2.2.1.3 On-line particle size measurements

Besides the above mentioned methods, in some experiments the appearance and growth of particles are followed by a simple, practical approach: automatic particle size analysis with a Fiber Optical Quasi Elastic Light Scattering (FOQELS). The method allows measurements of the particle diameter in a great range of sizes and concentrations, based on the standard Dynamic Light Scattering (DLS) theory.

Principally, in DLS, one measures the time dependence of the light intensity scattered from a very small region of the solution. When a beam of light passes through a colloidal dispersion, the particles or droplets scatter some the light in all directions. When the particles are very small compared with the wavelength of the light, the intensity of the scattered light is uniform in all directions (Rayleigh scattering); for larger particles the intensity is angle dependent (Mie scattering). [28, 38]

If the light is coherent and monochromatic, as from a laser for example, it is possible to observe time-dependent fluctuations in the scattered intensity using a suitable detector such as a photomultiplier capable of operating in photon counting mode. These fluctuations arise from the fact that the particles are small enough to undergo random thermal (Brownian) motion and the distance between them is therefore, constantly varying. Depending upon whether the particles are moving towards or away from the detector, the *Doppler effect* shifts the light to higher or lower frequencies, thus, the frequency broadening occurs.

Analysis of the time dependence of the Doppler shift can therefore, yield the diffusion coefficient of the particles (cf. equation 29).

$$I(Q,\omega) = \frac{A \cdot D \cdot Q^2}{\omega^2 + D^2 \cdot Q^4} \qquad \textbf{Equation 29}$$

where $Q \equiv \frac{4\pi \cdot n_0}{\lambda_0} \sin\left(\theta/2\right)$

$\boldsymbol{Q}$ is the "scattering factor", $\boldsymbol{\omega}$ is the frequency shift, $\boldsymbol{A}$ is a constant and $\boldsymbol{D}$ is the Fickian diffusion coefficient of the particle, $\boldsymbol{\lambda_0}$ is the vacuum wavelength of the light and $\boldsymbol{n_0}$ is the refractive index of the medium.

Theoretically, from equation 29 one can obtain the value of $\boldsymbol{D}$ directly from the half width at half height of the scattered beam (cf. equation 30).

$$\omega_{1/2} = D \cdot Q^2 \qquad \textbf{Equation 30}$$

from which, via the Stokes Einstein equation, (cf. equation 31), knowing the viscosity of the medium, $\boldsymbol{\eta}$, the hydrodynamic radius of the particles, $\boldsymbol{a_h}$, can be calculated.

$$a_h = \frac{K_B \cdot T}{6\pi \cdot \eta \cdot D}$$ **Equation 31**

where K_B is the Boltzmann's constant.

However, DLS uses another effect, namely intensity fluctuation due to the constructive and destructive interference of light scattered by neighbouring particles within the scattering column. The dependence of the intensity fluctuation is most commonly analysed using a photon counting autocorrelator. Such a device determines the intensity of autocorrelation function, ***G(τ)***, which can be described as the ensemble average of the product of the "signal", $I_s(t)$, with a delayed version of itself, $I_s(t+\tau)$, as a function of the delay time, **τ**, as stated in equation 32:

$$G(\tau) = \langle I_s(t) \cdot I_s(t+\tau) \rangle$$ **Equation 32**

The signal in this case is the number of photons counted in one sampling interval. At short delay times, correlation is high. Over time, as particles diffuse, correlation diminishes to zero. The exponential decay of the correlation function is characteristic of the diffusion coefficient of the particles:

$$G(\tau) = 1 + \exp(-2D \cdot Q^2 \cdot \tau)$$ **Equation 33**

Analysis of the autocorrelation function in terms of particle size distribution is done by numerically fitting the data with calculations based on assumed distributions. A truly monodisperse sample would give rise to a single exponential decay to which fitting a calculated particle size distribution is relatively straightforward. In practice, polydisperse samples give rise to a series of exponentials and several quite complex schemes have been devised for the fitting process. [4, 38]

Dynamic light scattering is particularly suited in determining changes in the average diameter. The lower limit of particle size depends on the scattering properties of the particles concerned (relative refractive index of particle and medium). The smallest polystyrene particles detected with the on-line measurements, (FOQELS) have a diameter below 5 nm. However, in the time of nucleation, when complex series of very fast changes in the size and number of scattering objects take place, applying the DLS might be very challenging. Furthermore, in the vicinity of the stirrer, the Brownian motions of the scattering objects are strongly perturbed. However, this

influence can be calculated, and correction procedures have been developed allowing the on-line estimation of the average particle size. [32] Another complexity is the presence of micelles, which are in similar size range. Hence, it is practically impossible to distinguish between particles and micelles.

On the other hand, off-line DLS of the particles with higher monomer conversions provides helpful data for studying the growth behavior, as well as the concentration and number of polymer particles.

2.3 Off-line Investigations

Perhaps the oldest and the most trivial way to study processes is to follow them by eyes. Carrying out the polymerization in the glass reactor offers the opportunity for visual investigation and for sampling for the off-line characterizations without disturbing the on-line measurements.

For the sake of comparison, complementary polymerizations are done in a glass reactor according to exactly the same procedure used for the on-line investigations. The polymerizations are carried out in a four-neck double jacketed reactor equipped with nitrogen inlet, condenser, mechanical stirrer, heating and cooling thermostat. The polymerization recipe is based on the "standard run" mentioned in table 1. To get a better visualization, the monomer is used in excess, so that the undisturbed monomer layer can be easily seen throughout the experiments on top of the aqueous phase. The reaction temperature and the "standard" stirring speed are kept constant at 70 °C and 50 rpm, respectively. In order to investigate the effect of stirring rate on the polymerization, some experiments are repeated under quiescent condition, as well as stirring with stirrer speeds of 150 and 300 rpm. The influence of various parameters, for instance: monomer solubility, monomer-water equilibrium time, and type of initiator are investigated by selecting the corresponding reaction condition.

Samples are taken from the aqueous phase (latex phase) at specific time intervals. A portion of the sample is analyzed for the solids content by the moisture analyzer. The dried products are collected for the molecular weight determinations by Size Exclusion Chromatography, (SEC). Another portion of the sample is used for particle

size measurements by DLS. The rest is kept for the electron microscopy and more analytical methods, if necessary.

The reproducibility of the reported results is confirmed by two repeats of each polymerization.

Comparing the off-line and on-line results, the following points should be considered. First, the hydrodynamics in both reactors is different. Second, the off-line samples are always investigated after cooling down to room temperature. Looking form thermodynamic point of view, lower temperature leads to a lowered solubility and faster nucleation. Hence, there is not always a one to one correlation to expect.

However, comparison of the analytical results accompanied by the on-line investigations provides a complete overview of the nucleation event, as will be discussed in chapter 4.

3 Results and Discussions

Particle formation in emulsion polymerization is an important and complex process. Several theories have been proposed to account for particle nucleation in emulsion polymerization, as for instance, micellar nucleation, [6, 7] homogeneous nucleation, [11, 13, 15, 39, 40] and aggregative nucleation. [16, 18, 19, 22, 37] All models are largely based on experimental data obtained at fairly high conversions of several percent, that is far beyond the particle nucleation step. The crucial point is that no experimental data are available for the complete polymerization process: from the first appearance of particles up to the growth and high conversion. Thus, it was not possible so far to get direct experimental proof to support or to refute one of the mentioned mechanisms.

Within this work the early stages of the polymerization systems have been recorded starting from the monomer addition to water followed by initiator addition up to high conversion range. Based on the experimental results and examining their compatibility with the existing nucleation theories, a better understanding of the particle nucleation mechanism has been achieved.

The experimental results presented in this chapter starts with the surfactant-free emulsion polymerization of styrene as the “standard run”. Indeed, surfactant-free polymerization is the simplest system to investigate particle nucleation as it contains only three starting components: water, monomer, and initiator. Moreover, in such systems the possibility of particle nucleation via the micellar nucleation mechanism is virtually precluded.

In the next parts of this chapter, the nucleation behavior is investigated with various initiators and in the presence of either surfactant micelles or seed particles as absorbing species. The obtained results provide a unique overview of the different polymerization systems. Thus, the results allow developing a consistent nucleation mechanism for emulsion polymerization.

3.1 Standard run: surfactant-free emulsion polymerization

Surfactant-free emulsion polymerization has inspired scientists in heterophase polymerization research for over 30 years. Special interest has been devoted to peculiarities of particle nucleation, in situ stabilizer formation, and polymerization kinetics. [18, 22, 37, 41-46]

A typical result of on-line monitoring of the ab-initio emulsion polymerization is shown in Fig. 6.

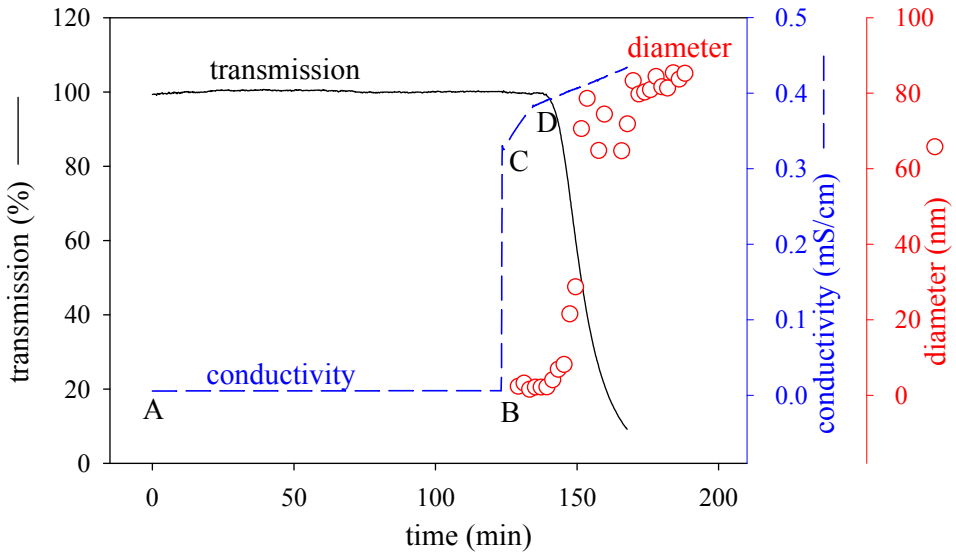

Figure 6 Typical record of the initial period of surfactant-free styrene emulsion polymerization with on-line determination of transmission (solid line), conductivity (dashed line) and particles diameter by FOQELS (circles).

Polymerization is carried out under the standard polymerization procedure. First, water is degassed under vacuum and elevated temperature and is charged into the reactor at a temperature higher than 70 °C. After certain time allowing the thermal equilibration of water, monomer is placed on top of the water through the glass funnel. This is the starting point denoted as point *A* in Fig. 6. At defined times after allowing the monomer to equilibrate in water, (t_{equ} = 120 min), the polymerization is started by injection of the initiator solution into the aqueous phase. Using the described methods, the conductivity, transmission and particle size in the aqueous phase are measured.

3.1.1 On-line conductivity measurement

During the equilibration time of monomer and water, period *A*-*B*, the conductivity is almost constant at a value very close to the conductivity of pure water. Polymerization is initiated at point *B* by the injection of the initiator (KPS) solution into water. The conductivity rises sharply till point *C*. After this point, the decomposition of the initiator causes a continuous increase in the concentration of ionic species, and thus, a linear development of the conductivity (cf. Appendix for the detailed mechanism of the thermal decomposition of persulfate).

Conductivity in the aqueous phase is controlled by the concentration and the mobility of the charged species, as discussed in chapter 2.1.1.2. The mechanism of KPS decomposition leads to equation 34 for the changes in the overall conductivity during the prenucleation stage of the polymerization. [37]

$$\kappa(t) = \Lambda_{K^+}[K^+] + \Lambda_{S_2O_8^{2-}}[S_2O_8^{2-}] + \Lambda_{H^+}[H^+] + \Lambda_{SO_4^{2-}}[SO_4^{2-}] + \Lambda_{HSO_4^-}[HSO_4^-]$$

Equation 34

Table 2 Molar conductivities of the different charged species involved in the KPS decomposition. [37]

Ion	Λ_m (m^2S/mol) (25 °C) measured	Λ_m (m^2S/mol) (60 °C) calculated
H^+	349.65	507.1
HSO_4^-	50	95.4
K^+	73.48	132.2
SO_4^{2-}	160	290.2
$S_2O_8^{2-}$	172	328.3

Comparison of the molar conductivities of different ionic species generated by the decomposition reaction (cf. table 2) reveals that the overall conductivity is governed by the protons. This is a rationalized conclusion as the protons are the smallest ions and contain the highest charge density. Therefore, the slope of the conductivity is practically determined by the proton concentration.

After a particular time, at point *D*, the slope of the conductivity curve changes towards lower values. The bend in the conductivity curve is interpreted as the

appearance of the first particles, i.e., the onset of the nucleation. At the time of the conductivity bend, mobile species loose their mobility due to the incorporation in the electrical double layers of the newly-formed particles. The duration *C*-*D* is called pre-nucleation period, and is indicated as t_N. Within the frame of the classical nucleation theory, t_N corresponds to the time needed for establishing the supersaturation of the nucleating species. During this period of time, the reaction takes place essentially in the continuous aqueous phase.

The development of the nucleation process, like any other chemical event, strongly depends on the concentration of the reacting species. According to the aggregative nucleation theory, the rate of nucleation is controlled by the supersaturation, and hence, by the concentration of the nucleating oligomers. The higher is the concentration of the oligomers, the faster the nucleation, and the shorter the pre-nucleation period. However, in heterophase polymerization the components distribute among all phases present in the reaction medium. Therefore, the kinetics of formation of the nucleating oligomers in water phase depends on the contribution of the monomer. One way to adjust the partitioning is, for instance, to vary the solubility of the monomer in water, as will be shown in section 3.4.2.

Besides the solubility, it is experimentally observed that the equilibration of water and monomer has an important influence on the rate of nucleation. Figure 7 shows the comparison of the conductivity curves for the polymerization with different equilibration times. Curve κ is in accordance of the standard-run (t_{equ} = 120 min), with the points *A*, *B* and *D* as: addition of styrene, KPS injection, and the onset of the nucleation, respectively. On the other hand, for the case of curve κ′ t_{equ} is zero. The points *A′*, *C′* and *D′* are therefore: the injection of KPS, addition of monomer, and the onset of the nucleation, respectively. The period of *B′*-*C′* is the continuous increase in conductivity due to the initiator decomposition. At point *C′*, immediately after the monomer addition, the ion-radicals start to polymerize generating oligomers of higher sizes. The decrease in the conductivity slope at this point is then contributed to the decrease in the mobility of charged species. The duration *C′*-*D′* is the pre-nucleation period, when the oligomers are constantly growing, but they are still water-soluble and do not form stable clusters. Only at point *D′* the critical supersaturation is reached and particles are formed.

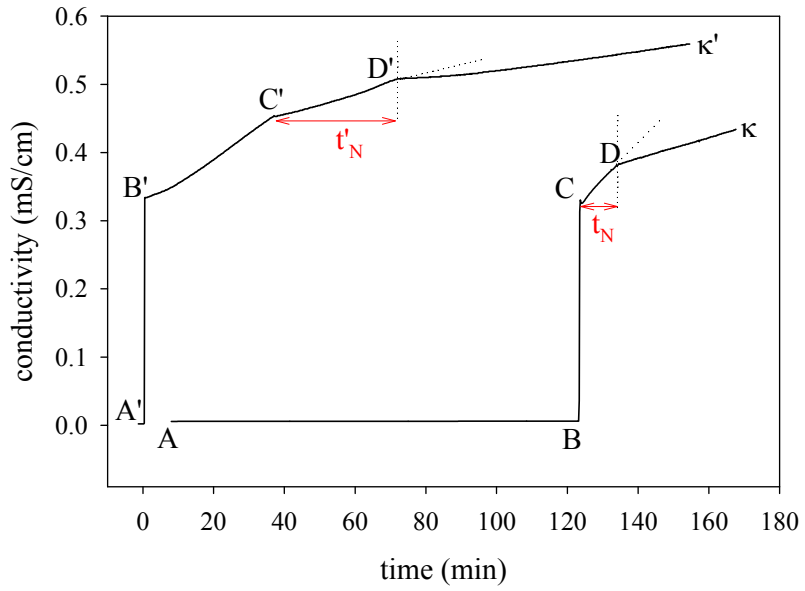

Figure 7 Comparison of the conductivity curves for the polymerization with and without the equilibration time (curves denoted as κ and κ′, respectively). Dotted lines are for a better visualization of the conductivity bends.

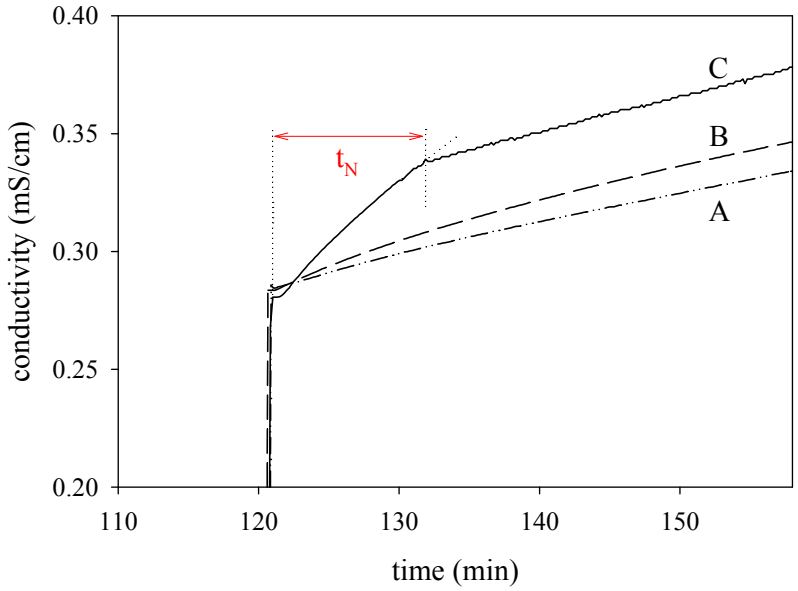

Figure 8 Comparison of the conductivity curves during the decomposition of KPS in pure water (A) and in the presence of ethyl benzene (B), and styrene (C). t = 120 min is the initiator injection. Dotted lines are for a better visualization of the conductivity bend.

Note that the duration of the pre-nucleation for the polymerization with $t_{equ} = 0$, t'_N is more than three times as long as t_N, the pre-nucleation time for the polymerization with t_{equ} = 120 min. This is an expectable behavior due to different monomer concentration for both systems. Obviously, the limited monomer concentration in the aqueous phase in the polymerization with t_{equ} = 0 is responsible for the longer

nucleation time. Moreover, the duration *C-D* has a higher slope than the periods *B´-C´* or *C´-D´*, as the reaction conditions in both systems are different. One can say the period *C-D* corresponds to period *B´-C´-D´*, as both decomposition and formation of oligoradicals are superimposed. However, the higher conductivity slope for the polymerization with t_{equ} = 120 min indicates a higher KPS decomposition rate than that for the decomposition in pure water (duration *B´-C´*). [47] This is not surprising as it is well known that the decomposition of persulfate is strongly influenced by organic compounds (cf. Fig. 8). Factors of up to 100 compared to the decomposition in pure water have been observed in the presence of organic compounds. [48]

The conductivity slopes after the bends are different, too. Also in this period, the conductivity slope for the polymerization with t_{equ} = 120 min is higher than the polymerization with t_{equ} = 0, pointing to differences in the average particle size and concentration under both conditions.

3.1.2 On-line turbidity measurement

A few minutes after the conductivity bend in Fig. 6, the transmission of the aqueous phase starts to decrease continuously to zero as a result of the growth of the polymer particles. In order to get an insight to the transmission variations during the monomer equilibration time and at the time of nucleation, transmission curves have been evaluated carefully during the monomer equilibration period and after starting the polymerizations. Figure 9 shows the comparison of the transmission curves for the polymerization with t_{equ} = 0 and 120 min.

The result reveals that before the final drop due to the particle growth, both transmission graphs exhibit two points of inflections, where the curves undergo a local minimum followed immediately by a maximum. This behavior is more dominant in the case of the polymerization without any equilibrium time. Appearance of the local minimum and maximum in the transmission curve, the so-called *Jumbo*-effect, has been extensively discussed previously. [32, 33, 49] It has been shown that during the monomer equilibration period, the transmission decreases from 100 to about 91 % continuously during 3 hours before reaching a constant value. In a detailed analysis by means of multi-angle laser light scattering, the authors observed that scattering signals appear in the aqueous phase a few minutes after the styrene is

placed quiescently on top of the water phase. The size and the number of the scattering objects increased continuously with time till reaching a saturation state.

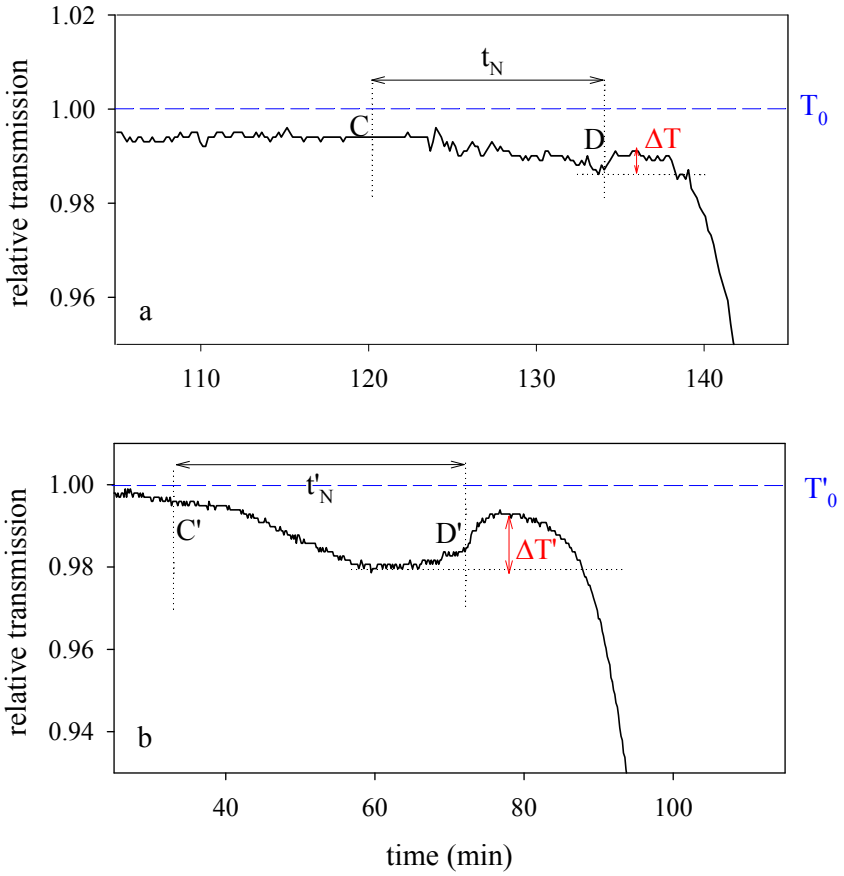

Figure 9 Comparison of the transmission curves for the polymerizations with (curve a), and without the equilibration time (curve b). Dotted lines are for a better visualization of the pre-nucleation period and the Jumbo-effect, and the dashed lines indicate the initial transmission in both cases. In curve a, t = 0 is the monomer addition and in curve b, is the initiator addition.

From this data, they concluded that the scattering results from *spontaneous emulsification*, i.e., the formation and continuous growth of styrene droplets in water. These droplets are formed spontaneously as soon as two phases are brought into contact, and are responsible for the decrease in the transmission. Based on this picture, the Jumbo-effect can be explained by the monomer consumption during the pre-nucleation stage in the continuous phase. This consumption causes a shrinkage of the styrene droplets and leads to a decrease in the scattering intensity, or an increase in the transmission. Another possible explanation for the occurrence of Jumbo-effect in the transmission curve is based on the changes in relative refractive indices. After the nucleation, particles imbibe monomer. Consequently, the difference in the

refractive indices between monomer swollen particles and the continuous phase (water saturated with the monomer) becomes slightly smaller.

The fact that the transmission variations are more significant in the case of the polymerization with t_{equ} = 0 can be explained with the coincident formation and consumption of monomer droplets, which causes a driving force and accelerates the spontaneous emulsification. Indeed, in the polymerization run with t_{equ} = 120 min, emulsification has started long ago: form the first moment that the monomer is brought into contact with water. Though, addition of the initiator at point *C* facilitates the droplet formation as it lowers the interfacial tension and the energy barrier. In any case, the droplet formation occurs in a more gradual process compared with that of the polymerization with t_{equ} = 0. The latter is accompanied with a steeper change at point *C´*, as the monomer emulsification is eased by the presence of radicals from the beginning. The continuous consumption of monomer in the aqueous phase accelerates the emulsification.

However, the overall concentration of monomer in water is limited in the polymerization with t_{equ} = 0, leading to a longer pre-nucleation period. Note that the kinetic of polymerization is not influence by the monomer droplets as the number of aggregates decreases inversely with the third power of their size. Hence, the number of single monomer molecules or dimers and trimers is orders of magnitude larger than that of bigger drops. Thus, the molecularly dissolved monomers determine the kinetics of the reaction with the primary radicals in the aqueous phase.

3.1.3 Particle growth and morphology

The formation and growth of particles can be followed by on-line FOQELS, as demonstrated by the continuous increase in the particle diameter (cf. Fig. 6). The reported diameters are corrected with respect to the stirring effects, by the method introduced in [32].

The first particles are detected a few minutes after the bend, with the diameter below 5 nm. The measured molecular weight of the oligoradicals forming these particles are in the range of 600 to 1000 g/mol. One can determine the aggregation number of these oligoradicals based on the calculated particle mass. The particles are composed of between 4 and 12 oligoradicals having the critical chain lengths ($\boldsymbol{j_{cr}}$) between 5 and

10. The experimental results are in an excellent agreement with the results from the nucleation modeling based on the aggregative nucleation theory [19] where a critical chain length of 6 for the surfactant-free polymerization of styrene at very similar conditions is predicted.

From the turbidity data, the polymer concentration and the particle number are calculated (cf. Fig. 10) according to the method described in section 2.1.1.1.

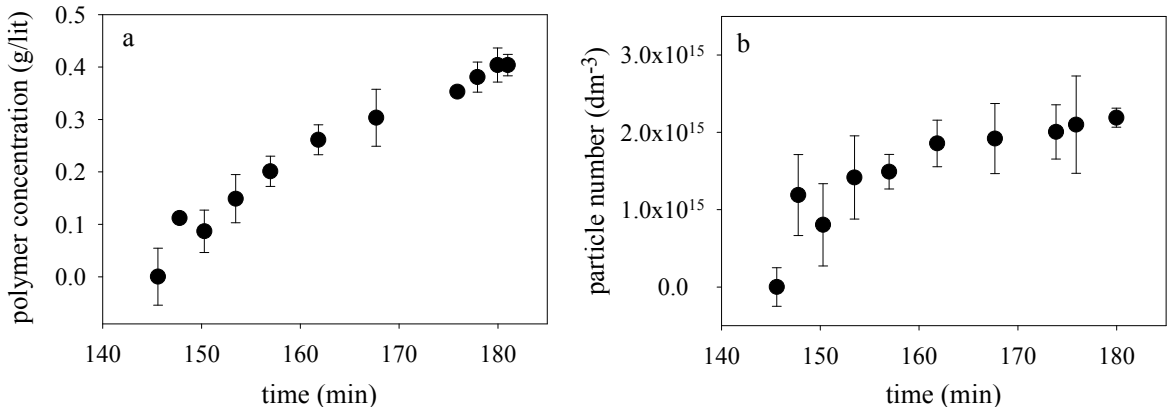

Figure 10 Development in (a) polymer concentration and (b) particle number of the surfactant-free styrene emulsion polymerization, standard run. Results are the averaged values with standard deviations of three polymerization runs. t = 0 is the monomer addition and t = 120 min is the start of the polymerization.

Figure 10 reveals that the polymer concentration increases from the values lower than 0.01 g/lit shortly after the onset of the nucleation to the maximum value of 0.4 g/lit at the time of zero transmission. These concentrations correspond to monomer conversions of 0.1% and 4.9%, respectively. The fact that the conductivity measurements can detect the onset of the nucleation even at this extremely low solid content confirms the suitability of the applied method. On the other hand, the estimated particle number shows a quite extended nucleation period under these particular experimental conditions of slowing down the reaction rate.

An independent experimental proof for the mechanism of particle formation and important role of the monomer droplets comes from the off-line investigations. Figure 11 shows the development of the particle morphology in dependence on the monomer equilibration time. Figure 12 shows the comparison of the number average molecular weight and the hydrodynamic average particle size during the polymerizations with t_{equ} = 0 and 120 min.

The results reveal that the equilibration time between monomer and water has a strong influence on the particle morphology.

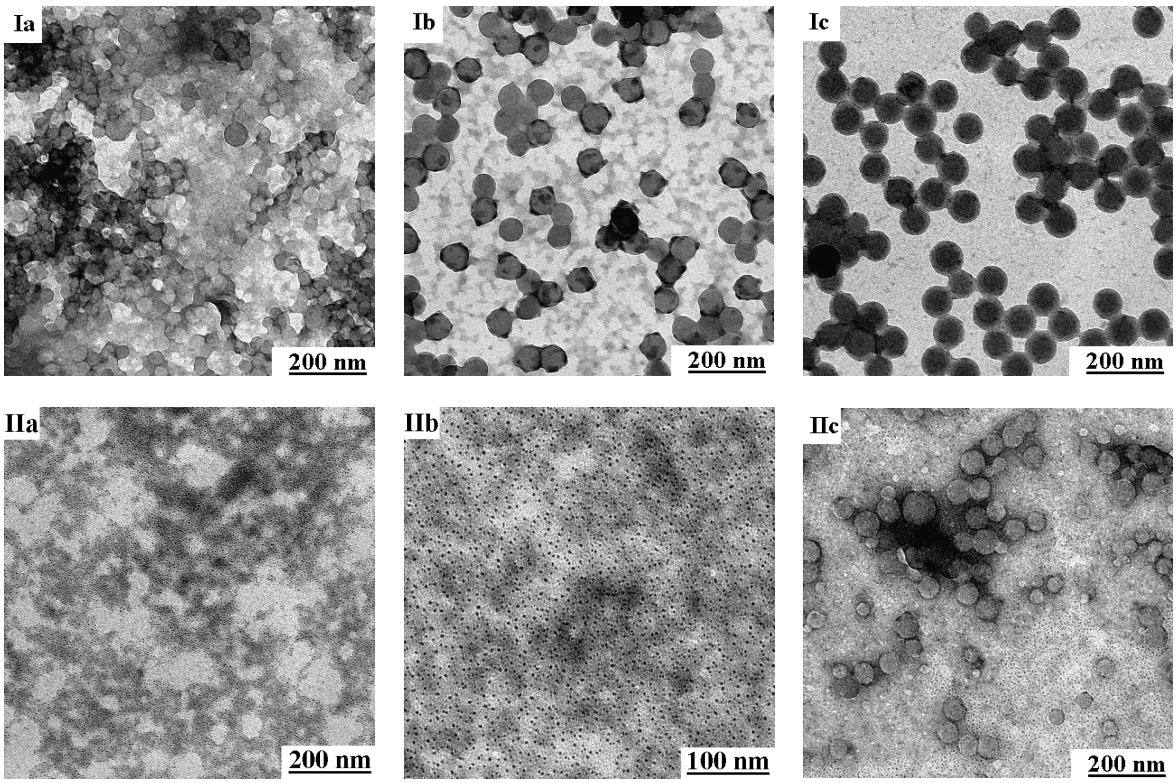

Figure 11 TEM images of the particle morphology during the surfactant-free emulsion polymerizations of styrene in the glass reactor, polymerization starts by injection of initiator (run I, polymerization with t_{equ} = 120 min) and by addition of monomer (run II, polymerization with t_{equ} = 0). Stirring rate is 50 rpm. The images show the polymerization mixture at 5 minutes (a), 15 minutes (b), and 30 minutes (c) after starting the polymerizations.

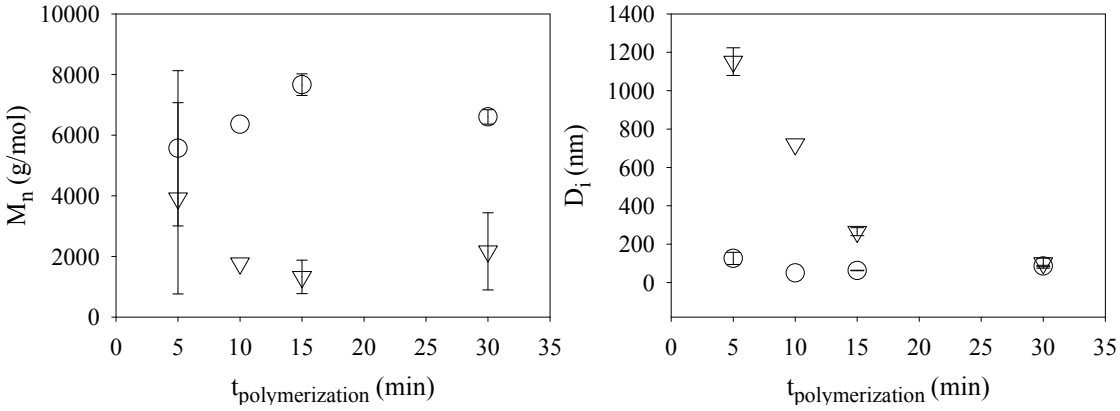

Figure 12 Development of the number average molecular weight (M_n) and the intensity averaged particle size (D_i) during the surfactant-free emulsion polymerizations of styrene in the glass reactor, polymerization starts by injection of initiator (run I, polymerization with t_{equ} = 120 min, circles) and by addition of monomer (run II, polymerization with t_{equ} = 0, triangles). Time zero is the start of the polymerizations; results are the averaged values and standard deviations of two polymerization runs.

The TEM images show different behavior for the polymerizations with t_{equ} = 0 and 120 min. In the polymerization with t_{equ} = 120 minute spherical objects are visible in only 5 minutes after the initiation (image Ia, Fig. 11). However, their size distribution

is quite broad. These objects possess clearly a core-shell morphology, as indicated by the darker edges. However, the core-shell morphology disappears with time and solid particles are formed. Image Ic shows solid-like particles having a darker core and brighter shell. The molecular weight is constantly increasing and levels off at higher conversions (cf. Fig. 12).

Contrary to this picture, in the polymerization with $t_{equ} = 0$, much smaller objects are observed at lower conversions. Very small dark spots of a size below 10 nm form immediately after the initiation (image IIa and IIb, Fig. 11). Later, these small spots are replaced by the objects with core-shell morphology (image IIc), which resemble the first image for the polymerization with t_{equ} = 120 min. It seems that, the development of the particle morphology follows the same trend as for the polymerization with t_{equ} = 120 min, but with a time delay. Only at higher conversions expected solid-like morphologies are formed (image not shown here). The molecular weight is almost constant and particle size decrease with time.

These observations can be explained considering different states of the monomer in water during the early stages of polymerizations. Obviously, equilibration of the monomer and water allows faster aqueous phase polymerization, thus a high number of low molecular weight oligomeric particles are formed within a short polymerization time. The oligomeric particles may nucleate and precipitate at the interface of the monomer drops, as they are neither soluble in water nor in styrene. The polymeric chain ends having higher water solubilities are oriented towards the water phase and are observed as thin dark layer due to the higher electron density of sulfur and oxygen groups. With ongoing polymerization, the morphology of the particles is changed as the polymerization is more and more shifted inside the templated monomer droplets leading eventually to the solid sphere morphology in the following way. The higher molecular weight polymers form the solid cores of the particles and imbibe monomer. Here is now the main locus for initiation of new polymer chains of lower molecular weights, which are visible as the bright shells.

However, in the polymerization with $t_{equ} = 0$ addition of monomer to the initiator containing aqueous phase leads to a rapid formation of oligoradicals. These oligomers nucleate to the primary particles which are visible as the dark spots, in both images IIa and IIb (as lower number of monomer drops are present, only the nuclei composed

of oligomers are visible). The high electron density is due to the high sulfur and oxygen contents. After formation, these oligomeric particles absorb monomer and continue to grow. However, their growth rate is restricted by the limited monomer concentration. Indeed, the low molecular weight data of these polymers confirm this hypothesis. The size measurement, on the other hand, suggests the presence of extremely large particles at low conversions. The particle size decreases sharply with time and reaches the same size range as for the polymerization with t_{equ} = 120 min. This result can be explained reminding the fast formation of monomer droplets from transmission data. Seemingly, the large scattering objects detected by DLS at low conversions are the monomer droplets formed by the spontaneous emulsification. Note that the scattering intensity varies with the sixth power of diameter. Thus, the tiny oligomeric particles contribute only little to the scattering. As the polymerization goes on, these droplets are consumed and become smaller in size, or disappear completely. At this time, the polymer particles are responsible for the scattering signals.

It is worth to mention two points here. First, the average hydrodynamic particle size measured by DLS reveals always higher values comparing with the size observed in the TEM images, as the diffusion rate of the particles is influenced by the internal interactions in the solution, and so is the estimated particle diameter. Second, the time scales in the off-line analysis can not be compared with those in on-line measurements, as the hydrodynamics of two polymerization reactions is different.

The importance of the hydrodynamics of the reactor (mainly the stirrer speed) on the state of the monomer in water and hence on the whole polymerization is shown in figures 13 and 14.

The TEM images reveal almost solid particle morphologies under different stirring conditions. Some of the particles exhibit darker edges as already discussed above. Note that the morphology is mainly determined by the initiator concentration, which is constantly kept low in these polymerization systems. At higher initiator concentration the influence of the stirring becomes more substantial. [50] In any case, the growth rate is the faster the higher the stirring speed, thus only a minor fraction of stabilized particles are available in the quiescent condition.

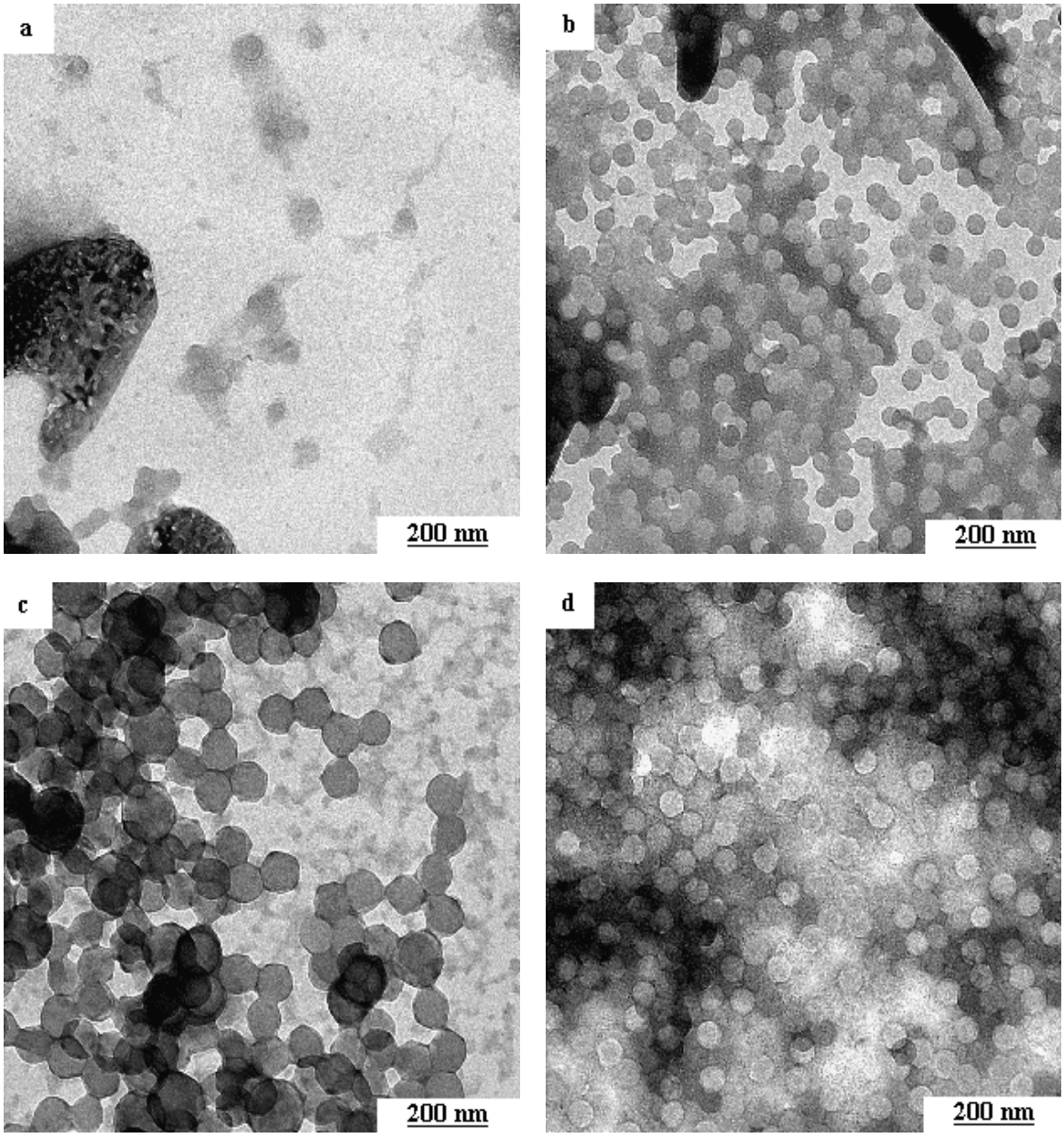

Figure 13 TEM images of the particle morphology 5 minutes after the initiation in the surfactant-free emulsion polymerizations of styrene in the glass reactor, with equilibration time, quiescent condition (a), stirred at 50 rpm (b), stirred at 150 rpm (c), and stirred at 300 rpm (d).

The molecular weight is affected by the stirring condition, especially at high conversions. The errors accompanied with results are significant (especially for the polymerization with 150 rpm stirring rate); however, one might conclude an increase in the molecular weight from quiescent to the stirred conditions due to the higher monomer concentration present in the water phase.

Neglecting the initial high diameter values corresponding to the monomer droplets, the particle size grows continuously with time in all the polymerizations, independently from the stirring speeds.

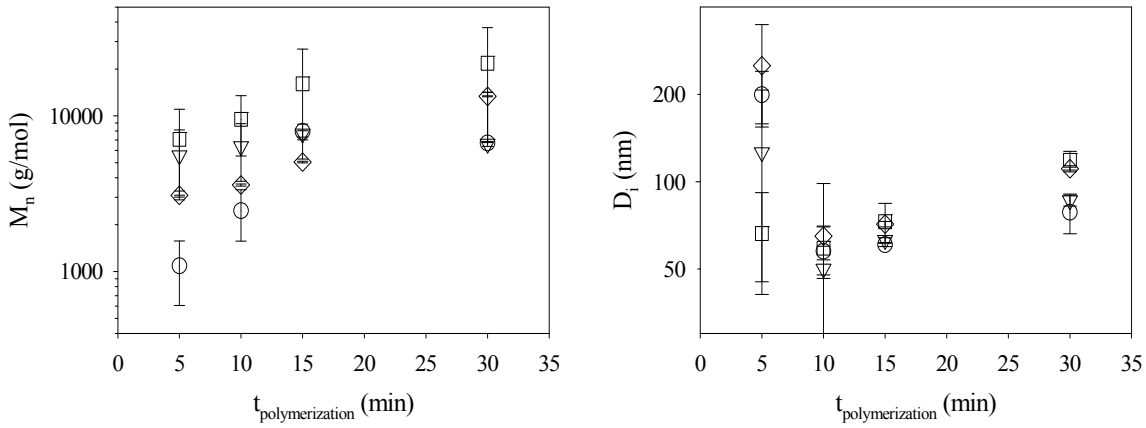

Figure 14 Development of the number average molecular weight (M_n) and the intensity averaged particle size (D_i) during the surfactant-free emulsion polymerizations of styrene in the glass reactor with equilibration time, quiescent condition (○), stirred at 50 rpm (△), stirred at 150 rpm (□), and stirred at 300 rpm (◇). Time zero is the start of the polymerizations.

In fact, the hydrodynamic conditions can neither change the basics of the particle formation mechanism nor the particle morphology, but have a strong impact on the transportation of the monomer to the reaction loci. The higher the stirrer speed, the higher is the rate of monomer emulsification, and the faster the transportation of the monomer to the reaction loci, and hence, the growth rate.

Surprisingly, the monomer droplets can be seen in the TEM images. It was observed repetitively in different polymerization systems that the monomer droplets are templated or stabilized by small oligomeric particles. These oligomeric particles are formed by the aggregation of the primary oligoradicals. The latter are the products of the reaction of the primary sulfate ion radicals with styrene molecules (or dimers or trimers). These oligomeric particles have a size below 5 nm and are visible as small dark spots on the TEM images. They consist of a few oligomers with higher electron density due to the higher sulfur and oxygen content than the polymer. According to the consideration of the classical nucleation theory, the energy barrier for the nucleation is lower at the interface. [51] Thus, these oligomeric particles nucleate at the interface between the styrene droplets and water. Also, they might adsorb at the interface after the nucleation as they are neither soluble in water nor in styrene, and thus, forming the hollow sphere morphology. In some cases, these templated particles coalesce during drying and form a foam-like structure, as they are softened by high amount of monomer (cf. image 2, table 9, Appendix). An example illustrating the

deposition of the oligomeric particles around the monomer droplet is shown in Fig. 15.

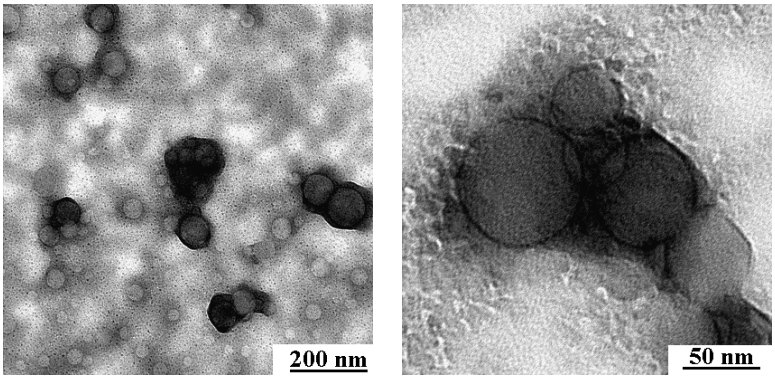

Figure 15 TEM images of the particle morphology 30 minutes after the initiation in the surfactant-free emulsion polymerizations of styrene in the glass reactor, without equilibration time, under quiescent condition. Images show the deposition of oligomeric particles onto styrene droplets during the early stage of the polymerization.

Although the monomer droplets do not change the reaction mechanism, but the consequences of their existence for the polymerization are enormous. The huge interface of the droplets facilitates monomer diffusion into water and hence, decreases the nucleation time, enhances the polymerization rate, and alters the particle morphology.

Indeed the above scenario can explain all the experimental observations as the parameters influencing the rate of the spontaneous emulsification and consequently, the rate of the droplet formation. Higher stirrer speed eases the formation of the droplets on the one hand, and enhances the growth rate by increasing the rate of monomer supply to the growing oligomers on the other hand.

If however, the polymerization conditions are changed in a way resulting in oligomers with higher molecular weight which are soluble in the droplets, solid particles should be formed. Indeed, this is proven by the data put together in Fig. 16 and 17. Here, two polymerizations with different KPS concentrations are compared. [52] The polymerization with the lower initiator concentration (standard run) leads to solid particles, as the more hydrophobic oligoradicals are soluble in the droplets. Regarding the radical generation in the continuous aqueous phase, the polymerizations with low KPS concentrations correspond to polymerizations with a more hydrophobic initiator, as will be discussed in the next section. On the other hand, polymerization with the higher initiator concentration leads to templated

droplets and, at higher conversions, very special particle morphologies resembling rather vesicular or hollow particles than solid spheres (cf. Fig. 17).

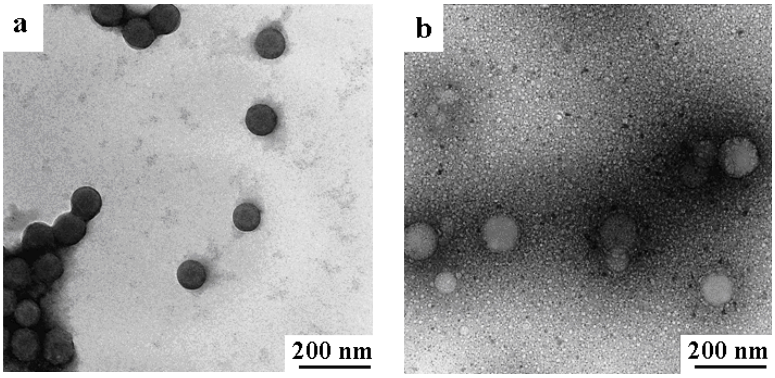

Figure 16 TEM images of particle morphology after polymerization time of 30 min of non-stirred surfactant-free emulsion polymerizations of styrene with 120 min monomer equilibration time in the glass reactor; polymerization is started with initiator concentration of 0.064 g (a), and 0.89 g (b).

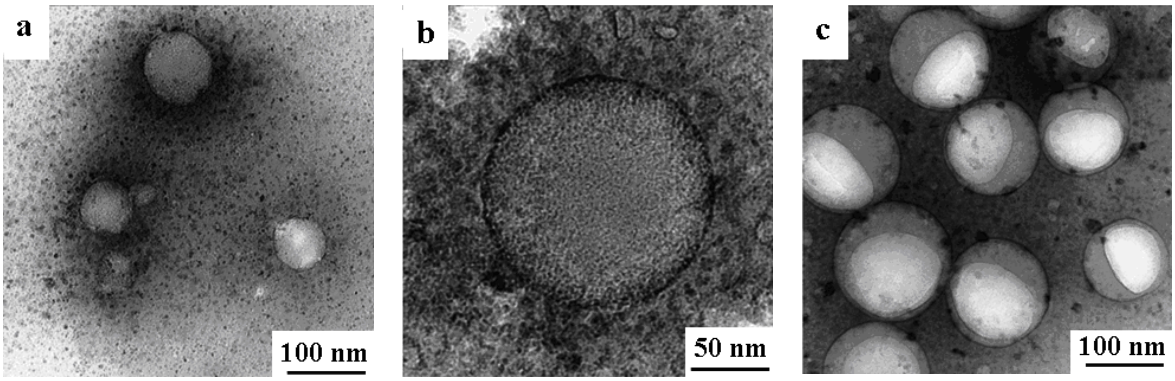

Figure 17 TEM images illustrating the particle morphology as result of the deposition of oligomeric particles onto styrene droplets during the early stage of unstirred emulsion polymerization of styrene in the glass reactor. (a): t_{equ} = 5 min after 40 minutes polymerization time, (b) t_{equ} = 120 min after 30 minutes polymerization time, (c): t_{equ} = 180 min after 30 minutes polymerization time. Polymerization is initiated with high initiator concentration of 0.89 g. Data in collaboration with O. Lazareva. [52, 53]

3.2 On the role of initiator

Understanding the kinetic and mechanistic role of initiators in free radical heterophase polymerizations is challenging as the initiators are distributed among all phases: monomer droplets, water phase, monomer-swollen polymer particles and, if present, monomer-swollen micelles. On the other hand, the choice of a specific initiator is crucial because the initiators residues as the chain-ends become parts of the polymer molecules and consequently, they influence the polymer properties. Moreover, for aqueous heterophase polymerization the initiator residues determine the particle morphology. The initiator plays an extremely important role in the case of

surfactant-free emulsion polymerization where the colloidal stability is achieved by hydrophilic initiator end groups.

As shown in the previous section, potassium peroxodisulfate (KPS) is much suited to carry out surfactant-free emulsion polymerization. Surprisingly, a very similar behavior of the aqueous phase conductivity is observed if KPS is substituted with azo-initiators leading to carbon-centered free radicals. Figure 18 shows the general behavior of the conductivity measurements for the azo-initiators of AIBN, V-59, VA-086, and PEGA200. These azo-initiators possess a quite different solubility in water but for all of them a bend in the conductivity – time curve has been observed, though, both the sharpness and the magnitude of the changes are different.

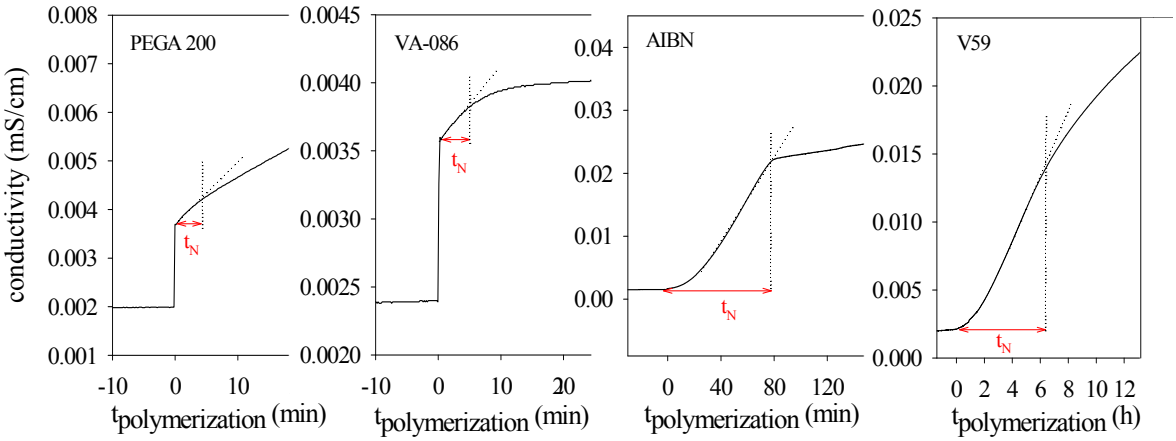

Figure 18 Conductivity – time curves measured during the initial period of surfactant-free emulsion polymerization of styrene with different azo-initiators; the dotted lines are for better visualization of the conductivity bend and the pre-nucleation period. Time zero is the start of the polymerizations.

The application of polyethylene-azo macroinitiator of PEGA200 for the heterophase polymerization of sterically stabilized latex particles is already known. [54] Formation of ionic species from the partially water-soluble VA-086 and electrically stabilization of the final particles are to some extent expectable. However, the fact that non-ionic initiators, even the extremely low water soluble V59, generates ionic species in the aqueous phase is not easy to explain. Apparently, a side reaction of carbon radicals with water molecules leads to the formation of ionic species that increase the conductivity in the aqueous phase and stabilize the particles even in the absence of surfactants. This hypothesis will be discussed in detail for the AIBN polymerization.

Figures 19a and 19b are comparison graphs of the duration of the pre-nucleation period for the above initiators compared with KPS. The obtained data show that the nucleation time decreases as the water solubility of the initiator increases. These data can be explained with different rate of radical generation in the continuous aqueous phase (cf. equation 4). The more water-soluble the initiator, the higher is the rate of the radical formation in the aqueous phase and the faster the nucleation.

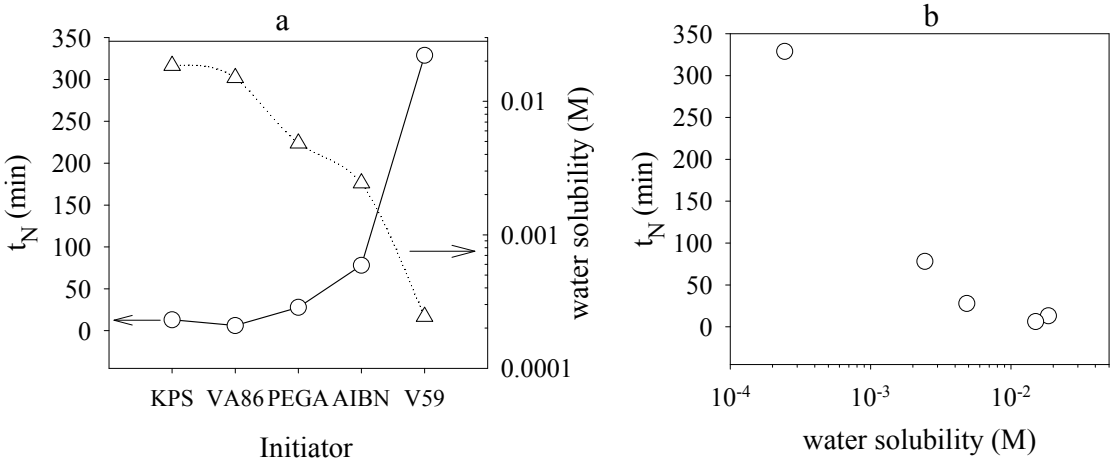

Figure 19 (a) Comparison of the duration of the pre-nucleation period (t_N, circles) for different types of initiators. The water solubility of the initiators is compared in the right axis (triangles). (b) Duration of the pre-nucleation period for different water solubilities. The water solubility data are at 25°C and taken from Ref. [55, 56] and estimated for V59 according to [57, 58]. The lines are just for guiding the eyes.

Medium hydrophobic initiators such as AIBN have been found to be the optimum choice for carrying out macro- and mini-emulsion polymerization. [59] Hence, it would be useful to study the surfactant-free polymerization of styrene initiated with AIBN in particular. Figure 20 compares the initial stage of the polymerization of styrene followed by the conductivity and the transmission measurements for the AIBN and KPS initiators.

Clearly, the general behavior for both types of initiators is identical. The slope of conductivity curves and the duration of the pre-nucleation periods are different, but explainable. [18, 19] The initiators decompose and free radicals are produced pairwise in both water and oil phase. The water-solubility of the initiator determines the partitioning of the radicals between the two phases. The generated free radicals in the aqueous phase react subsequently with water or monomer molecules. However, the initiator molecules in the continuous phase are surrounded by orders of magnitude more water than styrene molecules, and consequently, the free radicals attack water

molecules. This reaction sequence leads eventually to conducting species also for AIBN initiated polymerization and cause an increase in the conductivity.

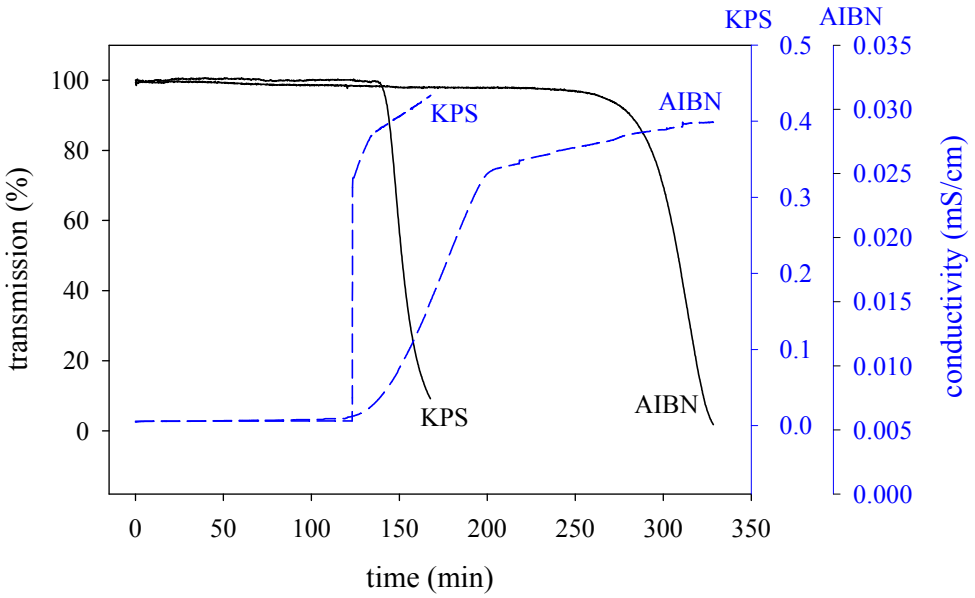

Figure 20 On-line monitoring of transmission (solid lines) and conductivity (dashed lines) during an ab-initio surfactant-free styrene emulsion polymerization initiated with KPS (first right axis) and AIBN (second right axis). Time zero is the monomer addition, and t = 120 min is the start of the polymerization.

The slope of the conductivity curve is much lower in the case of AIBN, although the decomposition rate coefficient of AIBN [60] is one order of magnitude higher than that of KPS [61]. This fact can be explained with a much lower water solubility of AIBN (the partition coefficient of AIBN between styrene monomer and water phase, $\lambda = [I]_d/[I]_{water}$ is 120 at 25 °C [62]). Consequently, both a lower concentration of initiating species and a lower concentration of oligomers are present in water at given time. Therefore, the onset of the nucleation which is controlled by the concentration of the cluster forming species, as well as the decrease in the transmission which is determined by the formation of a corresponding number of larger particles are delayed.

The different growth behaviors of water and oil soluble initiators are also reflected by the development of the average particle size and particle number with time, as shown in Fig. 21. The results confirm the generation of less but bigger particles after longer reaction times for AIBN compared with KPS as initiator.

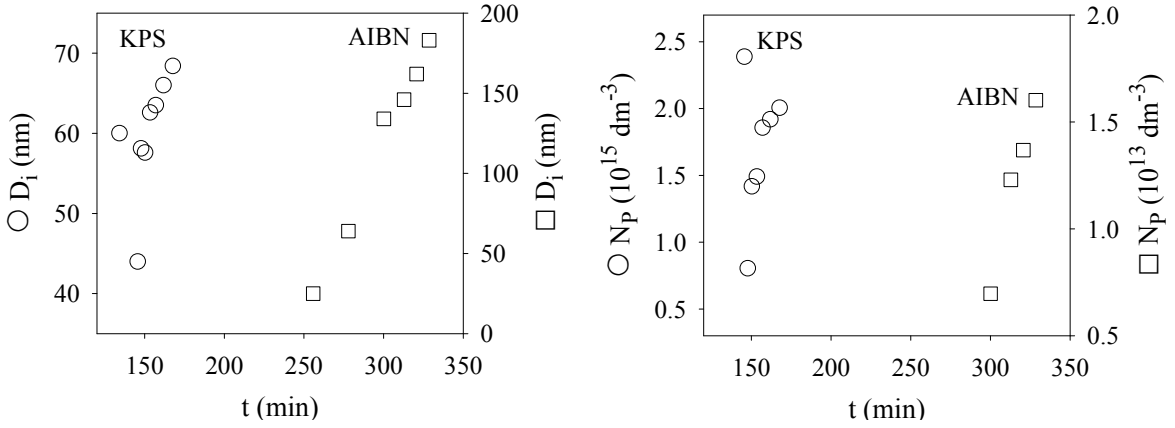

Figure 21 Comparison of the development of the measured intensity averaged particle size, D_i, and the calculated particle number, N, during the surfactant-free emulsion polymerization of styrene initiated with KPS (squares) and AIBN (circles). Time zero is the monomer addition, and t = 120 min is the start of the polymerization.

The TEM images of Fig. 22 obtained from the off-line polymerizations compare the growth of the latex particles initiated with AIBN and KPS.

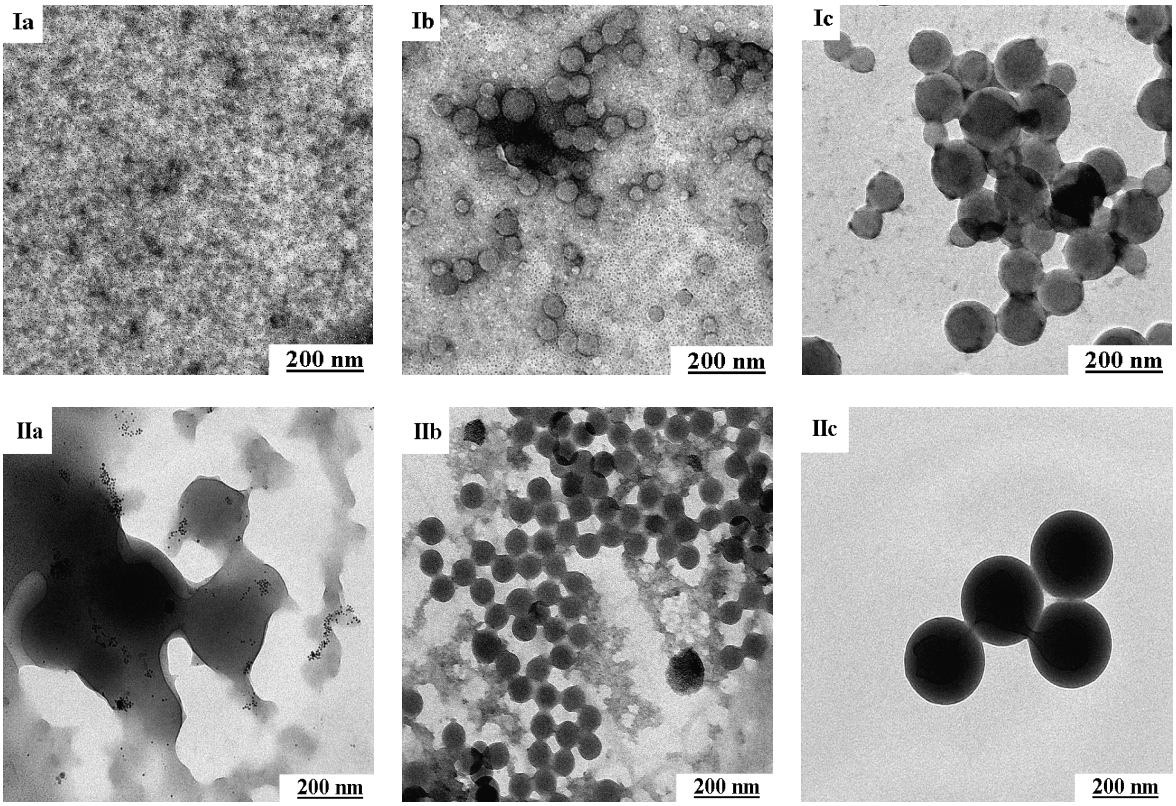

Figure 22 TEM images of the particle morphology during the surfactant-free emulsion polymerizations of styrene in the glass reactor, without equilibration time, stirring at 50 rpm, initiated with: KPS (I), and AIBN (II). Samples are taken 15 minutes (Ia), 30 minutes (Ib), and 60 minutes (Ic) after the initiation in the polymerization initiated with KPS and 30 minutes (IIa), 45 minutes (IIb), and 80 minutes (IIc) after the initiation in the polymerization initiated with AIBN.

Regarding the radical generation in the continuous aqueous phase the polymerizations with AIBN correspond to polymerizations with low KPS concentrations. Consequently, the particle morphology is always solid like. The images of Fig. 23 demonstrate that with AIBN quite nice monodisperse latexes can be obtained however at quite low solids content and with lower conversions compared with KPS.

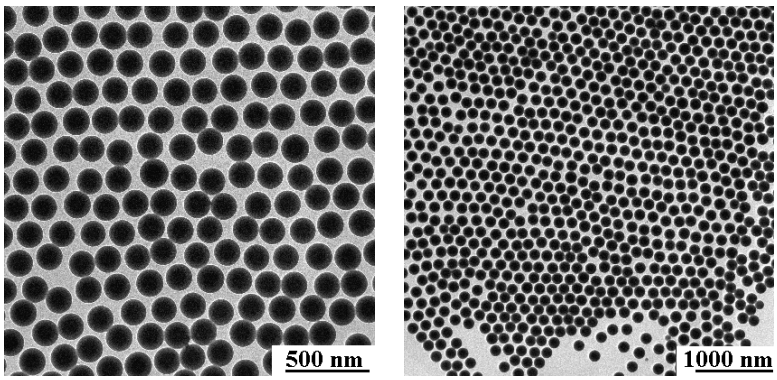

Figure 23 TEM images of the polystyrene particles obtained by surfactant-free emulsion polymerization of styrene initiated with AIBN in the glass reactor, without equilibration time, stirring at 50 rpm, 90 minutes after the initiation.

The only gradual difference between AIBN and KPS is also demonstrated by the development of the number average molecular weight and the average particles size with polymerization time, as shown in Fig. 24. This figure shows data for the initial period of the polymerizations at low conversions, so the minimum in the average particle size can be explained by the replacement of the monomer droplets to the latex particle [33], which continue to grow at higher conversions, as shown by the data of Fig. 21.

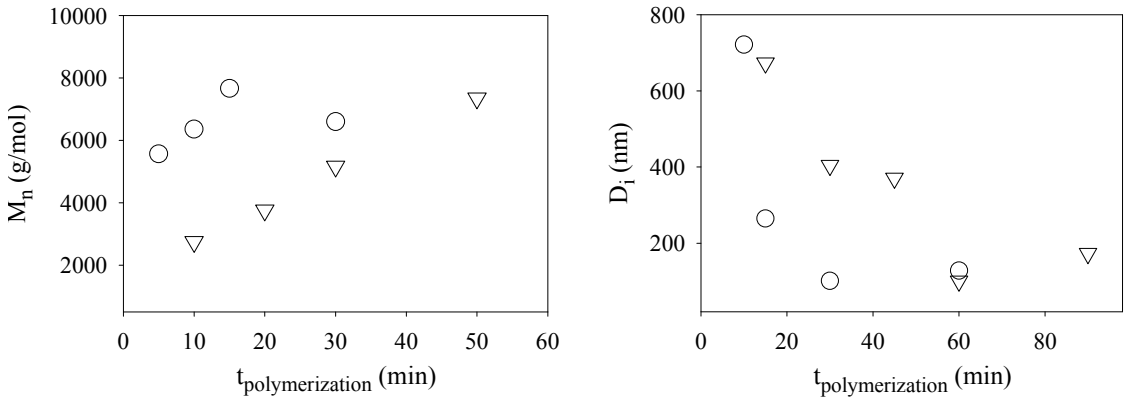

Figure 24 Development of the number average molecular weight (M_n) and the intensity averaged particle size (D_i) during the surfactant-free emulsion polymerizations of styrene with equilibration time and stirring at 50 rpm, initiated with: KPS (circles) and AIBN (triangles), polymerization in the glass reactor. Time zero is the start of the polymerizations.

Comparing the polymerization systems initiated with the AIBN and KPS, one can conclude that the AIBN leads to polymers with similar or slightly higher average molecular weights (at higher conversions, cf. table 26, Appendix) and particles with higher average diameters (cf. Fig. 24). Both results can be explained by a reduced concentration of the initiator which leads to a lower termination rate (and higher molecular weights), as well as a decreased concentration of the stabilizing species (and higher particle sizes). However, excessive bulk polymerization of styrene in the monomer layer restricts the monomer supply to the continuous aqueous phase and limits the solids content.

The available concentration of the monomer in the aqueous phase is an extremely important parameter influencing the nucleation and growth of the particles, as was shown in the previous section. Varying the equilibration time of the water with monomer (t_{equ}) from 40 to about 140 minutes reduces both the nucleation time (t_N) and the time of the drop in the transmission (t_T), as shown in Fig. 25.

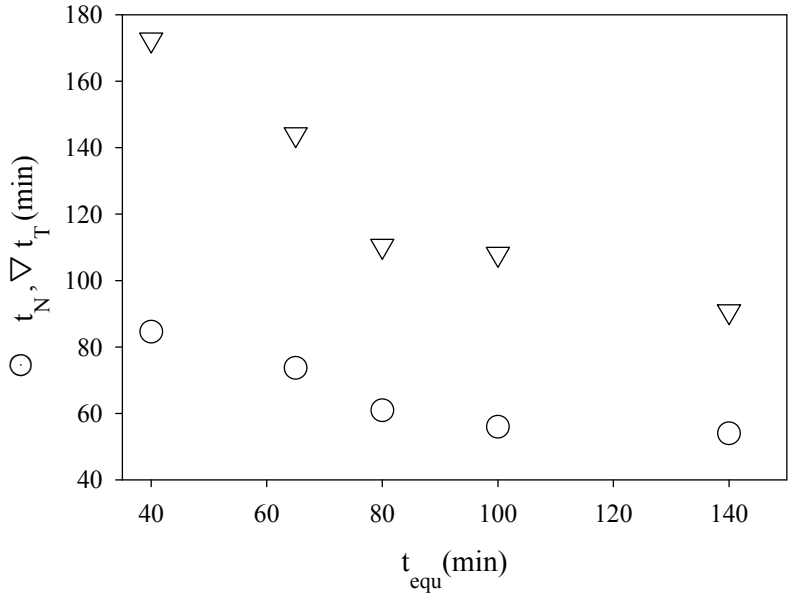

Figure 25 Dependence of the duration of the pre-nucleation period (t_N, circles) and the time of the drop in the transmission (t_T, triangles) on the equilibration time of the monomer with the aqueous phase with monomer in the surfactant-free styrene emulsion polymerization initiated with AIBN.

Moreover, the TEM images of Fig. 26 and the data of Fig. 27 obtained from the off-line polymerizations reveal the importance of the equilibration time on the nucleation

time, growth and morphology of the latex particles. In the same figures, the influence of the stirring on the morphology and the growth is demonstrated.

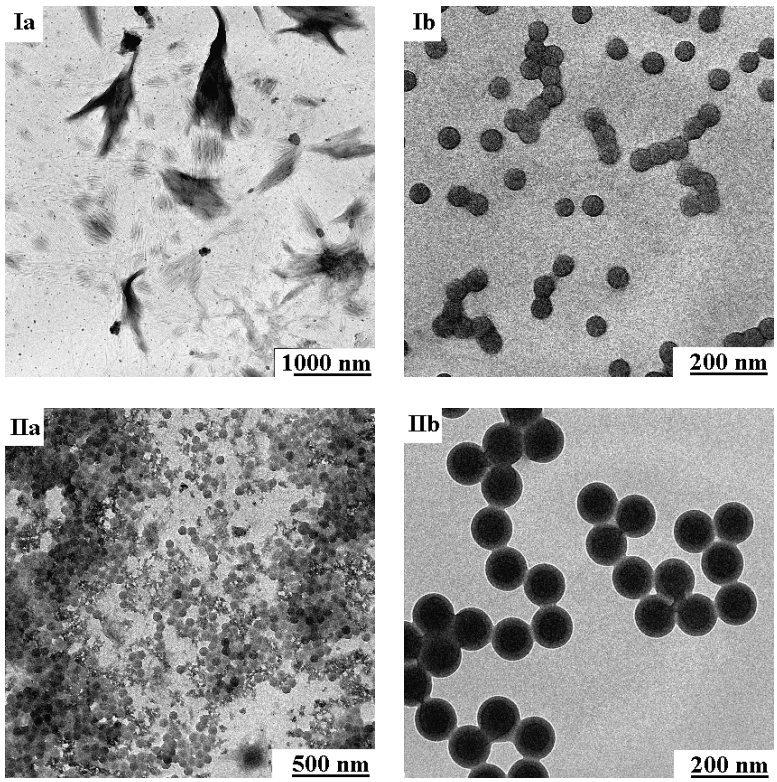

Figure 26 TEM images of the particle morphology during the surfactant-free emulsion polymerizations of styrene in the glass reactor initiated with AIBN, without equilibration time (I), and with 120 min equilibration time (II), at quiescent condition (a), and stirred at 50 rpm (b). Samples are taken 60 minutes after initiation.

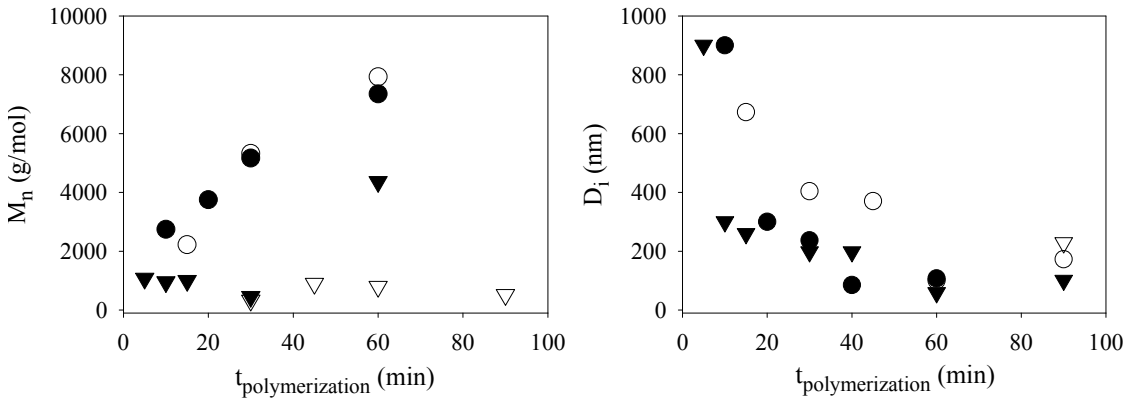

Figure 27 Development of the number average molecular weight (M_n) and intensity averaged particle size (D_i) during the surfactant-free emulsion polymerizations of styrene in the glass reactor initiated with AIBN, with equilibration (filled symbols) and without equilibration (empty symbols). The reaction was either under quiescent condition (triangles) or stirred at 50 rpm (circles). Time zero is the start of the polymerizations.

Obviously, a longer equilibration time leads to a better availability of the monomer during the polymerization. The effect is more substantial during the particle growth period (triangles in Fig. 25 and the data in Fig. 27), that is after particle nucleation.

This is a reasonable result as the behavior during the pre-nucleation period is essentially determined by the initiator concentration which is however, not changed during these experiments. Nevertheless, the duration of pre-nucleation period reduces from about 84 to about 54 minutes by increasing the monomer equilibration time from 40 to 140 minutes.

The influence of the reaction kinetics on the duration of the pre-nucleation period can be understood within the frame of the aggregative nucleation mechanism (equation 18, section 1.2) where the rate of nucleation (r_N) is controlled by the supersaturation. The higher the availability of monomer in water, the higher is the supersaturation and hence, the shorter is the pre-nucleation period. Once more, the results presented in figures 25 and 26 reveal the importance of the t_{equ} and the stirring on increasing the concentration of the monomer droplets as well as the molecularly dissolved monomer in water. Both experimental parameters influence the nucleation and growth kinetics. In general, longer equilibration time of the monomer in water leads to polymers with higher molecular weights and particles of slightly smaller size due to the increased concentration of the monomer in the continuous phase. The available monomer concentration influences all three the particle nucleation, the particle growth, and the propagation kinetics of the chains. In the absence of both stirring and equilibration no particles are formed even 60 minutes after the initiation. The TEM image (Ia, Fig. 26) shows arbitrary shaped precipitatation structures formed during sample preparation for electron microscopy. On the other side, in the case of having both equilibration and stirring, solid particles of high molecular weight are produced (image IIb).

These data raise immediately the question regarding the site of the initiation and the contribution of the AIBN radicals stemming from both phases (between bulk monomer, the droplets, and water). In order to get an idea, the polymerization has been carried out with AIBN injection either in the monomer phase (mode 1) or in the water phase (mode 2), as shown in Fig. 28. At the end of the polymerization, the monomer phase is separated from the aqueous phase and the products formed in each phase are analyzed. The data summarized in the following figures compare the results obtained for both injection modes with respect to the conductivity and transmission – time curves (Fig. 29), and the particle morphology (Fig. 30), as well as the molecular weights of the polymers (Fig. 31) at the end of the reaction.

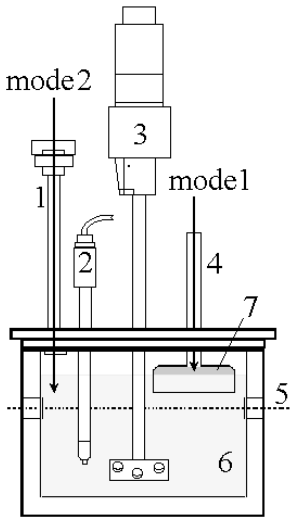

Figure 28 Schematic representation of the Teflon reactor; (1) initiator injection, (2) conductivity and temperature probe, (3) stirrer, (4) monomer funnel, (5) optical path for monitoring of transmission, (6) aqueous phase, (7) monomer phase; modes1 and 2 denote possibilities to inject oil-soluble initiators.

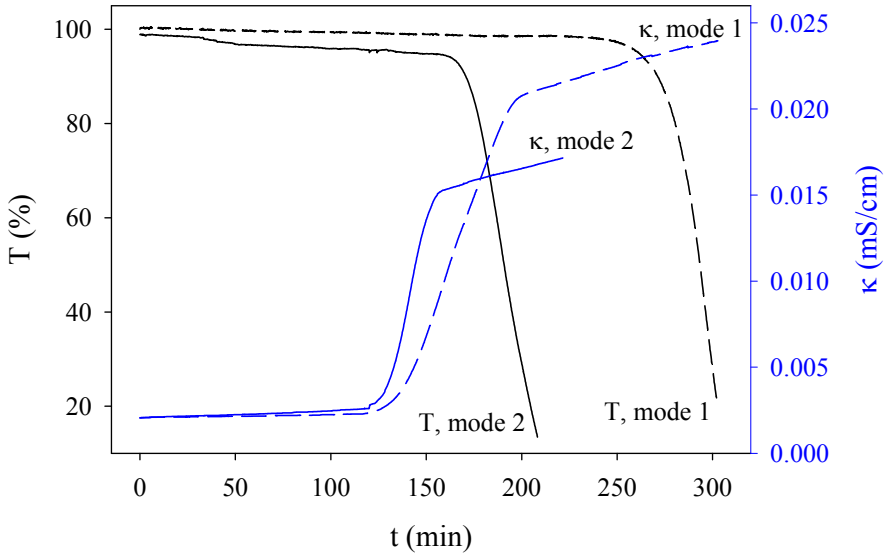

Figure 29 On-line record of the changes in transmission and conductivity during AIBN-initiated surfactant-free styrene emulsion polymerization; the curves represent averages of 5 repeats. AIBN is added into the monomer, mode 1 (dashed lines) and to the water phase, mode 2 (solid lines), respectively

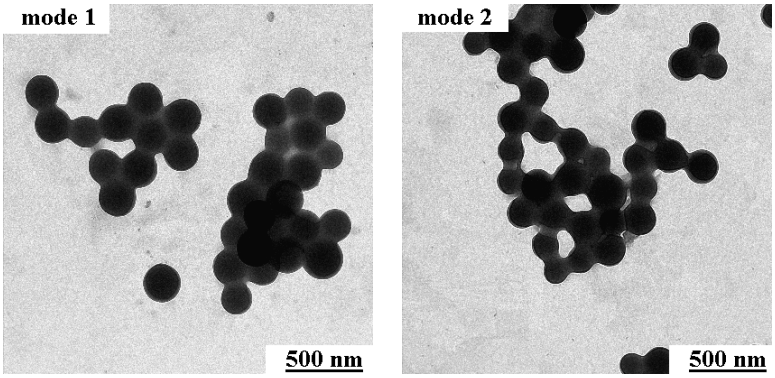

Figure 30 TEM images of latex particles obtained during surfactant-free emulsion polymerization of styrene in the Teflon reactor initiated with AIBN with two injection modes: monomer phase (mode1) and water phase (mode 2)

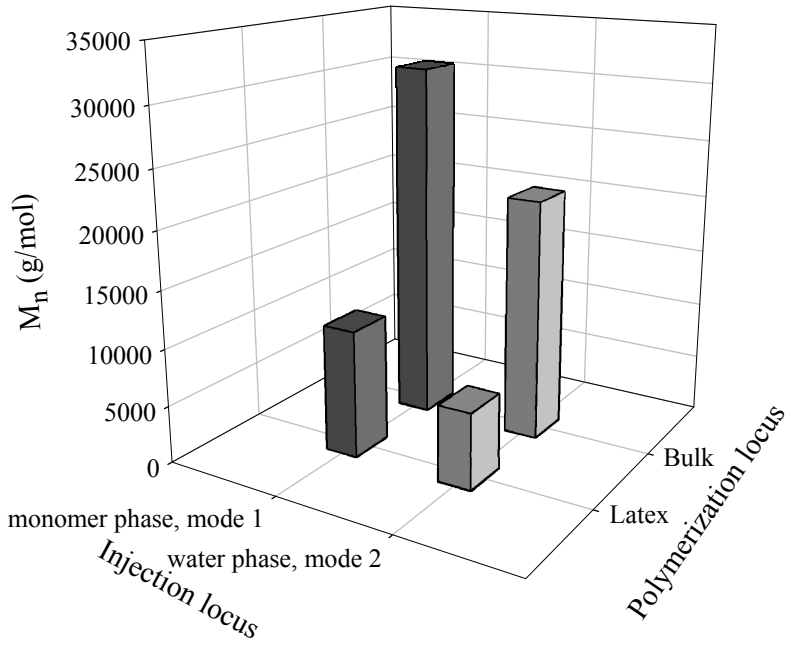

Figure 31 Number average molecular weight of the polymer formed during surfactant-free emulsion polymerization of styrene in dependence on the AIBN injection mode and the polymerization locus; results are the averaged values of six polymerization runs.

Either initiator addition mode leads to qualitatively similar behavior. Nevertheless, regarding the role of the AIBN addition mode the following conclusions can be drawn:

1. If the AIBN solution is injected to the monomer phase, that is confined in the glass funnel with an area of 31 cm^2, the interface through which the AIBN can diffuse into the water is reduced by more than a factor of two. On the other hand, the initiator addition mode 2 leads to a thin monomer layer at the water air interface, which obviously facilitates AIBN diffusion into the water phase

compared to mode 1. Thus, mode 1 favors a higher AIBN concentration in the thicker bulk monomer phase possessing a smaller interface to the water phase. The higher is the amount of AIBN in the bulk monomer phase (mode 1 vs. mode 2) the lower the initial slope of the conductivity – time curve, the longer the pre-nucleation period, and the later the transmission starts to drop.

2. After the bend (i.e. after particle nucleation), the slopes of both conductivity curves are almost identical, indicating the same overall surface area of the nucleated particles. This conclusion is confirmed by the average size of the particles which is almost the same (D_i of 190 and 184 nm for mode1 and 2, respectively). Moreover, the morphology of the particles at the end of the polymerization is similar (cf. Fig. 29).

3. The molecular weight data scatter a lot, especially those obtained for the polymer formed in the latex particles after AIBN addition to the monomer phase (mode 1). Despite the scatter, which might be due to a post-effect situation in the latex particles before isolating the polymer, the order of the molecular weights demonstrated in Fig. 30 can be explained as follows. The polymerization to high molecular weight polymers starts in the monomer phase soon after initiator addition. Whereas the formation of polymers in the latex can only start after nucleation, which is 30 minutes (for mode 2) or 70 minutes (for mode 1) after initiation (cf. Fig. 28). The polymer formed during this pre-nucleation period inside the monomer phases retains the monomer and reduces swelling of the particles with monomer. Thus, the polymerization inside the monomer phase prevents the formation of high molecular weight polymers inside the latex particles. Comparing two modes of the injection, mode 1 leads to higher molecular weights, both in latex and bulk. The latter can be explained by higher monomer concentration and the former by lower initiator concentration.

4. Production of high molecular weight polymer chains in the aqueous phase is accompanied with a bitter almond smell of benzaldehyde in the reaction medium and high conversions (cf. Appendix for the reaction details). It is worthful to mention that the rate of the transfer of polymer chains from bulk to

the latex phase is negligible. Molecular weight measurements of the product in the bulk phase isolated right after the conductivity bend proves this scheme, as high molecular weight polymers are already formed in the bulk at this time stage, whereas no polymer is found in the latex phase.

In conclusion, the formation of latex particles in surfactant-free emulsion polymerization of styrene initiated with AIBN obeys the same rules of aggregative nucleation as verified for KPS. However, initiation of surfactant-free emulsion polymerization with oil-soluble initiators offers the unique possibility to control the duration of the pre-nucleation period by the interfacial area between the monomer and the water.

In order to get an idea about the nature of the hydrophilic groups stabilizing the particles prepared by AIBN-initiated surfactant-free emulsion polymerization of styrene, the zeta potential of the particles was measured. These data (Fig. 32) reveal that the particles are electrically stabilized and their charge is pH dependent. The particles loose their stability below pH = 2 - 3. Obviously, carboxylic acid groups contribute essentially to particle stability.

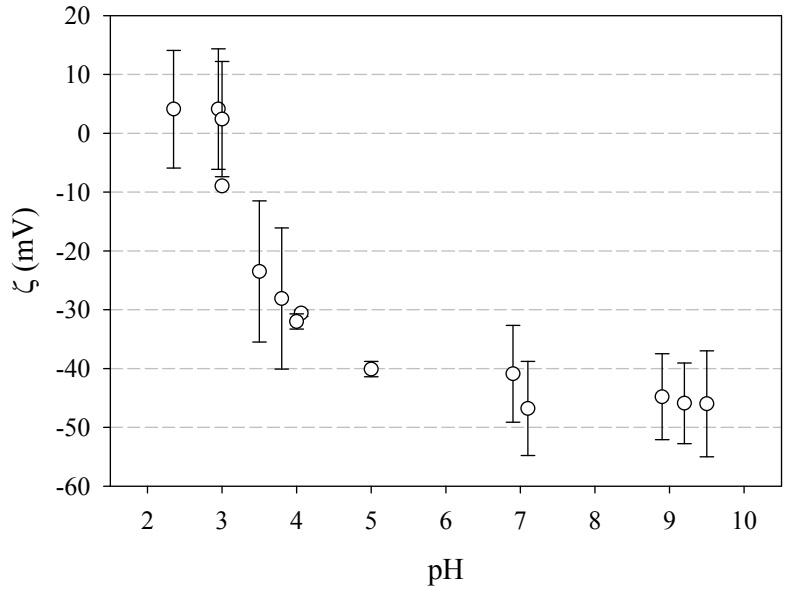

Figure 32 pH-dependent zeta potential measurement of latex obtained by surfactant-free emulsion polymerization of styrene initiated with AIBN, results are the averaged values and standard deviation of four polymerization runs.

The data presented so far (zeta potential, conductivity) allow the conclusion that side reactions of carbon-centered radicals in water lead to the formation of conducting species. Similar observation has been reported for the emulsion polymerization of

styrene initiated with poly(ethylene glycol)-azo-initiators, [63] where side oxidation reactions between carbon-centered radicals and water molecules are concluded based on NMR, FT-IR and elemental analysis data. A possible reaction path is shown in Fig. 33, where side reaction initiated by cyanoisopropyl radicals under participation of water molecules generates hydroxyl radicals and subsequently hydrogen peroxide. The ability of the latter to oxidize hydroxyl chain ends of oligomer or polymer molecules to carboxylic groups is well known. [64]

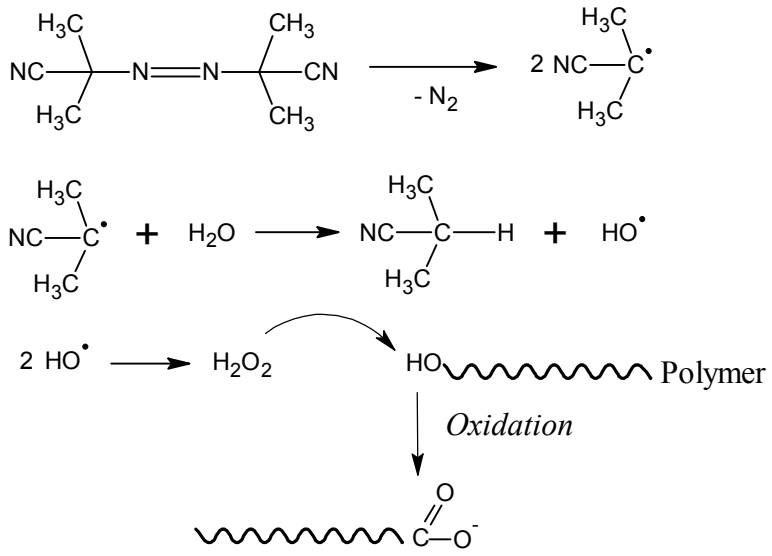

Figure 33 Possible side reaction of AIBN with water molecules leading to oxidizing agent and the following reaction with the polymer chain generating ionic species.

Another possible reaction is the hydrolysis of nitrile group to carboxylic acids, via the amide (cf. Appendix). [65] At room temperature, the reaction between nitriles and water would be so slow as to be completely negligible. But at elevated temperature and more effectively in an acid catalysed medium, the nucleophilic addition followed by the nucleophilic acyl aubstitution reaction is highly feasible. The positive zeta potential at acidic pH is then explained by the positively charged nitrogen functionalities.

First confirmations for such side reactions are obtained from IR and NMR investigations of the extracted latex. A part of the NMR spectrum is illustrated in Fig. 34, which reveals additional signals indicating carboxylic or benzoic acid groups besides the polystyrene and the cyanoisopropyl signals (cf. table 3).

The next confirmation comes from the AIBN decomposition experiment. Indeed, the side reaction of azo-initiators while decomposing is an experimental fact reported by different authors. [55, 63, 66] Table 4 shows a summary of the results concerning the

NMR investigations of the AIBN decomposition products formed in a benzene-water mixture and in the pure benzene (more details and the spectra in the Appendix).

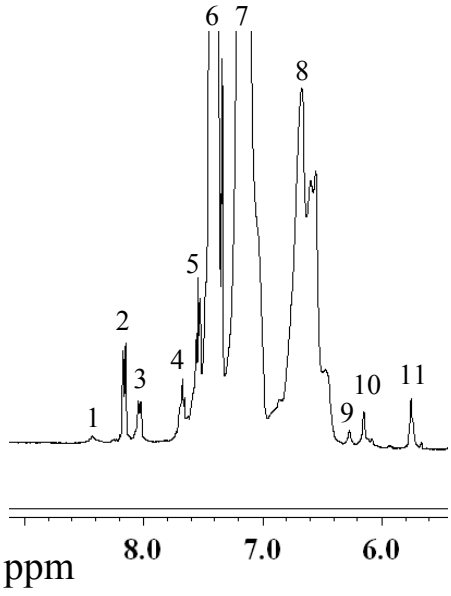

Figure 34 Part of the 400 MHz ^{1}H-NMR spectrum of the final latex obtained by surfactant-free emulsion polymerization of styrene initiated with AIBN.

Table 3 Chemical shifts in 400 MHz ^{1}H-NMR spectrum of the final latex obtained by surfactant-free emulsion polymerization of styrene initiated with AIBN, numbers correspond to the signals in figure 34.

Peak number	1-4	5	6	7	8	9-11
Polystyrene peaks		$\delta 1H_4$	$\delta 2H_3$		$\delta 2H_2$	
				Solvent peak		
End groups	δC_6H_5COO, δCOO, δC_6H_5OH					$\delta CONH_2$

Obviously, in pure benzene the cyanoisopropyl radicals recombine completely to tetramethylsuccinodinitrile (TMSDN), as it is well known. [55, 66] However, in the presence of water, the cyanoisopropyl primary radicals undergo in both phases side reactions leading to a mixture of ionic (or ionizable) products. This is clearly to be seen in the NMR spectrum since the CH_3 signal splits into two signals, and additional signals occur corresponding to a CH group and carboxylic or benzoic acid groups. The side reaction of cyanoisopropyl radicals with water molecules, generating ionic

species is observed in different organic solvent-water mixture (cf. conductivity data of Fig. 35).

Table 4 100 MHz ^{13}C-NMR chemical shifts of AIBN decomposition products.

	δCH_3 (ppm)	δCH (ppm)	δC quaternary (ppm)	δCN (ppm)	δC_6H_5COO (ppm)	δCOO (ppm)
AIBN in benzene-water mixture, Products in water phase	23.41-26.14	30.16	75.30	112.21-119.94	128.87	161.55
AIBN in benzene-water mixture, Products in benzene phase	23.86-26.51	39.40	67.79	111.3-119.1	129.19-141.45	161.3
AIBN in pure benzene	23.34		39.28	121.34		

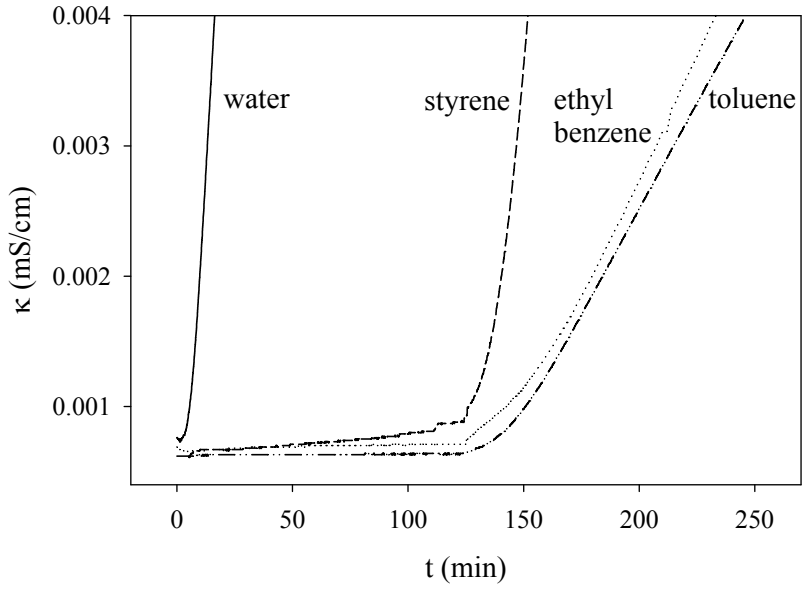

Figure 35 On-line record of the conductivity rise during the AIBN decomposition in water. AIBN powder is added to the water (solid line), dissolved in styrene (dashed line), dissolved in ethyl benzene (dotted line), and dissolved in toluene (dash-dotted line).

Interestingly, ionic species are formed even in pure AIBN-water mixture. In pure water, formation of these conducting species occurs with the highest rate (highest conductivity slope) compared with the cases where AIBN was dissolved in organic solvents. In the latter case, AIBN is partitioned between the two phases and the reaction rate with water leading to the conducting species is reduced. Organic

solvents with different hydrophobicities have been chosen, but all behave similarly. The results of two examples (toluene and ethyl benzene) are plotted in Fig. 35. Styrene leads exceptionally to a very high decomposition rate, as the polymerization and consumption of oligoradicals accelerate the decomposition reaction.

The results regarding the decomposition of AIBN in pure water need more clarification. At this experimental condition, AIBN decomposes continuously and it is not possible to distinguish between the dissolution and the decomposition reactions. This means, any solubility value of AIBN at higher temperature is just a fictive number. To gain a more quantitative result of the behavior at different temperatures, various amounts of AIBN were added as powder to water and placed in glass flasks for 24 hours at 80° C. After cooling down to room temperature the remained solid was separated from the aqueous phase. Elemental analysis and IR data show that the solids are AIBN (cf. Fig. 36 and table 5).

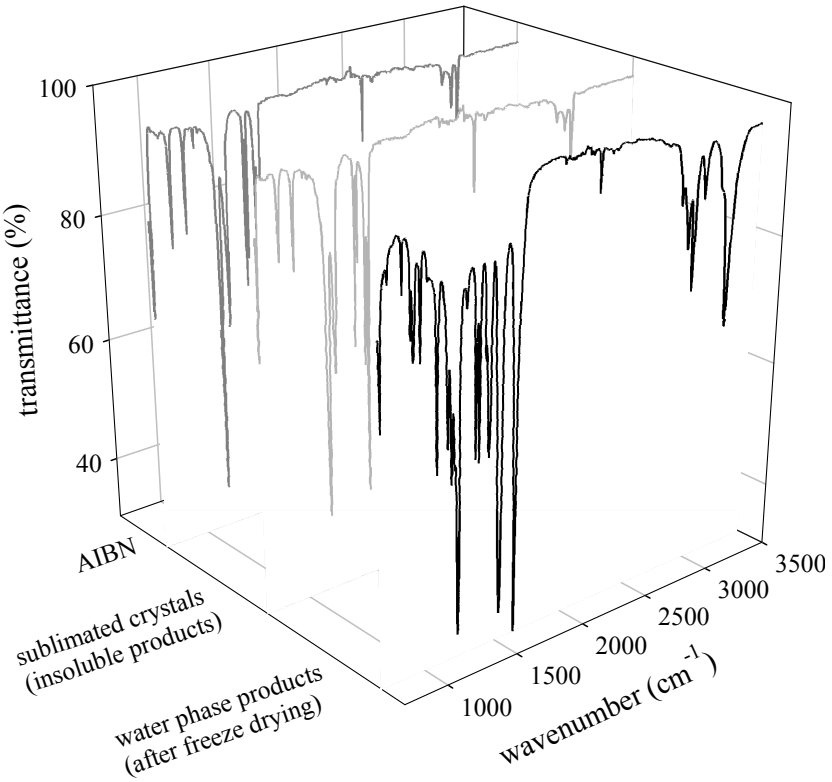

Figure 36 FTIR spectra of pure AIBN, and the decomposition products heated at 80°C in the rotation thermostat. Curves represent the sublimated products after cooling, and curve III represents the products in the aqueous phase after freeze drying.

The products dissolved at the end of the reaction in the aqueous phase were isolated by freeze drying and analyzed also by IR and elemental analysis. Figure 36 shows the comparison of the IR spectra of pure AIBN, sublimated crystals and the products in water phase, and table 5 shows the elemental analysis data for both solid (insoluble) and soluble products.

Table 5 Elemental analysis of the products of decomposition and reaction of AIBN in pure water at various temperatures; Theoretical values for AIBN and TMSDN are calculated and given as the references. Reaction time 24 h, results are the average values of three repeats.

T (°C)	% C		% H		% N		% O	
	Insoluble	Soluble	Insoluble	Soluble	Insoluble	Soluble	Insoluble	Soluble
90	71.99	62.32	9.40	8.87	19.76	17.12	-	11.68
70	61.28	65.38	7.97	9.63	32.1	18.21	-	6.27
50	58.35	63.63	7.3	9.23	31.89	22.35	2.46	4.29
25	58.31	59.78	7.3	7.94	31.78	33.72	2.69	-
AIBN	58.28		7.31		34.12		-	
TMSDN	70.25		8.88		20.57		-	

The analysis reveals that the soluble products are the decomposed species and contain, besides the tetramethylsuccinodinitrile (TMSDN), traces of unknown products with oxygen functionality. It is clearly to be seen that new signals are appeared in the IR spectra arose from the reactions of AIBN and water. Expectedly, the amount of side-products that are other products than TMSDN (the “normal” recombination product) and AIBN depends strongly on the decomposition temperature. A summarized result of the product distribution is presented in table 6.

Table 6 Product distribution of decomposition and reaction of AIBN in pure water at various temperatures; reaction time 24 h, AIBN and TMSD sublimate easily and hence larger losses occur during both thermal treatment and freeze drying. Values are given in percent in relation to used AIBN.

Temperature (°C)	filterable products (%)	aqueous phase products after freeze drying (%)
90	0.4	27.8
70	44.7	10
50	80.3	< 1
25	81	< 1

Despite all peculiarities and the scatter of the experiments, the data of table 6 are reasonable as with increasing temperatures aqueous phase side reactions become more and more important.

In conclusion, AIBN can be successfully applied to produce stable latexes with low solids content in surfactant-free emulsion polymerization. The formation of latex particles can be perfectly explained within the frame of the aggregative nucleation theory. The latex particles are electrostatically stabilized by ionic or ionizable groups which are formed by side reactions of carbon radicals under participation of water.

3.3 Are surfactant micelles crucial for the nucleation?

Although the surfactant-free polymerization has its own advantages of gaining non-contaminated polymers, in a general industrial emulsion polymerization, surfactants are used as a key formulation variable. According to Dunn [67] surfactants can:

1. act to solubilize the monomer and to stabilize the monomer droplets in an emulsion form
2. stabilize the formed latex particles as well as the particles which continue to grow during polymerization
3. act as chain transfer agents or retarders
4. serve as the site for the nucleation of particles.

The latter point, which is the basic assumption of micellar nucleation theory, has for some time been disputed. In accordance with this theory originally proposed by Harkins, [6] the nucleation of particles takes place solely in the monomer swollen micelles which are transformed smoothly into polymer particles by absorption of radicals from the aqueous phase. Based on this core assumption, Smith and Ewart [7] derived the famous relation for the number of polymer particles, N, depending on the concentration of micellar surfactants [S] and initiator [I], as $N \sim [S]^{0.6} \cdot [I]^{0.4}$. However, Roe pointed out [68] that this relation has only little to do with the mechanism of particle formation but rather with the question when does particle formation cease. This relation is not helpful to learn about particle formation as it is in fact independent of the particle nucleation mechanism! Moreover, there are all

kinds of data published showing various exponents for experimentally found $N - S^{\alpha}$ relations. Some results evidence Smith and Ewart's relationship and others do not. [16, 69, 70] Exemplarily, Bartholomé et al. determined $\alpha = 0.615$ for emulsion polymerizations of styrene with Amphoseife C18 as emulsifier and 0.361 g/l KPS at 45 °C. [8] Contrary, Hansen et al. obtained $\alpha = 2.67$ also for styrene emulsion polymerization but with SDS as emulsifier and 0.6 g/l KPS at 60 °C. [9, 50]

The experimental data that have been hitherto employed to provide support for the various proposed mechanisms are somewhat limited. Roughly speaking, there has been available only the particle number density (N) and the average particle diameter (D) at the end of the polymerization and the dependence of these observables on surfactant and initiator concentrations. Unfortunately, such data are obtained at a time stage far from the nucleation, and hence, are insufficiently sensitive to eliminate or confirm any postulated nucleation mechanisms.

In the context of this thesis, on-line conductivity measurements are applied to study the role of surfactants (and micelles) in particle nucleation. The micellar nucleation theory expects the monomer swollen micelles to be transformed smoothly into polymer particles by absorption of radicals from the aqueous phase. Hence, in the presence of surfactant micelles, the conductivity-time curve should posses a smooth pattern without sharp transitions. At least, no bend towards smaller slopes should be observed, if no additional particles are formed (no secondary nucleation). However, the conductivity data put together in Fig. 37 show bends towards lower slopes for a variety of surfactants at concentrations above their CMC, with KPS as initiator. The surfactants tested comprise examples of anionic, nonionic, and polymeric natures in order to be compatible with the initiator. Note that applying a cationic surfactant (for instance CTAB) in combination with anionic KPS leads to the formation of insoluble complex that precipitates as indicated by the decrease in transmission. Thus, an accurate decision regarding the onset of the nucleation is not possible with this recipe. However, a combination of CTAB and cationic Azo-initiator V50, or nonionic AIBN show the normal behavior and a bend towards lower slopes (cf. Appendix).

Despite this peculiarity in the case of CTAB, for all surfactants similar conductivity behavior is observed, and the onset of nucleation is clearly visible. However, the duration and the slope of that during the pre-nucleation period, as well as the slope of

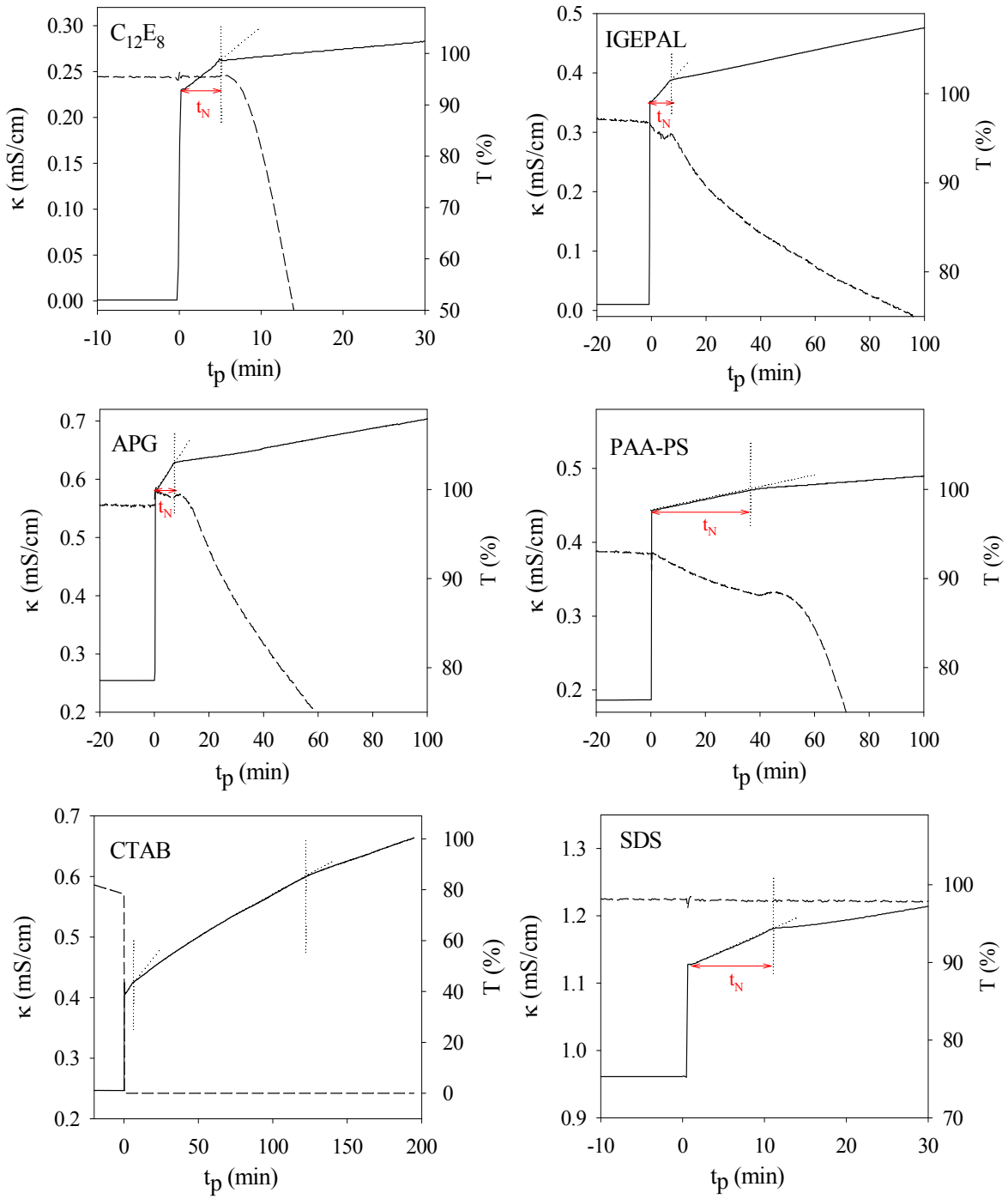

Figure 37 On-line monitoring of conductivity (κ, solid lines) and transmission (T, dashed lines) during ab initio styrene emulsion polymerization initiated with KPS, in the presence of different types of surfactant above their micellization concentrations. The dotted lines are for better visualization of the conductivity bend and the pre-nucleation period. Time zero is the injection of the initiator two hours after monomer addition to the surfactant solution. The $C_{12}E_8$ surfactant system exists in a meta-stable state, as the reaction temperature (70°C) is close to its phase separation temperature (80°C). The cationic surfactant (CTAB) forms complexes with the KPS.

the decrease in transmission are dependent on the type of emulsifier. These data allow an experimental verification of the influence of surfactants on the nucleation rate or

the duration of the pre-nucleation period (t_N). Surfactants lower the interfacial tension between the nucleating particles and the continuous phase, and hence, in the presence of surfactants the nucleation rate should be increased according to the classical nucleation theory. On the other hand, surfactants increase the solubilization of the monomer, and thus, increasing the polymerization rate during the pre-nucleation period. Hence, they lead to a decrease in t_N.

In contrast, the influence of surfactants on the growth rate reflected in the transmission curves is significant. Indeed, the data obtained here prove that surfactants serve in a large extent to stabilize the formed latex particles. As a result of the hindered aggregation, the number of latex particles is considerably higher compared with the case of surfactant-free polymerization. However, their size is smaller and thus, the transmission decrease slower.

Another interesting behavior is the occurrence of the Jumbo-effect in the transmission curves except for CTAB and SDS. For CTAB in the presence of KPS, this is due to the formation of the precipitates and for SDS, the change in the transmission is extremely low due to the high efficiency of this emulsifier to stabilize a high number of small particles. Unusually large Jumbo-effects are observed for nonionic surfactant (IGEPAL) and for PAA-PS. In the case of PAA-PS block copolymer, the magnitude of the Jumbo-effect increases with increasing the block copolymer concentration, as shown in Fig. 38. The magnitude of the Jumbo-effect for this system leads to the conclusion that block copolymer micelles play a role as scattering species. Indeed, the microscopy investigations prove the formation and swelling of the block copolymer micelles in water. In this case, styrene was replaced by the non-polymerizable ethyl benzene. Interestingly, after a while micelles are observed in either phase (cf. Fig.39).

In water, the hydrophobic polystyrene domains form the core and the hydrophilic PAA units stabilize the micelle (shell). In contact with an oil phase, there is a driving force for the organic solvent to swell the polystyrene core, that is to enter the aqueous phase and swell the micelles. On the other hand, there is a driving force for the micelles to enter the organic phase. As a result of equilibration in the chemical potential, and minimizing free energy, block copolymer micelles can diffuse across the interface to the oil phase. Consequently, micelles are to be seen in both phases (cf. image b and c Fig. 39). However, the morphology of the micelles is inversed at

the interface, so that the PAA domain collapses to the core in ethyl benzene and PS domain forms the stabilizing shell.

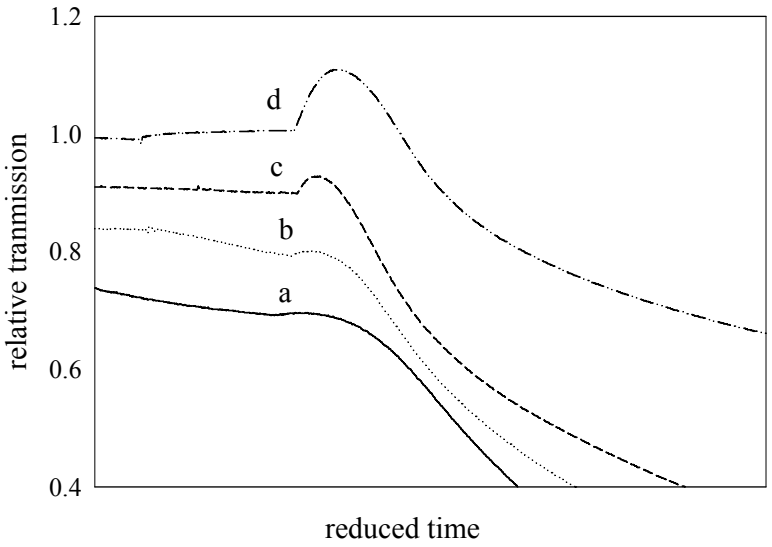

Figure 38 Dependence of the magnitude of the Jumbo-effect on the concentration of PAA-PS block copolymer surfactant during styrene emulsion polymerizations initiated with KPS. Different curves correspond to (a) 0.048 g, (b) 0.072 g, (c) 0.084 g and (d) 0.05 g of block copolymer dissolved in the aqueous phase. The transmissions are normalized and the times are shifted with respect to the highest surfactant concentration.

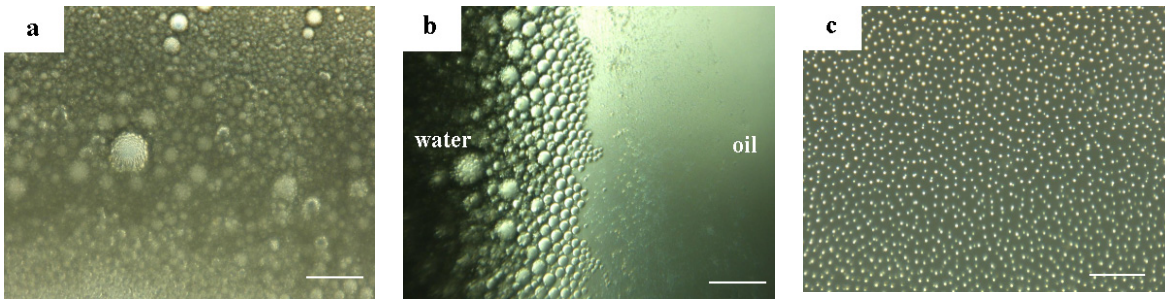

Figure 39 Light microscopy images of the formation of PAA-PS block-copolymeric micelles on both water and oil phase (ethyl benzene). Block copolymers are dissolved in water at high concentration and are brought into contact with the oil phase in a specially designed glass cuvette, as described in [49]. The bars indicate 100 µm. The images are taken 96 h after bringing two liquids into contact, from the water phase (image a), at the interface (b) and from the oil phase (c).

Consequently, the block copolymer micelles are simultaneously presented in both phases, and not only at the interface. There is no sharp interface between two liquids and an exchange of matter takes place as soon as two liquids are brought into contact. Similar observation was observed for different block copolymers (cf. Fig. 40).

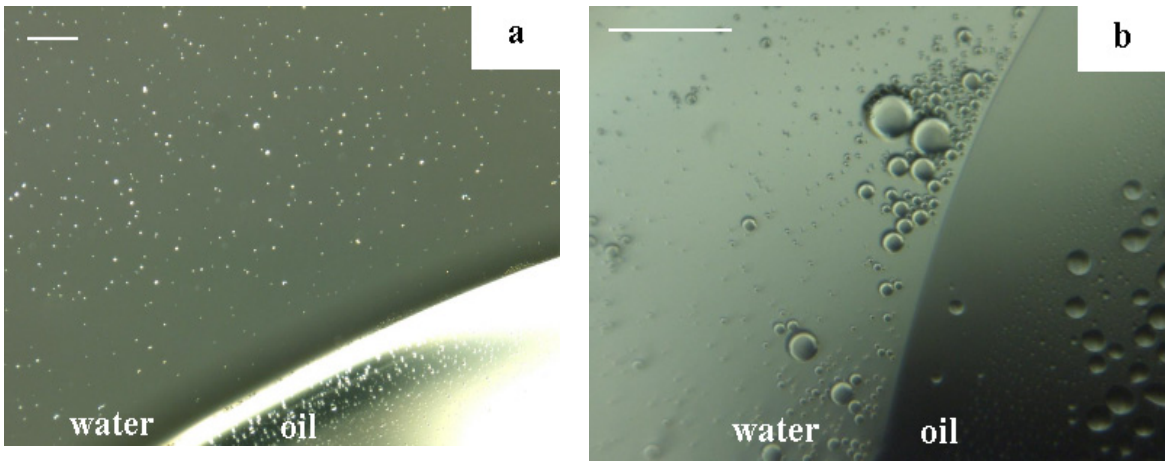

Figure 40 Light microscopy images of the formation and growth of PMMA-PAA block-copolymeric micelles on both water and oil phase (ethyl benzene). Block copolymers are dissolved in water and are brought into contact with the oil phase in a specially designed glass cuvette, as described in [49]. The bars indicate 10 µm. The images are taken from the oil-water interface (a) 24 h and (b) 240 h after bringing two liquids into contact.

If micelles are the loci of particle formation, one might expect that the critical micelle concentration (CMC) is a special point in the nucleation process. For further investigations regarding the nucleation in the presence of emulsifiers SDS was selected. This classical low molecular weight surfactant allows to use KPS as initiator and its concentration can be varied below and above the CMC in wide ranges. As it was shown in the previous section, two possibilities exist to start the reaction: either by the addition of the initiator to a monomer in water emulsion or by the addition of the monomer to an initiator solution. In the presence of surfactant micelles both situations might lead to different results as swollen micelles in which primary initiator free radicals could enter correspond to the micellar nucleation theory scenario. In the case of empty micelles, initiator free radicals and micelles compete for the monomer molecules. Again, if the micelles are the loci of the nucleation, no bend towards smaller slopes should be observed in the conductivity – time curves. The experimental results presented in Fig. 41 show for both situations after the pre-nucleation period a bend in the conductivity – time curves.

Despite the occurrence of the bend under both conditions, the conductivity curves are substantially influenced by the presence of SDS in the reaction system. In general, the decomposition of KPS is strongly influenced by the presence of foreign matter as it is a strong oxidizing agent. [48] Also surfactants such as SDS and polymer particles such as polystyrene can affect the decomposition rate. [71, 72] The consequences for the conductivity measurements are enormous as even in the absence of styrene

monomer, the decomposition of KPS in the presence of SDS is accompanied by apparently disordered changes. The conductivity curves exhibit a tendency to oscillations before again a constant slope is observed (cf. Fig. 42).

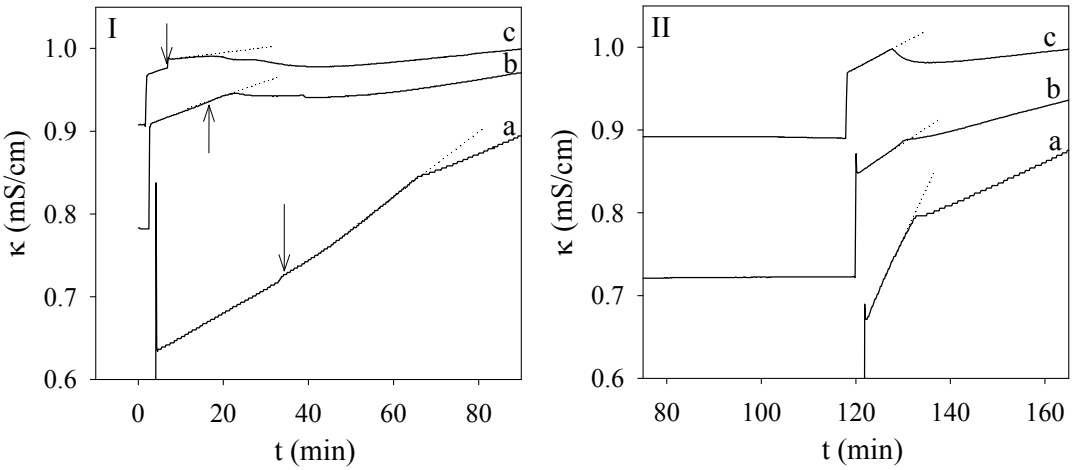

Figure 41 Conductivity – time curves for emulsion polymerizations of styrene in the presence of various amounts of SDS, curve a: 0.11 mM, b: 9 mM, c: 15 mM. Plot I corresponds to the polymerization with t_{equ} = 0, plot II corresponds to the polymerization with t_{equ} = 120 min. Dotted lines are for better visualization of the conductivity bends, arrows in plot I indicate the addition of monomer. The CMC of SDS under the experimental condition is about 8 mM. This value was determined at 70 °C by both surface tension and conductivity measurements whereby the influence of the styrene monomer was mimicked by toluene. [73]

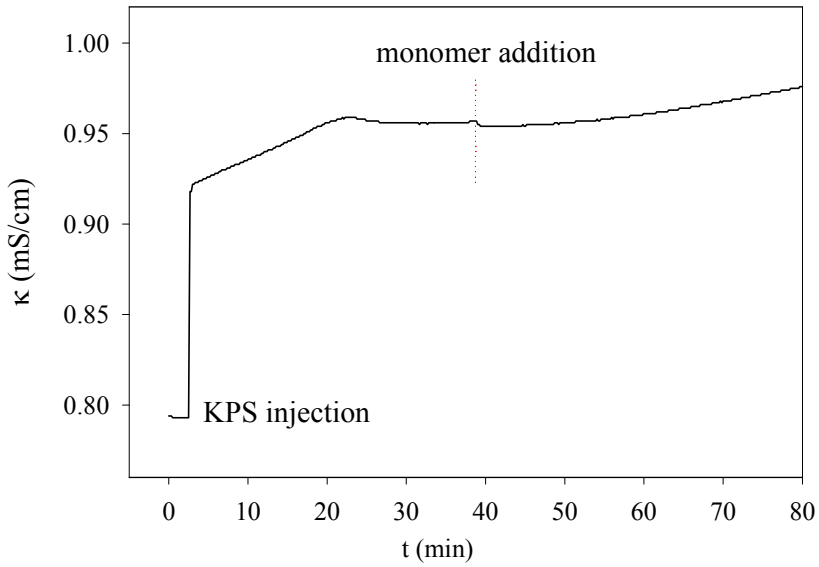

Figure 42 Conductivity – time curve during the decomposition of KPS in water in the presence of SDS micelles. The conductivity curve exhibits a bend, and then a plateau before addition of styrene. SDS concentration 15 mM, dotted line indicates the addition of monomer. The CMC of SDS under the experimental condition is about 8 mM.

A similar behavior is also found in the presence of monomer as depicted by the data in Fig. 41-II. For SDS concentrations higher than two times the CMC the conductivity drops after the pre-nucleation period quite sharply before it returns to a linear increase with lower slope. A possible explanation for such a behavior might be the re-orientation of the micelles and the structural changes due to the pH variations upon KPS injection, or occurrence of oxidation side reactions.

Despite these peculiarities, an evaluation of two slopes (before and after nucleation) is possible. Note, for the polymerization without monomer equilibration the first slope corresponds to the KPS decomposition in the absence of monomer (cf. Fig. 43).

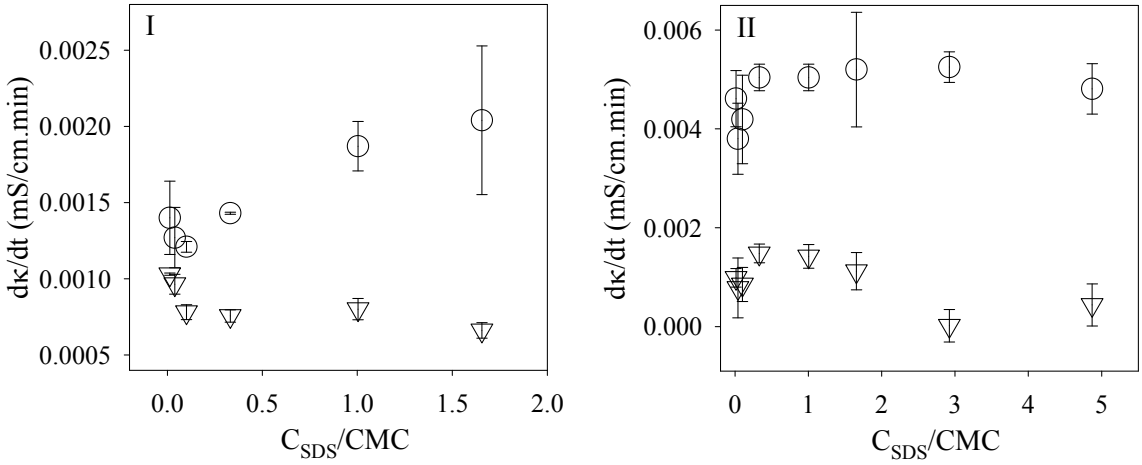

Figure 43 Dependence of the slopes of the conductivity curves on the SDS concentration during styrene emulsion polymerizations initiated with KPS; plot I corresponds to the polymerization starting by the addition of the monomer to the initiator solution (t_{equ} = 0), plot II corresponds to the polymerization starting by the addition of the initiator to the monomer in water emulsion (t_{equ} = 120 min). The triangles describe the conductivity slopes after particle nucleation, the circles of graph I describe the KPS decomposition in the presence of SDS, and in plot II, circles correspond to the slope of the pre-nucleation period. The CMC of SDS under the experimental condition is about 8 mM.

For the polymerization with t_{equ} = 120 min, the slopes before and after the bend are almost independent of the SDS concentration (Fig. 43II). Moreover, the slopes before the conductivity bends are about a factor of five higher than those after the bends. This is an interesting result as it proves that reactions inside micelles are only of minor importance during the initial period of emulsion polymerizations, and almost all particles are nucleated in accordance of the aggregative nucleation theory. For the polymerization with t_{equ} = 0, the slopes of the conductivity curves behave differently. The data before the polymerization show that the KPS decomposition is enhanced by

the presence of SDS micelles. After particle nucleation, the slope is smaller and the difference is the larger the higher the SDS concentration. This might be due to the much larger particle interface that can be stabilized with higher SDS concentrations.

The data obtained in the presence of SDS allow an experimental verification of the influence of surfactants on the duration of the pre-nucleation period (t_N) as they lower the interfacial tension between the nucleating particles and the continuous phase. In the presence of surfactants, the energy barrier for particle formation is decreased, i.e., the rate of nucleation should increase according to the classical nucleation theory. [18, 19] Thus, the time needed for the nucleation, t_N, should decrease. However, t_N is mainly determined by the polymerization kinetics in the aqueous phase. Consequently, one might expect only a minor influence of surfactant concentration on t_N for swollen micelles.

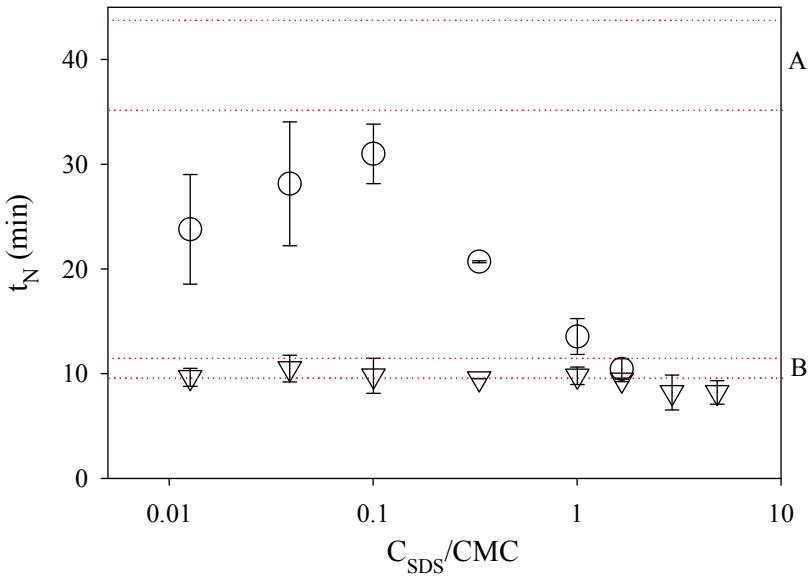

Figure 44 Dependence of the duration of pre-nucleation period (t_N) on the SDS concentration during styrene emulsion polymerizations initiated with KPS. Circles corresponds to the polymerization starting by the addition of the monomer to the initiator solution (t_{equ} = 0), triangles corresponds to the polymerization starting by the addition of the initiator to the monomer in water emulsion (t_{equ} = 120 min). Dotted lines mark the regions of t_N = 39 ± 4 min and t_N = 10.5 ± 1 min for surfactant-free polymerizations with zero (A) and 2 h (B) monomer equilibration time, respectively. The CMC of SDS under the experimental condition is about 8 mM.

Indeed, the experimental data put together in Fig. 44 reveal only a week influence of the SDS concentration on t_N for the polymerization with t_{equ} = 120 min. The difference between the nucleation time of surfactant-free polymerization (C_{SDS} = 0, t_N = 10.5 ± 1 min) and that of the highest SDS concentration (C_{SDS} = 5CMC, t_N = 8.2 ±

1 min) is marginal. This is not a really significant difference considering the inherent scatter of any nucleation experiment. For the polymerization with t_{equ} = 0, the duration of the pre-nucleation period at SDS concentrations below the CMC exhibits a strange behavior: t_N displays a maximum in dependence on the concentration. At higher concentrations, t_N decreases continuously until it reaches a constant value similar to that observed for monomer swollen micelles. The variation of the pre-nucleation period with surfactant concentration is much more significant in the polymerization with t_{equ} = 0. The nucleation time of surfactant-free polymerization (C_{SDS} = 0, t_N = 39 ± 4 min) and that of the highest SDS concentration (C_{SDS} = 2CMC, t_N = 10.5 ± 0.1 min) differs by almost a factor of four.

The data of Fig. 44 for emulsion polymerization in the presence of SDS covering a huge concentration range below and above the CMC give no hints that micelles are somehow involved in the particle nucleation process. Once more, these data reveal that the CMC is no extraordinary point and exhibits no special meaning for particle nucleation. Contrary, interesting features are observed at SDS concentration far below the CMC, where t_N displays a maximum. This behavior is more significant under monomer starved conditions (no equilibration time).

Explanation of this behavior is neither straightforward nor possible within the frame of ordinarily discussed emulsion polymerization mechanisms. [3] Obviously the presence of low amount of surfactants affects the rate of aqueous phase polymerization. One reason might be the influence of the foreign material on the acceleration of KPS decomposition reaction. [71, 72] However, an enhanced decomposition rate of KPS can not explain the occurrence of the maximum. The only remained explanation is the influence of surfactants on the monomer solubilization and consequently the available monomer concentration in water. The presence of hydrophobic surfactants can enhance the driving force for the monomer to enter the aqueous phase. This might be the reason for the initial drop of the nucleation time comparing the surfactant-free polymerization and the polymerization in the presence of surfactants. On the other hand, SDS micelles can act as absorbents capturing radicals and monomers, and thus, they can cause also a reduction in the rate of polymerization. However, below the CMC surfactant molecules are usually considered to be molecularly dissolved and consequently, the assumption of acting as absorbent is not very realistic. The situation is complicated and unraveling requires

more investigations especially regarding the state of the monomer and surfactant molecules in water.

Although the presence of surfactants does not vary the nucleation mechanism, it has an enormous influence on the growth rate and the particle size. This influence is evidenced by the transmission curves of Fig. 45.

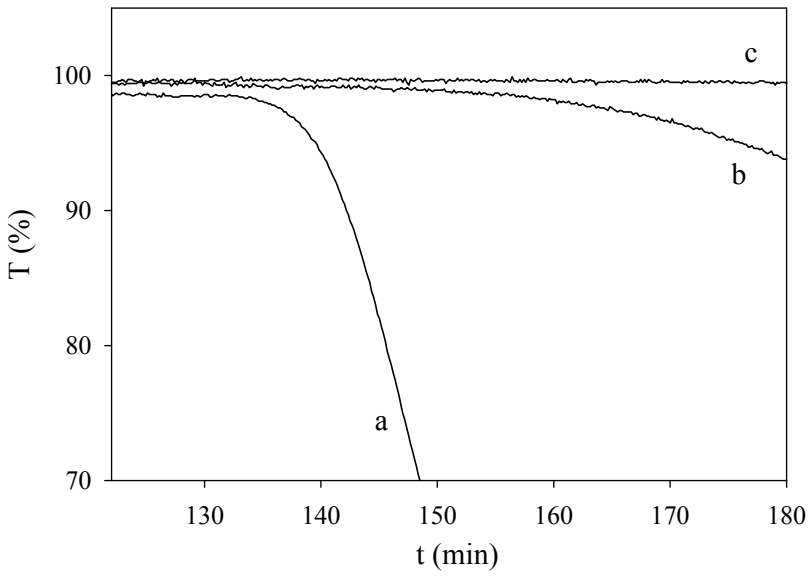

Figure 45 Transmission – time curves for emulsion polymerizations of styrene in the presence of various amounts of SDS, t_{equ} = 120 min, curve a: 0.11 mM, b: 9 mM, c: 15 mM. The CMC of SDS under the experimental condition is about 8 mM.

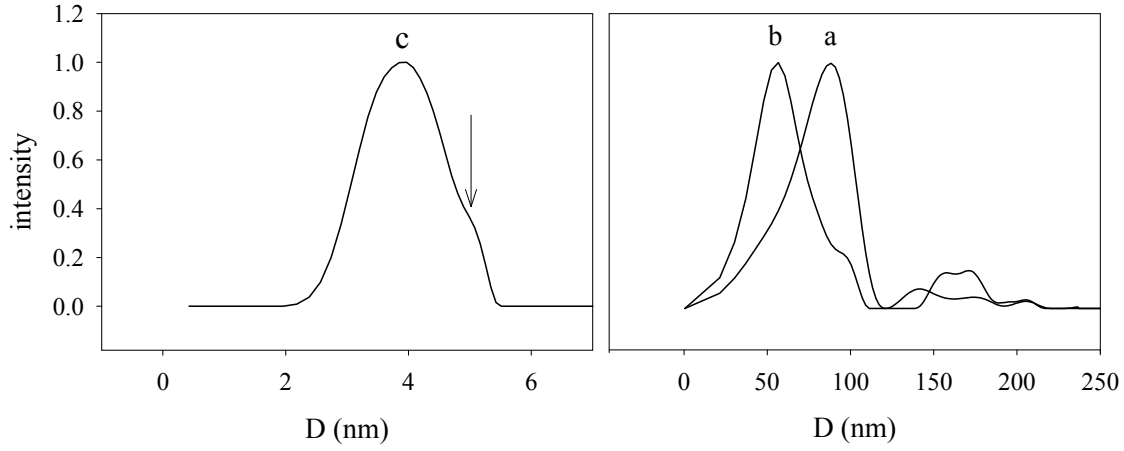

Figure 46 Analytical ultracentrifugation data of the particle size distributions of the final latexes for emulsion polymerizations of styrene in the presence of various amounts of SDS corresponding to the latexes of Fig. 41. Curve a: 0.11 mM, b: 9 mM, c: 15 mM. The CMC of SDS under these condition is about 8 mM; the arrow indicates a shoulder in the size distribution of latex c.

The significant influence of the SDS concentration on the particle size is illustrated by the particles size distributions shown in the graph of Fig. 46.

The data confirm that with increasing the SDS concentration the particle size decreases continuously. For SDS concentrations about twice the CMC the average particle size is below 10 nm and the turbidity did not decrease during the duration of the experiment (cf. Fig. 45, curve c). The arrow in graph c. Fig. 46 indicates the shoulder representing the latex particles. Obviously, the polystyrene particles coexist with a huge number SDS micelles, which are present with the highest concentration in the sample.

Additionally, micellar nucleation theory requires, compared with polymerization at surfactant concentration below the CMC, a higher molecular weight in the low mass region of the molecular weight distribution, as the swollen micelles are spots with higher monomer concentration in the aqueous phase. The polymer of the low molecular weight region originates from the reaction in the continuous phase before the onset of nucleation, whereas the polymer of the high molecular weight region comes from the post-nucleation growth of the polymer chains inside the monomer swollen particles. However, the molecular weight data put together in table 7 shows that there is almost no influence of the SDS concentration in the low molecular weight region.

Table 7 Average molecular weights of the high and low molecular mass regions of polystyrene particles obtained in the presence of various amounts of SDS surfactant.

C_{SDS} (mM)	M_n / M_w (g/mol) (low molecular weight range)	M_n / M_w (g/mol) (high molecular weight range)
0.11	360 / 480	$7.7 \cdot 10^4$ / $1.2 \cdot 10^5$
2.9	280 / 600	$1.0 \cdot 10^4$ / $2.4 \cdot 10^4$
15	360 / 700	None

Thus, also the molecular weight data eliminate the possibility that micelles being the locus of particle nucleation. On the other hand, the average molecular weights in the high mass portion of the molecular weight distribution strongly depend on the surfactant concentration. This is an expected behavior as the particles are the smaller

the higher the SDS concentration and smaller particles imbibe less monomer than larger particles. [74]

It is worth mentioning that the results of numerical simulations based on the Brownian dynamics [52, 75-77] reveal that at a surfactant concentration just above the CMC, the number of micelles is high enough in order that the capture rate of a radical from the water phase equals the propagation rate in water. In other words, the micelles can kinetically compete with the styrene molecules for the radical capture. That micellar nucleation is experimentally not observed might have several reasons. Either, the radical grows out of the micelle into the water phase as Harkins already suspected [78-81]. Another possibility is that the micelle is destroyed by the inside growing radical (either by the heat of propagation or due to the incompatibility between the surfactant and the polymer chain) and the only millisecond lifetime of a low molecular weight surfactant micelle [82] is effectively still further reduced. Moreover, there might exist an effective quite high energy barrier counteracting the entry of the radicals. [52]

As a conclusion from the experimental data presented here, surfactant micelles are not the nucleation locus, but they have an enormous influence on the growth mechanism by stabilizing the formed latex particles. As a result of both lower energy barrier of particle formation, and lower flocculation rate in the presence of surfactant molecules, higher number of smaller sized particles is formed.

However, if instead of micelles seed particles are used as absorbing species the conditions might change. Seeded emulsion polymerizations are an important procedure to carry out emulsion polymerizations in industry. [24] One important reason for the application of seeded instead of ab-initio emulsion polymerizations in industrial scale is the possibility to avoid the uncertainties connected with the particle nucleation. Therefore, it is mandatory to check the conductivity method to study particle nucleation for seeded polymerizations. The interesting question is whether it is possible to detect a critical volume fraction of seed particles where the nucleation of new particles is suppressed. Under such conditions no bend in the conductivity time curve should be observed.

The two possibilities to start the polymerization must be studied also in the present of seed particles, as both conditions are of practical importance. Starting the

polymerization by initiator addition after monomer equilibration means that the seed particles are swollen with the monomer and the aqueous phase is saturated. This situation is useful for the production of composite latex particles. Contrary, the other scenario where the polymerization starts with the addition of monomer and the seed particle remain unswollen, allows the formation of core - shell particles.

The conductivity data of Fig. 47 for the seeded polymerization reveal the strong influence of the seed volume fraction. For the lower seed volume fraction, the bend in the conductivity curve clearly proves secondary nucleation. In this case, the seed particles are unable to capture enough nucleable species to keep their concentration below the critical supersaturation (cf. Fig. 47 I). Small changes in the conductivity slopes immediately after monomer addition are due to the formation of less mobile species as free radicals react now with styrene molecules. However, for a seed volume fraction of 2 % the conductivity curve is a straight line without any sign of bending towards lower slope (Fig. 47 II).

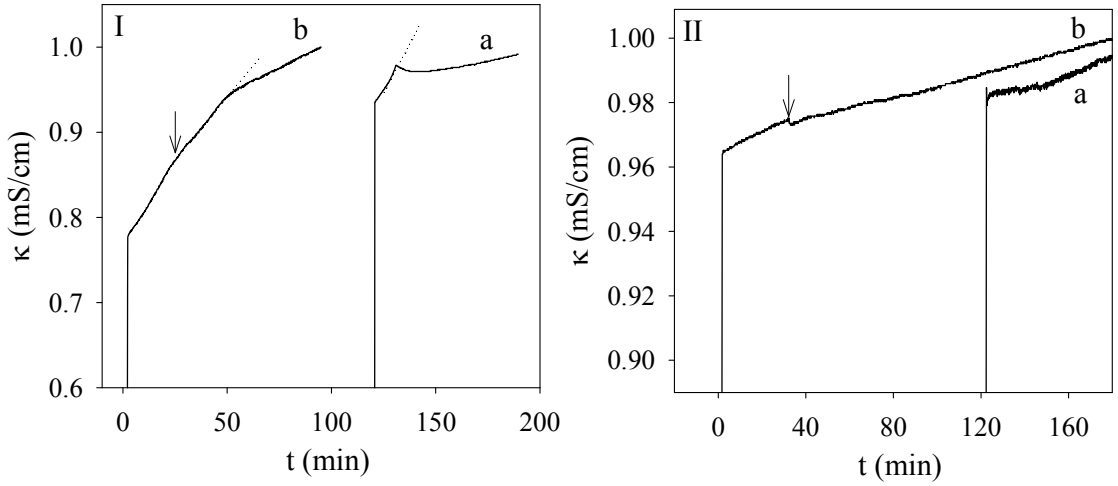

Figure 47 Conductivity – time curves for emulsion polymerizations of styrene in the presence of seed particles at two different volume fractions with 2 h (curve a) and zero (curve b) equilibration time. Plots I and II correspond to the seed volume fraction of 0.2 % and 2 %, respectively. Dotted lines are for better visualization of the conductivity bends, arrows in curves *b* indicate the addition of monomer.

The data of Fig. 47 reveal the existence of a critical seed volume fraction above which the secondary nucleation ceases. To find the critical point a series of seeded emulsion polymerization at different seed volume fractions and without monomer equilibration were carried out. The results presented in Fig. 48 show the behavior of the conductivity slopes. The first slope (circles of Fig. 48) which corresponds to the KPS decomposition in the absence of monomer shows an increasing trend with a discontinuity and sudden drop.

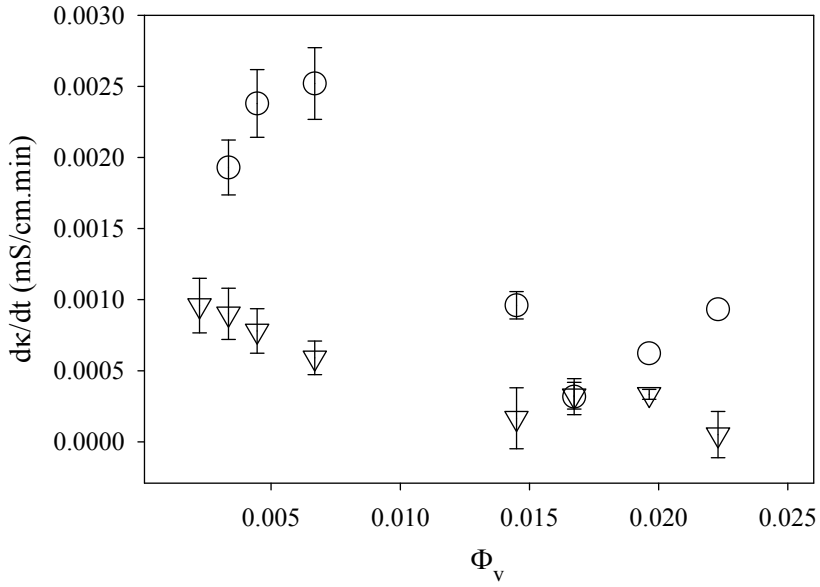

Figure 48 Dependence of the slopes of the conductivity curves on the seed volume fraction during seeded emulsion polymerizations of styrene initiated with KPS. Polymerization is started by the addition of the monomer to the initiator solution. The triangles describe the conductivity slop after particle nucleation, the circles describe the KPS decomposition in the presence of the seed particles.

Despite these peculiarities for the decomposition period, the second slope corresponding to the region after the particle formation (triangles of Fig. 48) is continuously decreasing until reaching to a constant value of zero within the experimental scatters. An evaluation of these behaviors is not straight forward; nevertheless the following conclusion can be drawn:

1. The maximum of the conductivity slopes before monomer addition points to the existence of counteracting influences. Seed particles can act as accelerator for the KPS decomposition reaction leading to higher concentration of smaller and hence more mobile species. Consequently, the value of dκ/dt increases. On the other hand, seed particles can act as absorbents capturing radicals, and thus, increasing their concentration leads to a reduced concentration of mobile species and a decreasing dκ/dt.

2. For the slope after particle nucleation, the water phase reaction between the mobile species and monomer molecules should be considered as well. Increasing the seed volume fraction enhances the driving force for monomer diffusion into water which increases the probability of particle nucleation. Thus, the overall surface area of the capturing species increases continuously

and, results in a decreasing dκ/dt. At higher volume fractions, the surface area of the absorbing objects reaches a critical value above which all nucleable species are captured, with the consequence that the slope of the consuctivity – time curve does not change.

A conclusion regarding the critical volume fraction grounded on the conductivity slopes is not possible. However, based on the data of Fig. 47-48 one can conclude that for the seed volume fractions of 2% and higher, growth of the seed particles is, under the particular conditions, the dominant mechanism. At lower volume fractions, aqueous phase polymerization leading to nucleation coexists with the seed growth.

In this context, a comparison between seed particles and surfactant micelles seems to be useful. Figure 49 shows the experimental result of the duration of the pre-nucleation period for polymerizations with seed particles and surfactants (previously presented in Fig. 44) in dependence on the volume fraction of the foreign material. For SDS concentrations below the CMC the resulting volume fraction is negative which has the physical meaning that no micelles but different amounts of non-micellar SDS are present.

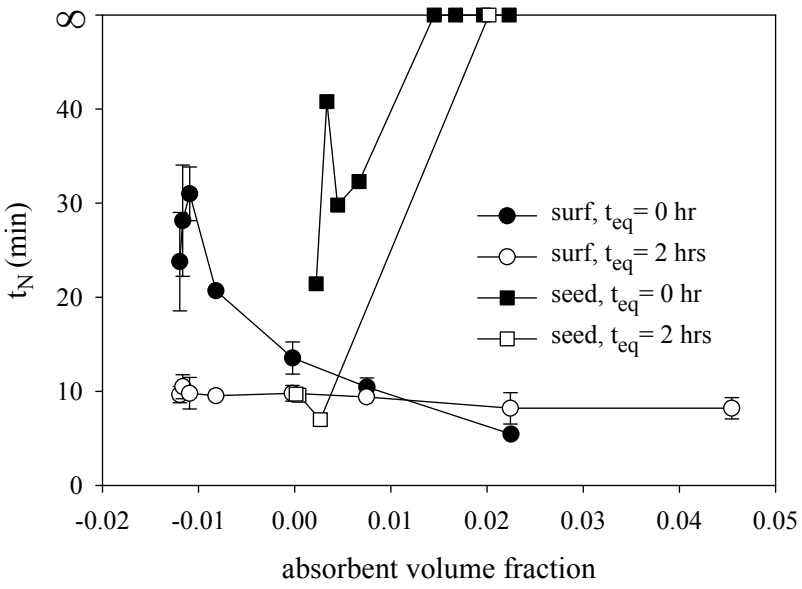

Figure 49 Nucleation time (t_N) in dependence on the volume fraction of absorbent particles: SDS molecules (circles) and seed latex particles (squares); the filled symbols represent data obtained with empty or unswollen particles (polymerizations started with monomer addition) and the open symbols data points for swollen absorbent particles after two hours equilibration time with monomer (polymerizations started with KPS addition).

The variation of the pre-nucleation period in the presence of a low amount of seed particles and a surfactant concentrations below the CMC exhibits qualitatively a

similar behaviour. For the scenario that the reaction is started by the addition of initiator, the duration of the pre-nucleation period is slightly decreasing, but remains basically in the range of absorbent-free condition (t_N = 10.5 ± 1). For the second scenario that the polymerization is started by the addition of styrene t_N displays a maximum in dependence on the volume fraction. Again, a decrease in t_N corresponds to a faster nucleation, which in both scenarios can be explained by an enhanced diffusion rate of the monomer. Whereas, an initial increase in t_N for the second scenario might be explained by the increased amount of immobilized monomer inside the absorbing particles.

However, the condition is different at higher volume fractions of the seed particles, where particles nucleation ceases and no conductivity bend is observed. In this situation, the duration of the pre-nucleation period might be referred to zero or infinite. An infinite value of t_N seems to be more rationalized, as is in agreement with other experimental data, [32] where the nucleation time can be infinitely long, but can not be smaller than a limiting value.

All the results presented in this section reveal the applicability of conductivity measurements to investigate particle nucleation during the initial state of emulsion polymerizations at different conditions. This technique allows clearly to detect the onset of particle nucleation and to find experimental conditions where it is suppressed. The present experimental data rule out the micellar nucleation mechanism as no hints have been found that even at SDS concentration five times higher than the CMC the micelles are the locus of particle nucleation. The probable roles of emulsifier in modifying particle formation process are (a) to reduce the activation energy of particle formation by lowering the interfacial energy and (b) to participate in the stability of incipient nuclei.

3.4 More special cases

3.4.1 Inisurfs

A major drawback of the emulsion polymerization process consists in the need of surface active agents in order to avoid coagulation of the polymer particles at higher solids content. In general, surfactants remain in the final product and affect its

properties as they are mobile and gather into hydrophilic spots. A strategy to avoid the negative influences is to use reactive surfactants, which become covalently bound to the polymer during emulsion polymerization. A reactive surfactant is an amphiphilic molecule with an additional functionality that provides chemical reactivity. An important class of reactive surfactants comprises substances that act in radical polymerizations as initiator (inisurfs). The inisurfs have the special feature of acting as both surface active and initiator agent while incorporating into the polymer chains. [54, 83] Because of these unique properties, it seems worthful to study particle nucleation in the presence of inisurfs. Figure 50 shows the conductivity data for the polymerizations initiated with two homologues of 2,2′-azobis (N-2′-methylpropanoyl-2-amino-alkyl-1)-sulfonates (AAS inisurfs, cf. Scheme in Fig. 50) synthesized by [84, 85].

Similar to the previous cases, nucleation occurs via aggregation of still water-soluble oligomers reflected as the bends towards the lower slopes in the conductivity curves. The difference between the two inisurfs is small. Nevertheless, increase in the number of methyl groups associated with the molecules from 10 to 16 leads to a slight increase in the duration of pre-nucleation period ($t_{N,\ DAS}$ = 13 ± 1 min, $t_{N,\ HDAS}$ = 18 ± 2 min).

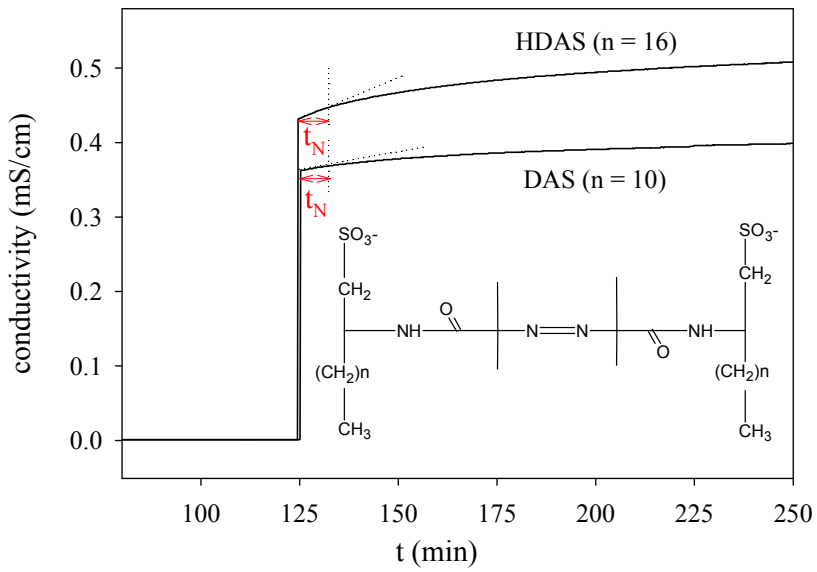

Figure 50 On-line monitoring of conductivity during ab-initio styrene emulsion polymerization initiated with inisurfs (HDAS and DAS) at concentrations above their CMC. The dotted lines are for better visualization of the conductivity bend and the pre-nucleation period.

The results seem contradictory with the expected behavior as the solubility decreases and the surface activity increases with increasing alkyl chain length. However, it has been shown that inisurfs exhibit a very low initiation efficiency as the recombination rate of primary radicals is high. [86] This means that the concentration of nucleating radicals in the case of HDAS (the inisurf with the longer alkyl chain) is lower than that of DAS, thus the nucleation time is longer.

Nonetheless, the main message is the compatibility of the results with those obtained with other types of conventional surfactants.

3.4.2 Other monomers

An intrinsic feature of heterophase polymerization is the tendency of the components to distribute among all phases from the first moment of mixing. Therefore, the available concentration of the reactants at the polymerization loci depends on their partitioning ratio between the phases. For example, it is expected that the solubility of monomer in water influences the critical chain length, concentration, and supersaturation of the oligomeric chains before nucleation and finally, the rate of particle formation. Hence, as the last part of this thesis it is mandatory to expand the experimental results to other monomers of different water solubilities.

Monomers with a lower water solubility than styrene are challenging due to the low concentration of monomeric residues present in the aqueous phase. Monomer drops or aggregates (formed via spontaneous emulsification) might compete effectively for the initiator free radicals. Moreover, for the ester monomers hydrolysis is an issue as the contributions regarding solubility, supersaturation and nucleation are influenced. The data put together in figures 51-52 summarize the conductivity behavior for monomers within a range of an extremely hydrophobic, low water-soluble 4-*tert*-butylstyrene ($C_W \sim 10^{-2}$ mM, estimated according to [58]) and lauryl methacrylate ($C_W \sim 10^{-4}$ mM, estimated according to [58]) to the hydrophilic, highly water-soluble methyl methacrylate ($C_W \sim 150$ mM, according to [87], all the values are reported at 25 °C).

The results obtained for the methacrylate monomers (cf. Fig. 51) show qualitative and quantitative differences in dependence on the hydrophobicity of the ester.

Compared with styrene the following points are worth to mention.

1. The conductivity starts to increase from the first moment of monomer addition (cf. Fig 51, hydrolysis plot) which is in agreement with the previous studies, reporting the hydrolysis of the ester groups. [34] Obviously, at these conditions, the methacrylate monomers are prone to the hydrolysis, resulting in a continuous increase in the conductivity. Apparently, the rate of hydrolysis increases as the hydrocarbon chain length decreases (MMA > BuMA >LMA). In any case, the hydrolysis of the monomers and formation of acid functionality have distinct influences on the nucleation behavior, as the solubility and the interfacial tension of the nucleating species are changed compared to the neat system.

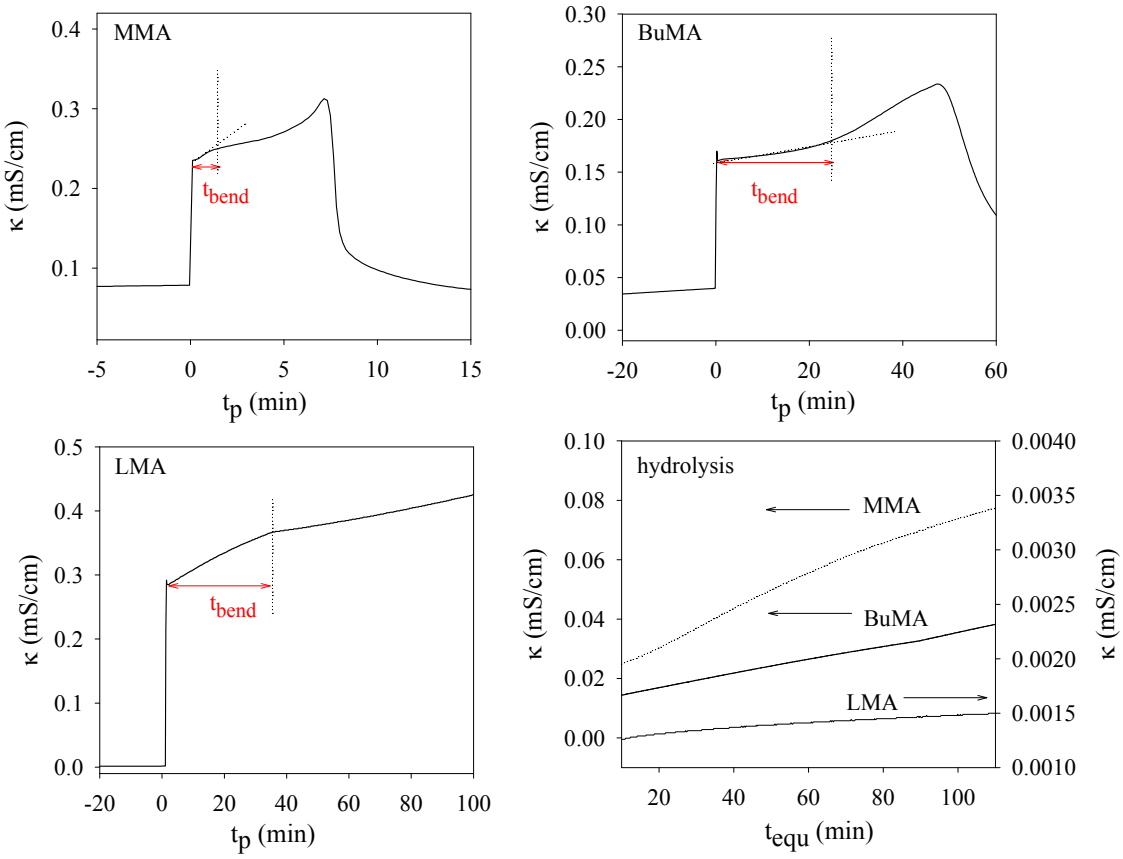

Figure 51 On-line monitoring of conductivity during surfactant-free ab-initio emulsion polymerization of methyl methacrylate, butyl methacrylate and lauryl methacrylate, as well as the increase in the conductivity during the equilibration time of these monomer with water as a result of the ester hydrolysis. The dotted lines are for better visualization of the conductivity bends and the pre-nucleation periods. Time zero is the start of the polymerization for the curves showing the polymerization of MMA, BuMA and LMA. For the hydrolysis graph, at time zero the monomer is added to water.

2. The measured conductivity is the sum of all involved processes. Consequently, a conclusion regarding the rate of nucleation based only on the solubility values of the monomer is not possible. However, the duration of pre-nucleation period seems to decrease with increasing solubility in water (MMA < BuMA < LMA).

3. After nucleation, the conductivity in the case of MMA is influenced by the fast particle growth (transmission drops within 10 minutes to zero). The PMMA particles absorb any species from the aqueous phase like a sponge. The fast polymerization rate (particle growth) is confirmed with the off-line analysis where within less than eight minutes, stable latexes are formed for methyl methacrylate polymerization (cf. Fig 52). Regarding the morphological development, the MMA polymerization corresponds basically to styrene polymerizations with hydrophilic initiators. The TEM images of the methyl methacrylate polymerization show similar morphological, where the oligoradicals are partially soluble in the monomer droplets and form the dark shell (cf. core-shell morphology of image b, Fig. 52).

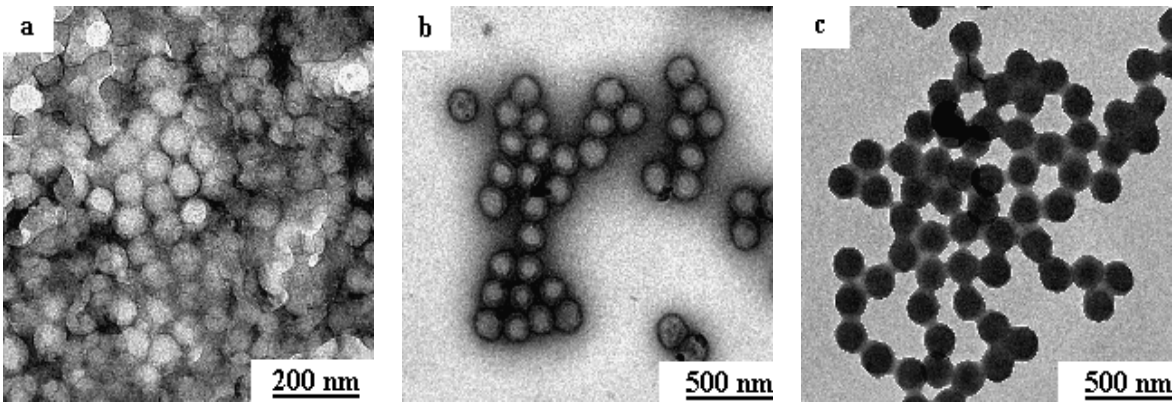

Figure 52 TEM images of the particle morphology during the surfactant-free emulsion polymerizations of methyl methacrylate in the glass reactor, the images are due to 2, 8 and 10 minutes after the initiation.

4. LMA with the lowest solubility in water and the lowest hydrolysis within the series of methacrylates shows the “ideal” behavior comparable with styrene.

5. The data for BuMA and MMA appears at a glance strange, but might be understood in the following way. After KPS addition, the conductivity jumps and rises as expected. However, the slope increases surprisingly. This might

be due to an enhanced hydrolysis by the H^+ formed during KPS decomposition. The drop in the conductivity indicates that particle nucleation and growth took place.

A consistent explanation of the influence of monomer hydrophobicity on the nucleation rate is not straightforward. Note that according to the classical nucleation theory two counteracting parameters are responsible for the rate of nucleation: on the one hand, a reduced solubility leads to a higher supersaturation. On the other hand, a lower water solubility causes a lower concentration of the nucleating species, and also a lower supersaturation. Moreover, a high water solubility of the monomer enhances the overall rate of polymerization, as the available concentration of monomer in water increases. Based on the conductivity data, it might be concluded that the influence of the concentration parameter on the supersaturation is more dominant: the higher the water-solubility of the monomer, the higher the monomer concentration and polymerization rate, the faster reaching of the critical supersaturation, and the shorter the pre-nucleation period.

In the case of tert-butyl styrene, the situation is more complicated. The conductivity curve reveals a unique behavior without any bend towards lower slopes (cf. Fig. 53).

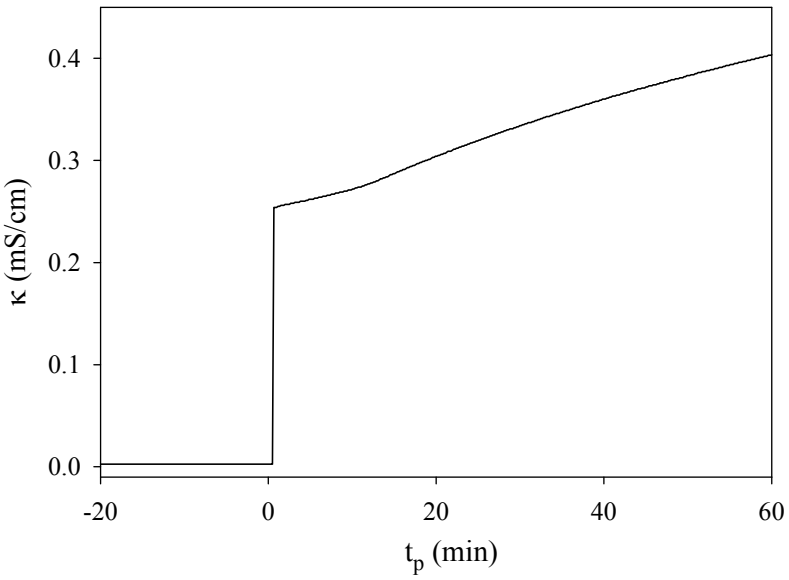

Figure 53 On-line monitoring of conductivity during surfactant-free ab-initio emulsion polymerization of t-butyl styrene according to the "standard" polymerization recipe, time zero is the start of the polymerization.

Instead, after ca. 10 minutes of constancy the slope is gradually decreasing with time. This behavior might be explained with a gradual particle formation. The continuously formed particles absorb continuously conducting species. It might be expected that at this range of solubility, oligomers with $\boldsymbol{j} = 1$ reach the critical supersaturation and nucleate new particle. Moreover it is found that the shape of conductivity – time curve is significantly influenced by the initiator concentration (cf. Fig. 54).

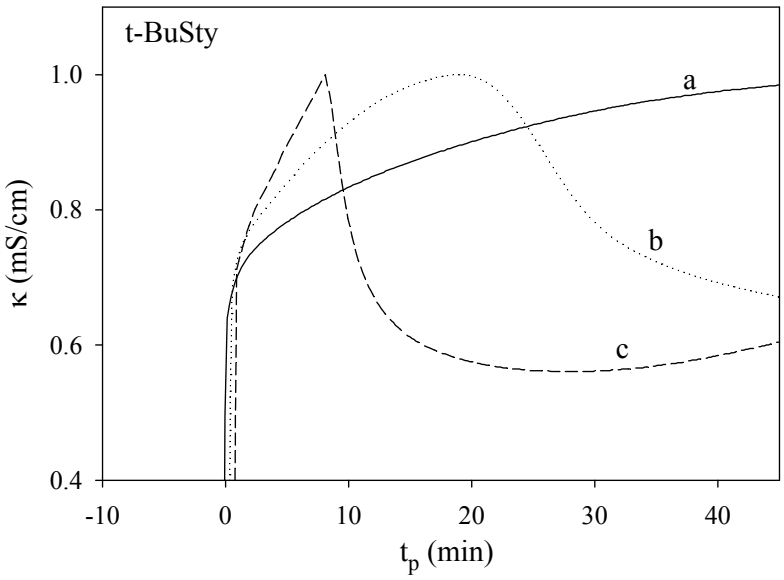

Figure 54 Normalized conductivity – time curves during surfactant-free ab-initio emulsion polymerization of t-butyl styrene with 1/2 (curve a), 2 (curve b) and five times (curve c) the standard initiator concentrations.

The TEM images of Fig. 55 show formation and growth of the tert-butyl styrene polymer particles. The particle morphology resembles that observed for the styrene polymerization with high concentration of KPS. Small dark spots with high electron density are templating low electron density spheres (cf. image a, Fig. 55). These hollow spheres are later on transformed into a core-shell morphology (cf. image b, Fig. 55). The shell is growing by time, so that after 50 minutes solid particles are to be seen. The transformation is the faster the lower the initiator concentration (cf. TEM images of Fig. 56). For the lowest initiator concentration solid particles are observed already 10 minutes after the initiation (cf. image a, Fig. 56). Whereas, at medium or high initiator concentration, a core-shell morphology or a combination of core-shell morphology and the hollow spheres is observed (cf. images b and c, Fig. 56).

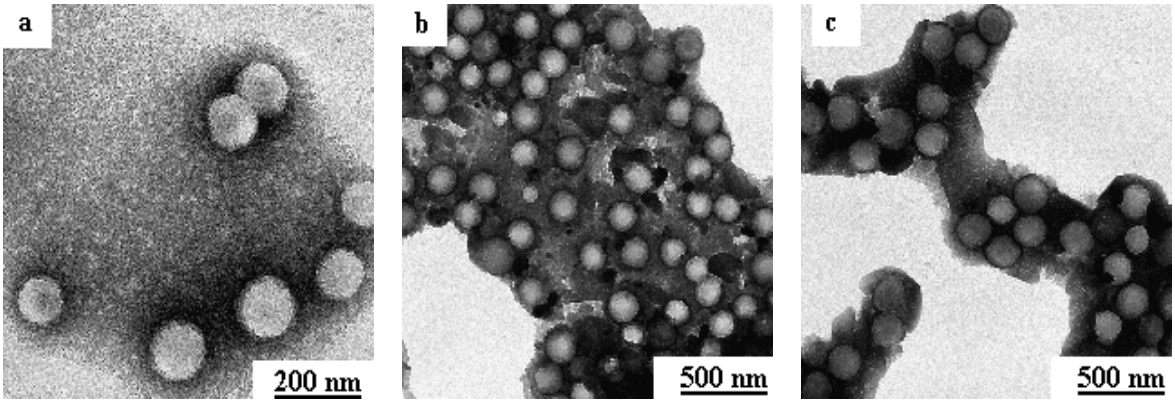

Figure 55 TEM images of the particle morphology during the surfactant-free emulsion polymerizations t-butyl styrene in the glass reactor according to the "standard" polymerization recipe, the images are due 15, 30 and 45 minuets after the initiation..

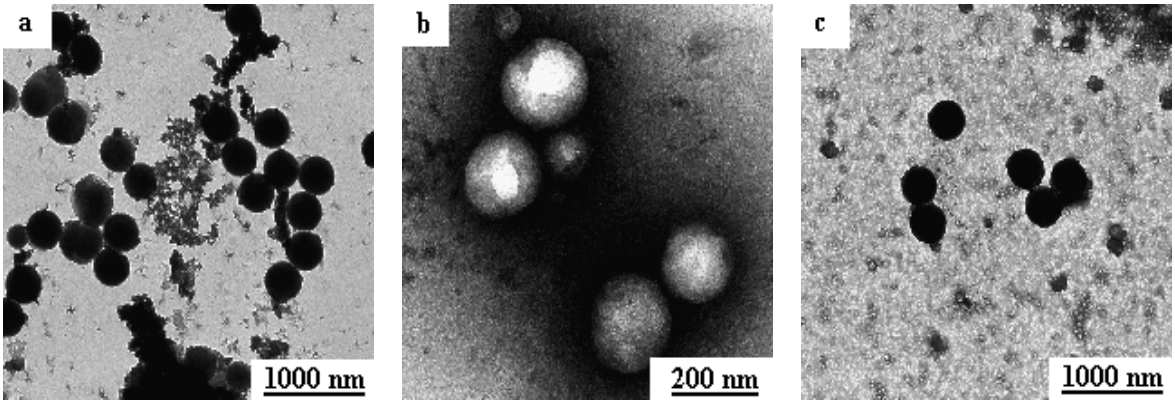

Figure 56 TEM images of the particle morphology during the surfactant-free emulsion polymerizations of t-butyl styrene with half (a), two (b) and five times (c) the standard initiator concentrations (corresponding to the curves of figure 47), 10 minutes (a), 30 minutes (b), and 90 minutes (c) after the initiation.

Molecular weight measurements reveal an interesting effect that is a decrease of the molecular weight with increasing polymerization time (cf. data of Fig. 57). Moreover, the molecular weight distribution is multimodal with peaks in the high and low molecular weight regions. With increasing polymerization time the peak in the high molecular weight region shifts towards lower molecular weights. Contrary, the peak in the low molecular weight region shifts to high molecular weights.

Appearance of two regions in the molecular weight distribution clearly reveals that the polymerization is going on at two different reaction sites: the water phase, and inside the monomer droplets. Indeed, the obtained morphology for the particles can only be explained by the bulk polymerization of the monomer droplets. The tendency of tert-butyl styrene in order to start spontaneous emulsification at much higher rates compared with styrene is already proved. [49] Apparently, highly hydrophobic monomer droplets absorb the water-phase initiated oligoradicals having limited water

solubility. The water-solubility of these oligoradicals decreases with decreasing the initiator concentration (due to the longer polymer chains formed), consequently their affinity to enter the monomer droplets and start a bulk polymerization increases (cf. image a, Fig. 56, dark particles only 10 minutes after the initiation). Hence, at higher initiator concentration, these solid spheres are coexisted with the water-phase nucleated oligomeric particles templating the monomer droplets. Consequently, at higher conversions core-shell morphologies are observed, too.

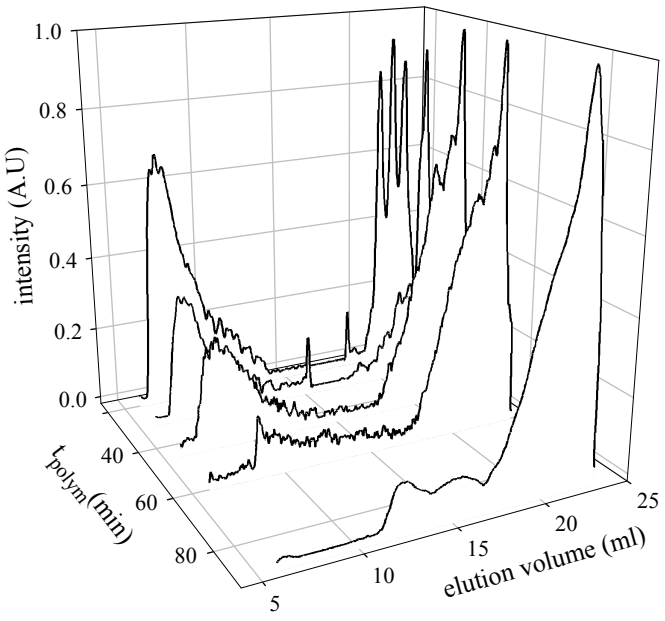

Figure 57 Molecular weight distributions of the polymer obtained during surfactant-free emulsion polymerizations of t-butyl styrene according to the "standard" polymerization recipe, at different conversions (polymerization times).

Within this frame, the conductivity data of figures 53-54 can be explained by the simultaneous water phase nucleation of extremely low water-soluble oligoradicals and the polymerization inside the monomer droplets, the so-called droplet nucleation. The former nucleation event leads to the low molecular weight region, whereas droplet nucleation is the origin of the high molecular weight products. With increasing polymerization time the particles formed via aggregative nucleation imbibe monomer which leads to the observed shift of the peak in the low molecular weight region to higher values. Parallel, the monomer concentration is reduced in the droplets and the peak in high molecular weight region shifts towards lower values.

Moreover, these results show that in order to get a clarification regarding the influence of the monomers hydrophobicity on the nucleation in aqueous heterophase polymerization, derivative of styrene are the monomers of choice as they are chemically stable.

4 Conclusion

Particle formation in emulsion polymerization is a quite complex process. The extremely fast nature of the nucleation event requires firstly, a slowing down the reaction rate and secondly, a combination of various methods to achieve the acquisition of experimental data as prerequisite for a better understanding of the mechanism. Within this study, on-line as well as off-line methods have been applied to obtain a consistent picture of the nucleation stage in emulsion polymerization. During the investigations it turned out that on-line conductivity measurement is a tremendously valuable tool to investigate particle nucleation. This technique allows clearly detecting the onset of particle nucleation and the exact determination of the duration of the pre-nucleation period during which a critical supersaturation of nucelable species is built up. The experimental data acquired support the model of aggregative particle nucleation in emulsion polymerization.

Experimental evidence has been presented for the first time that the non-ionic, oil soluble Azo-initiators like AIBN can be successfully applied to produce stable latex particles in a surfactant-free system. Stabilization of the particles is achieved by the presence of covalently bound ionic or ionizable groups on the particle surface. These charged species are formed by the side reactions of carbon radicals under participation of water. Furthermore, it was shown that the main characteristics of the particle formation process, like for instance the rate of nucleation or the duration of pre-nucleation period, obey the same rules of "standard" surfactant-free polymerization with ionic KPS initiator. The duration of pre-nucleation period can precisely be adjusted with the equilibration time of styrene in water as well as by choosing the injection phase of AIBN either to the monomer reservoir or into the aqueous phase. Moreover, the off-line characterizations reveal that these parameters affect substantially the particle morphology, too. Based on the obtained results, the key parameter is the "available" amount of monomer in water in the form of monomer droplets of various sizes ranging from a few nanometer up to several micrometer. These droplets which form by spontaneous emulsification of monomer in water phase, as soon as both phases are brought into contact, control the kinetically available monomer concentration, and hence, have a strong influence on the

nucleation of particles as well as their final morphology. Important reaction parameters such as the equilibration time of monomer in water, the hydrodynamics of the reactor, the hydrophobicity of the monomer, and the presence of foreign materials (surfactant molecules, micelles, seed particles, etc.) vary considerably the rate and the extent of the emulsification.

Based on clear experimental evidence, the particle nucleation during emulsion polymerization is a complex process, which is illustrated by the following scheme (cf. Fig. 58). Depending on whether the polymerization is started by initiator or monomer addition two pathways (case *A* and case *B*, respectively) are possible.

In case *A* where the polymerization is started by initiator addition and the aqueous phase is saturated with monomer (single molecules, aggregates, and droplets of various size), the *Heterogeneous* aggregative nucleation is facilitated by the monomer droplets-water interface. In case *B* where the polymerization is started by monomer addition, the extent of heterogeneous nucleation depends on rate of spontaneous emulsification, but is mainly homogeneous in nature.

In both cases, the formation of templated monomer drops and core-shell (hollow) particle morphology strongly depends on the initiator concentration and the solubility of the oligomeric particles in the monomer. At higher initiator concentration the oligomeric particles are neither soluble in water nor in the monomer and hence, they stay at the droplet-water interface. With ongoing polymerization and increasing molecular weight, solid particles are formed.

Within the frame of the aggregative nucleation, surfactants assist with the particle formation process in the following way. The presence of emulsifier lowers the activation energy by reducing the interfacial tension between the nucleus and water. Moreover, the surfactants increase the emulsification rate and the concentration of monomer (droplets and molecularly dissolved) in the aqueous phase. In this way, surfactants participate in forming more nuclei in a shorter nucleation period. On the other hand, presence of surfactants prevents or limits agglomeration of small particles and hence, produces higher number of stable particles.

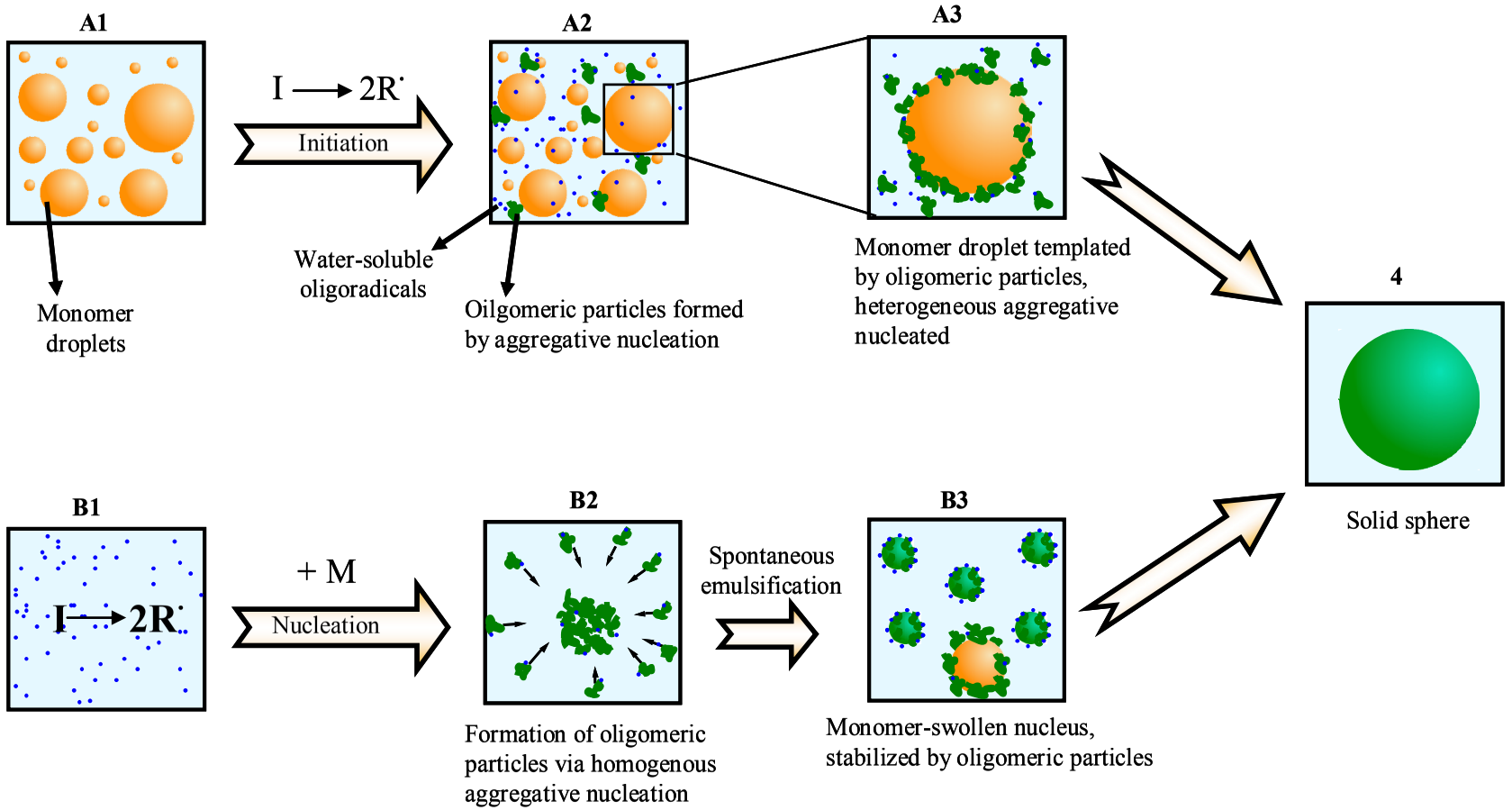

Figure 58 General scheme of surfactant-free emulsion polymerization obtained based on the TEM images for the polymerization started by initiator addition (A), and by the monomer addition (B).

The experimental data presented here rule out the micellar nucleation mechanism as no hints have been found that even at a surfactant concentration five times higher than the CMC the micelles are the loci of particle nucleation. The presence of seed particles on the other hand can suppress the nucleation of new particles above a critical volume fraction. Under this condition, the seed particles act effectively as absorbers for all radical species from the water phase.

The results of this thesis prove the value of conductivity measurements for nucleation investigations. The experimental data can be nicely explained with the aggregative nucleation model, strongly influenced by the presence of monomer drops.

The mechanism proposed above is in good agreement with the experimental results and can qualitatively explain the facts and trends in ab-initio polymerization. However, the position has not yet been achieved where a precise model can be formulated which predicts quantitavely the numbers and sizes of particles formed at any conditions. It is worthful bearing in mind that from practical points of view such a model is of the utmost importance. The development of a quantitative model requires both new experimental techniques and new modeling approaches taking into account the complex interplay between the thermodynamics and the kinetics of the nucleation process.

5 Appendix

5.1 Experimental details

Materials

• De-ionized water was taken from a Seral purification system (PURELAB Plus) with a conductivity of 0.06 µS/cm and degassed prior to use for polymerization.

• Styrene (Sigma Aldrich) was purified by standard procedures to remove stabilizers, distilled under vacuum, and stored in the refrigerator until use. Methyl methacrylate (Sigma Aldrich) and 4-*tert*-Butylstyrene (Lancaster) were distilled under reduced pressure. Methyl methacrylate, Butyl methacrylate, Benzene, Toluene, Cyclohexane, Ethyl benzene (all from Sigma Aldrich) and Lauryl methacrylate (Fluka) were used as received.

• Potassium peroxodisulfate (KPS), from Fluka, 2,2-azobis(2-methylbutyronitrile) (V59) from Wako, 2,2-azobis[2-methyl-N-(2-hydroxyethyl)-propionamide] (V86) from Wako were used as received.

• 2,2-azobisisobutyronitrile (AIBN) from Wako was re-crystallized from methanol before use.

• Sodium dodecylsulfate (SDS) ultrapure from Roth, Cetyltrimethylammoniumbromid (CTAB) from Roth were used as received.

• Reactive surfactant Allyl phenylpolyol ether sulphate with 20 EO, ammonium salt (APG 2019) from Clarient, Ethoxylated nonyl phenyl (IGEPAL CO-880) from Rhone-Poulenc, Octaethylene glycol ether ($C_{12}E_8$) form Fluka, block copolymer Polyacrylic acid - block- Polystyrene (PAA-PS) from Goldschmidt were used as received.

• PEGA200 with an average molecular weight of 568 g/mol had been synthesized as described elsewhere. [88]

• Inisurfs 2,2´-azobis (N-2´-methylpropanoyl-2-amino-alkyl-1)-sulfonates with 10 and 16 methyl groups (DAS and HDAS, respectively) had been synthesized by [84, 85].

• Polystyrene were prepared by batch emulsion polymerization in a 2000 mL all glass reactor, equipped with stirrer, reflux condenser, nitrogen inlet and outlet, heating jacket to control the temperature. The seed latex was produced by polymerizing 24 g of styrene in 2000 g of water containing 8.5 g of a reactive surfactant (APG 2019) and 3.2 g of KPS initiator at 70°C at slow stirrer speed (50 rpm) for 24 hours under N_2 atmosphere. The seed latex was cleaned by ultrafiltration through DIAFLO membranes with a molecular weight cut-off of 10^4 g/mol (type YM 10 from Amicon, Inc., USA) as long as the amount of original water was replaced at least five times. The final seed particles are quite mono disperse with an average diameter of 30.5 nm (measured by analytical ultracentrifuge).

On-line Investigations

All polymerizations to investigate particle nucleation were carried out at 70 °C in a specially constructed 500 mL all-Teflon reactor equipped with a stirrer working at 70 rpm, probes for on-line measurement of the temperature and conductivity, and two optical windows for an on-line monitoring of optical transmission in the aqueous phase, as described previously.

- Conductivity measurement: Radiometer Copenhagen, Conductivity Meter CDM 92, Conductivity Cell C-100-8-T, Beta Sensor, Sweden

- Turbidity measurement: SPEKOL 11, Carl Zeiss Jena, Germany

- Dynamic Light Scattering: FOQELS, Brookhaven Instruments Corporation, USA

Off-line Investigations

The off-line polymerizations were carried out in a four-neck double jacketed reactor equipped with nitrogen inlet, condenser, mechanical stirrer, and heating and cooling thermostat.

- Rotational Thermostat, VLM20 (VLM GmbH, Leopoldshöhe, Germany).

- Freeze drying, LMC-2 (Christ, Germany)

Characterization and Analysis

- Size Exclusion Chromatography (SEC): Thermo separation products.

Injected sample: 100 µl polymer solutions, solvent: tetrahydrofuran, Filter: Teflon-filter, mesh size of 450 nm, detectors: ultra violet (UV) (TSP UV1000) and refractive index (RI) (Shodex RI-71) flow rate: 1 ml/min. Column set: three 300 x 8 mm columns filled with a MZ-SDplus spherical polystyrene gel (average particle size 5 µm) having a pore size of 10^3, 10^5, and 10^6 Å. Standards: polystyrene (500 - $2 \cdot 10^6$ g mol^{-1} from PSS, Mainz, Germany).

- Dynamic Light Scattering (DLS): NICOMP particle sizer (model 370), PSS Santa Barbara, USA

- Transmission Electron Microscopy (TEM): Zeiss EM 912 Omega microscope, operating at 100 kV with sample preparation according to the suspension preparation technique, Carl Zeiss Jena.

- Light Microscopy: Keyence VH-X digital microscope (Keyence Corporation, Osaka, Japan), objectives: VH-Z100 or VH-Z500, x 1000, x 5000

- Nuclear Magnetic Resonance (NMR): Bruker DPX-400 Spectrometer at 400 MHz and 100 MHz ^{13}C-NMR, solvents: $CDCl_3$, D_2O, Deutrated benzene (for AIBN decomposition experiment).

- Elemental analyses (C, H, N, S): Vario EL Elementar (Elementar Analysensysteme, Hanau, Germany).

- Hydrodynamic Chromatography (HDC): Polymer Laboratories (PL-PSDA)

- Analytical ultracentrifuge (AUC): particles size distribution measurements, Beckman Coulter Optima XLI Analytical Ultracentrifuge (Palo Alto, CA), solvent: water, rotation speed: 20000, 60000 rpm, 25 °C, sedimentation coefficient distributions: 8.9 (Sedfit), data evaluation algorithm according to [89].

- Slids content: HR73 Halogen Moisture Analyzer (Mettler Toledo)

- Zeta-potential: standard procedures with the Zetasizer 4 (Malvern)

- Fourier Transform Infrared (FTIR) spectroscopy: FTS 6000 spectrometer (Bio-Rad)

5.2 Additional information

KPS decomposition

For the thermal decomposition of persulfate, Kolthoff and Miller [47] proposed the following mechanism:

$$S_2O_8^{2-} \rightarrow 2SO_4^{-\bullet}$$
$$SO_4^{-\bullet} + H_2O \rightarrow HSO_4^- + OH^\bullet$$
$$S_2O_8^{2-} + OH^\bullet \rightarrow HSO_4^- + SO_4^{-\bullet} + \frac{1}{2}O_2$$
$$OH^\bullet + SO_4^{-\bullet} \rightarrow HSO_4^- + \frac{1}{2}O_2$$
$$S_2O_8^{2-} + H_2O \rightarrow 2HSO_4^- + \frac{1}{2}O_2$$

Equation 35

In the presence of protons, the acid-catalyzed decomposition is changed to the following mechanism:

$$S_2O_8^{2-} + H^+ \rightarrow HS_2O_8^-$$
$$HS_2O_8^- \rightarrow SO_4 + HSO_4^-$$
$$SO_4 + H_2O \rightarrow SO_3 + \frac{1}{2}O_2$$
$$SO_3 + H_2O \rightarrow H_2SO_4 + H^+$$
$$S_2O_8^{2-} + H_2O \xrightarrow{H^+} 2HSO_4^- + \frac{1}{2}O_2$$

Equation 36

Conductivity in the aqueous phase is controlled by the concentration and the mobility of the all ions. Hence, the mechanism of KPS decomposition leads to equation 40 for the changes in the overall conductivity and can be applied for modeling the experimental conductivity behavior during the initial stage of a KPS-initiated emulsion polymerization.

$$\kappa(t) = \Lambda_{K^+}[K^+] + \Lambda_{S_2O_8^{2-}}[S_2O_8^{2-}] + \Lambda_{H^+}[H^+] + \Lambda_{SO_4^{2-}}[SO_4^{2-}] + \Lambda_{HSO_4^-}[HSO_4^-]$$

Equation 37

A comparison of the molar conductivities of different ions involved in equation 40 is shown in Table 6. [37] Accordingly, the protons have the highest molar conductivity and govern the overall conductivity behavior.

Table 8 Molar conductivities of the different charged species involved in the KPS decomposition.

Ion	Λ_m (m^2S/mol) (25 °C) measured	Λ_m (m^2S/mol) (60 °C) calculated
H^+	349.65	507.1

HSO_4^-	50	95.4
K^+	73.48	132.2
SO_4^{2-}	160	290.2
$S_2O_8^{2-}$	172	328.3

Oil-soluble initiators

Letting the AIBN initiated polymerization continues over night, very high molecular weight polymers are produced, both in latex phase and bulk phase. Viscous bulk polymer is formed in the same time in the monomer phase. For the extreme low water soluble V59, the bulk polymerization leads to the formation of glassy polymer in the funnel which hinders further diffusion of monomer to the water phase.

In any case, polymers are formed in both phases, confirmed by NMR analysis (cf. Fig. 59 for V59-initaiated polymerization, and Fig. 60 for AIBN-initiated polymerization).

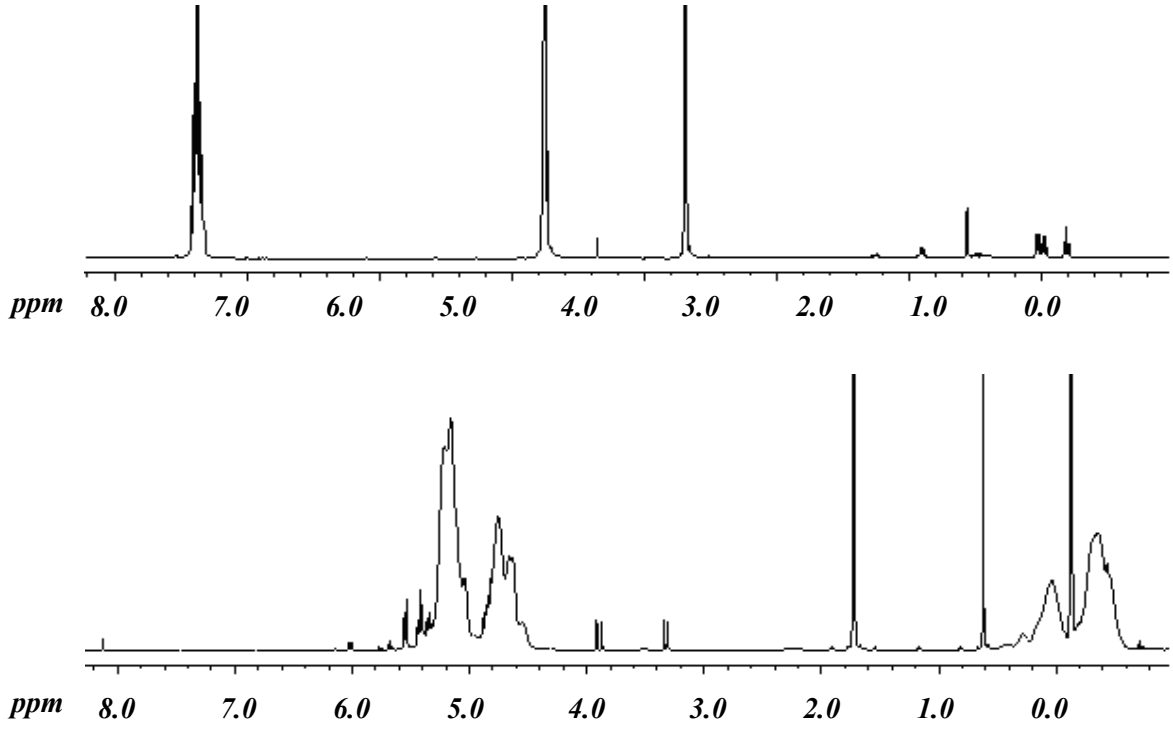

Figure 59 400 MHz ^{1}H-NMR spectra of the polymer obtained in the latex phase (I) and bulk phase (II) by surfactant-free emulsion polymerization of styrene initiated with V59.

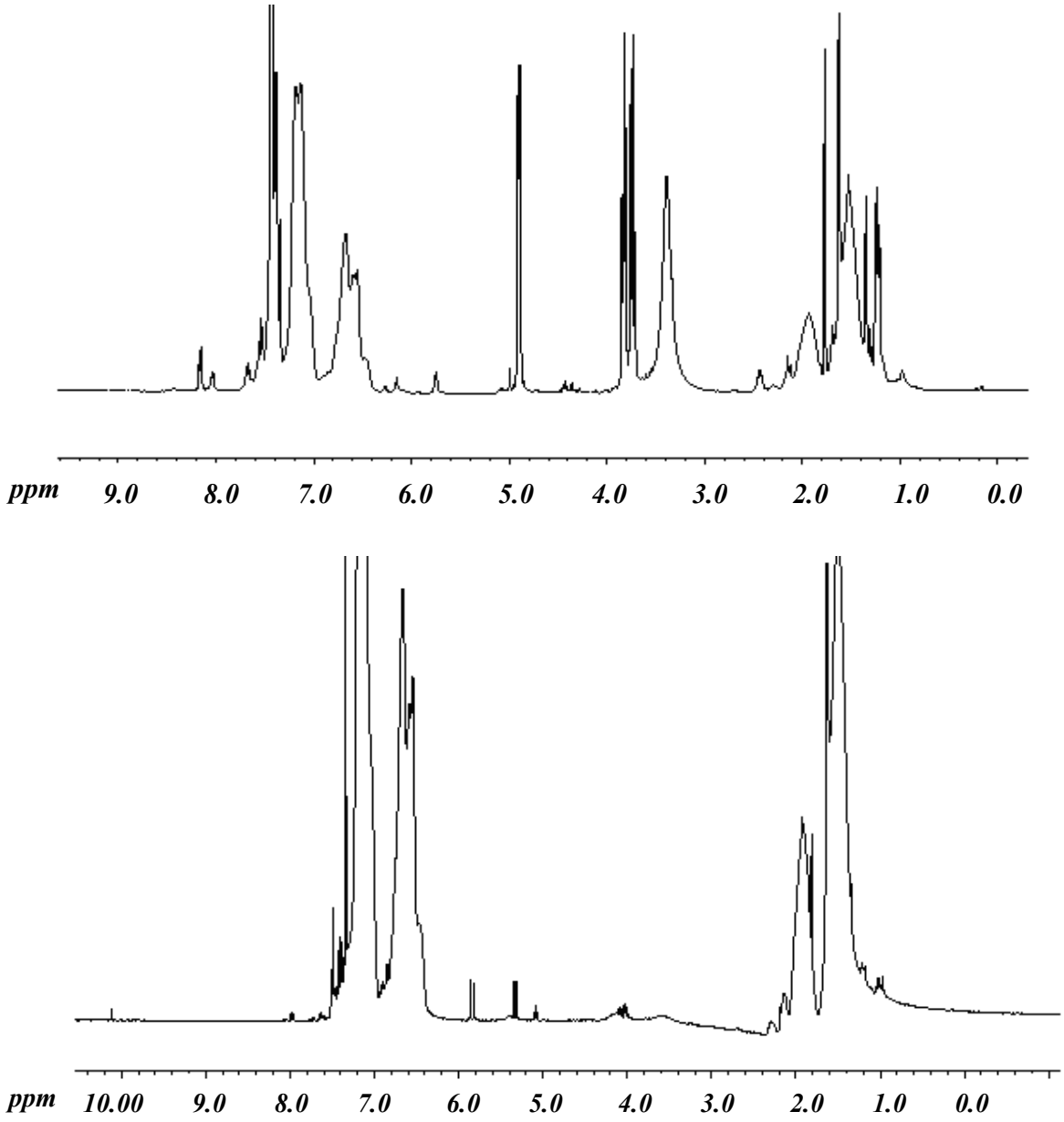

Figure 60 400 MHz ^{1}H-NMR spectra of the polymer obtained in the latex phase (I) and bulk phase (II) by surfactant-free emulsion polymerization of styrene initiated with AIBN.

AIBN decomposition

To follow the mechanism of AIBN initiation in the aqueous as well as the oil phase, the decomposition of AIBN in water was investigated by heating the mixture of heavy water (D_2O) and AIBN containing benzene for a long time. The mixture was heating at 70°C while stirring at 70 rpm for 7 days after which the two phases were isolated and studied by NMR and IR. In a separate experiment, AIBN was heated in pure benzene, and the extracted product was studied by NMR for the sake of comparison.

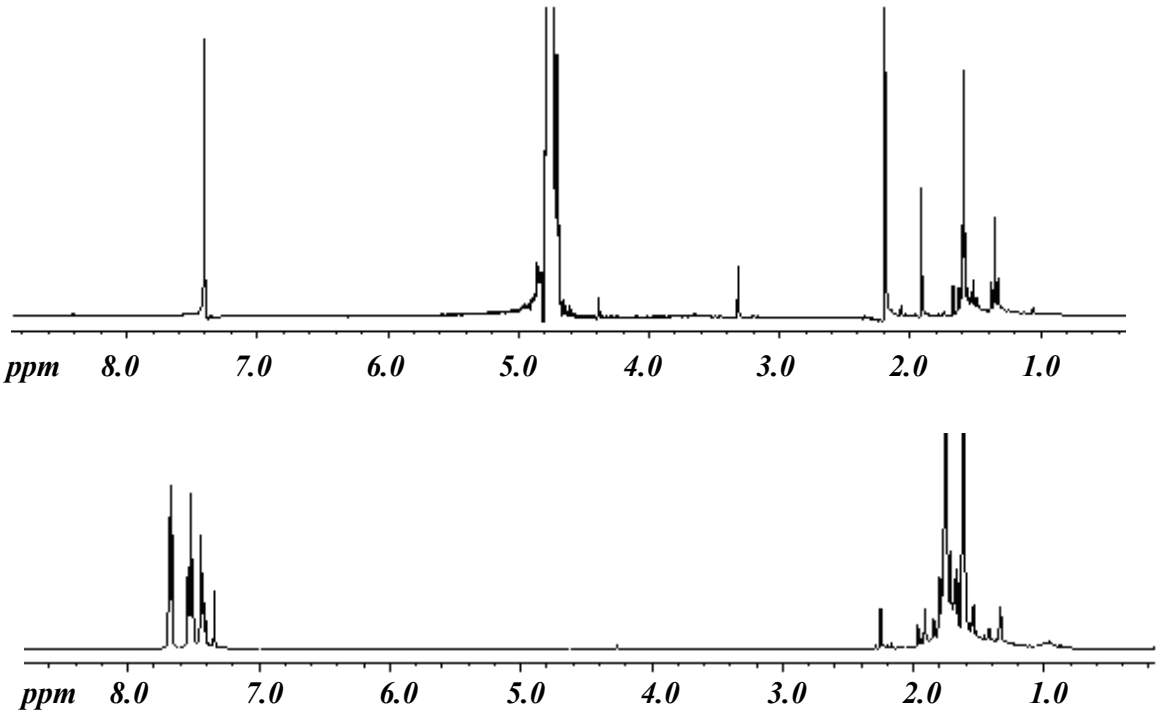

Figure 61 400 MHz ^{1}H-NMR spectra of AIBN decomposition products heated in the mixture of D2O/benzene; (I) D2O part, (II) Benzene part dried over P_2O_5 and dissolved in $CDCl_3$

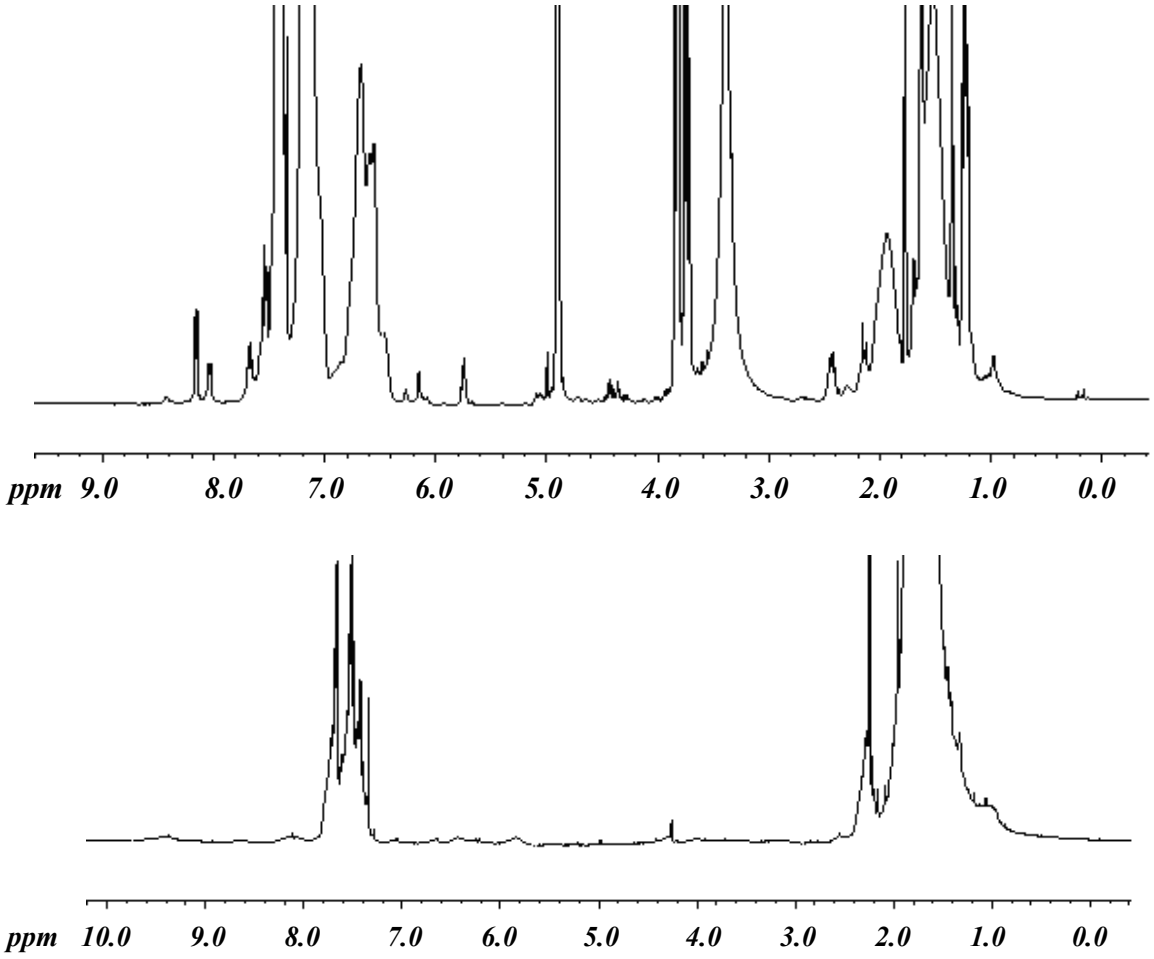

Figure 62 400 MHz ^{1}H-NMR spectra of the AIBN decomposition products, heated in benzene, (I), and the extracted products dissolved in deutrated benzene (II).

AIBN Hydrolysis

AIBN can undergo a hydrolysis reaction to produce carboxylic acids, via the amide, as shown in Fig. 63. [65]

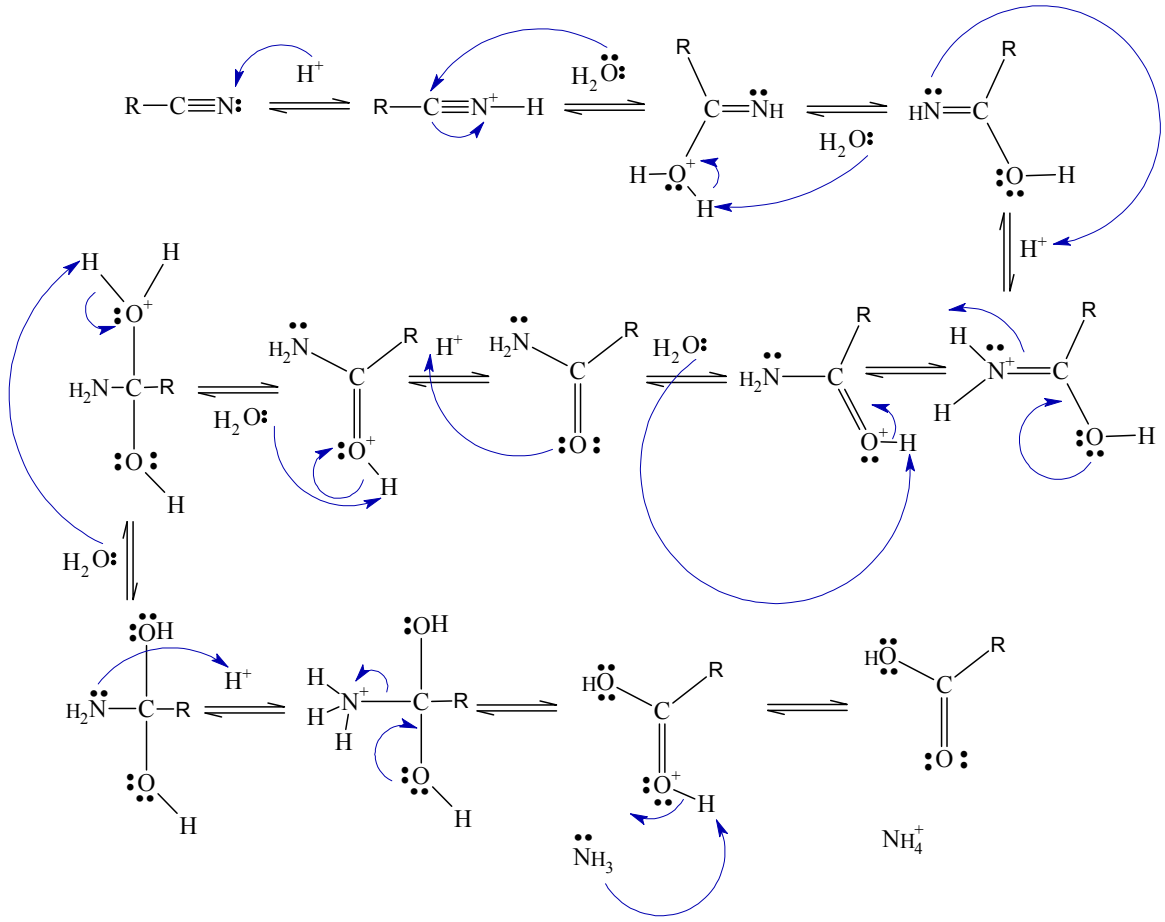

Figure 63 Acid-catalyzed hydrolysis of nitrile to carboxylic functionality.

5.3 Categorized library of results

A complete dataset is made available for the ab-initio emulsion polymerization of styrene at 70°C initiated with different types of initiators and monomers. In chapter 3 only examples of these data were selected for discussion. Here, for further reference, a categorized set of graphs demonstrates the influence of varying the type of initiator, equilibration time, stirring and monomer water-solubility on the morphology, molecular weights and the particle size during the whole course of the polymerization.

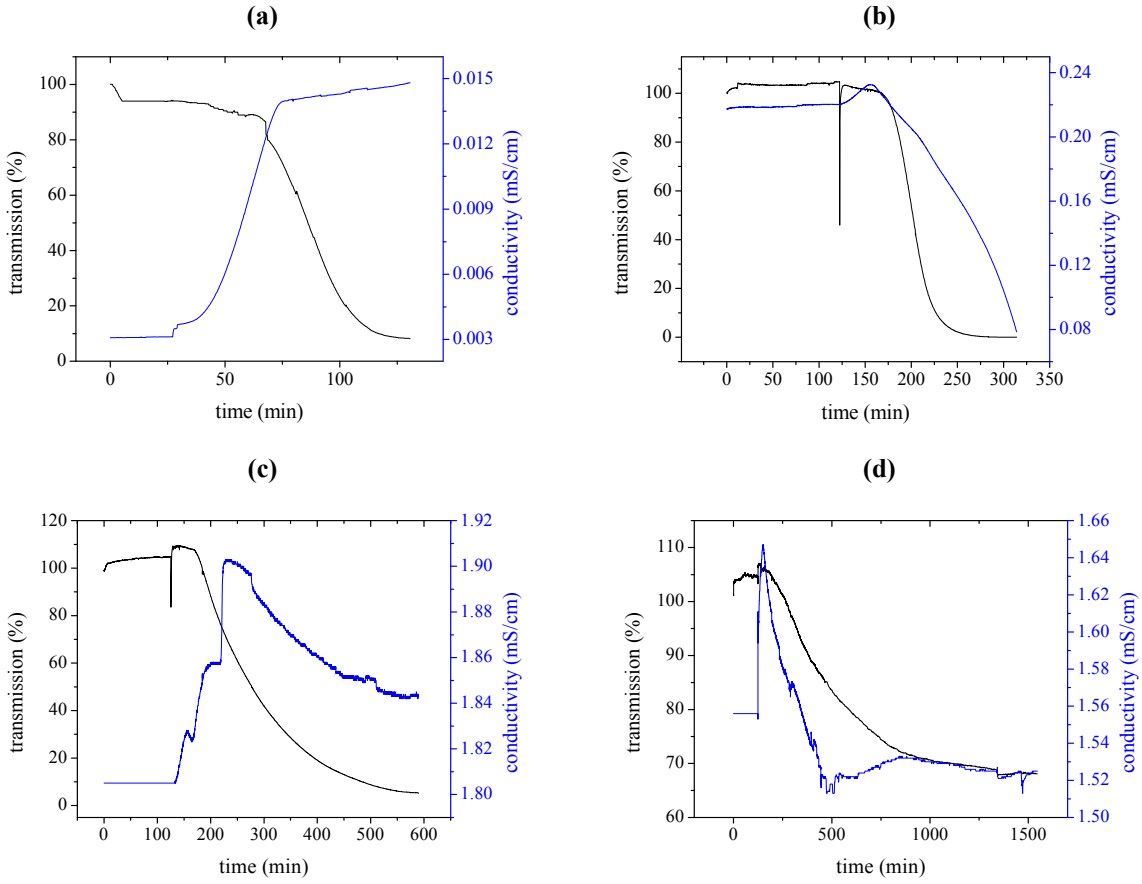

Figure 64 On-line measurement of the conductivity and transmission during styrene emulsion polymerization, with (a) AIBN - $C_{12}E_8$, (b) AIBN – CTAB, (c) AIBN – SDS, (d) V50 - SDS

Table 9 Off-line analysis, JAK2: Emulsion polymerization of styrene at 70° C with KPS, with equilibration time, surfactant free, NO stirring. TEM pictures of samples taken at: (1) -10 min, (2) 5 min, (3) 15 min, (4) 60 min, (5) 120 min. Time zero is the initiation.

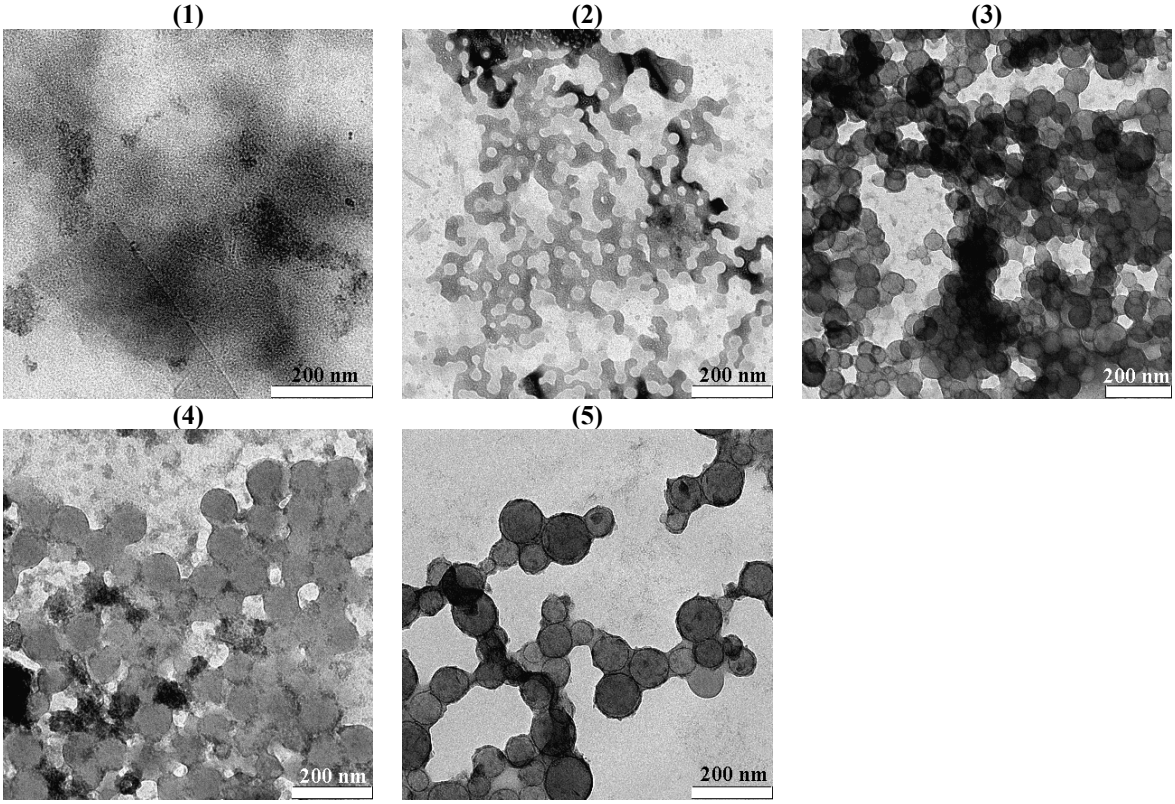

Table 10 Off-line analysis, JAK4: Emulsion polymerization of styrene at 70° C with KPS, No equilibration time, surfactant free, NO stirring. TEM pictures of samples taken at: (1) -5 min, (2) 5 min, (3) 15 min, (4) 30 min, (5) 60 min. Time zero is the initiation.

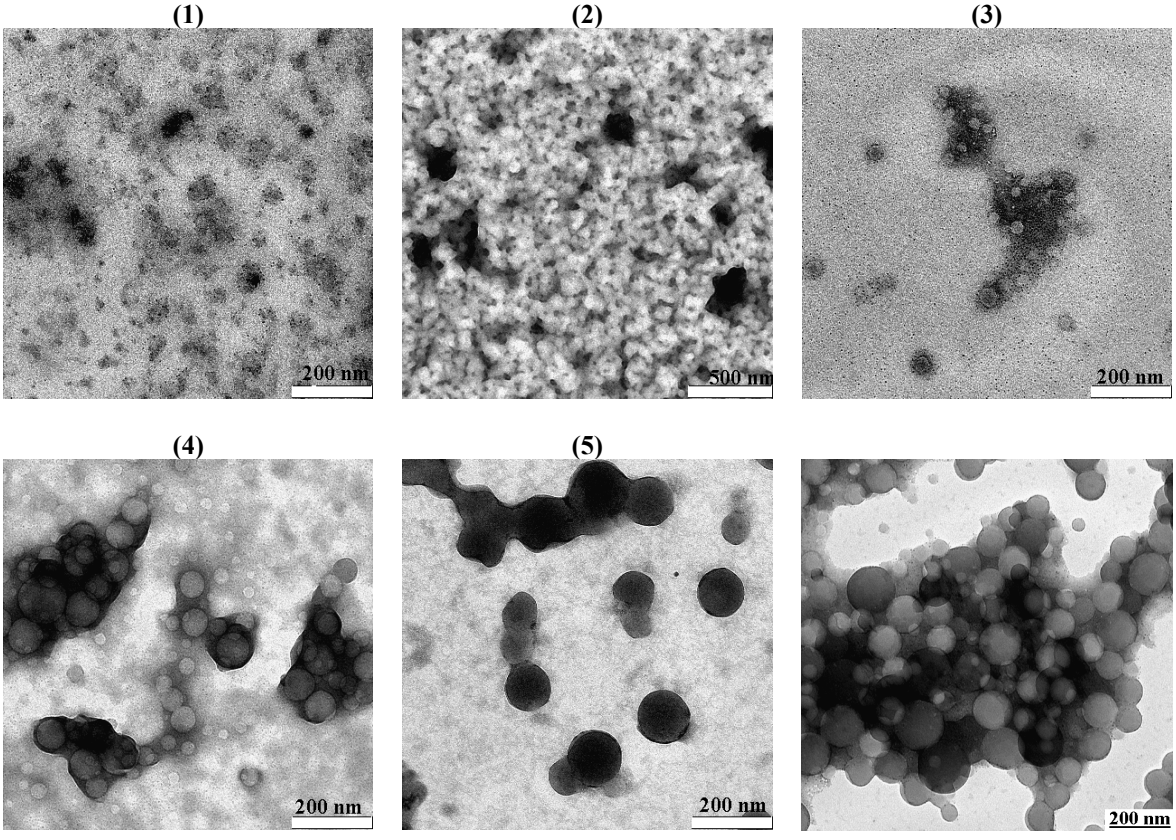

Table 11 Off-line analysis, JAK8: Emulsion polymerization of styrene at 70° C with KPS, with equilibration time, surfactant free, 50 rpm stirring. TEM pictures of samples taken at: (1) -10 min, (2) 5 min, (3) 15 min, (4) 30 min. Time zero is the initiation.

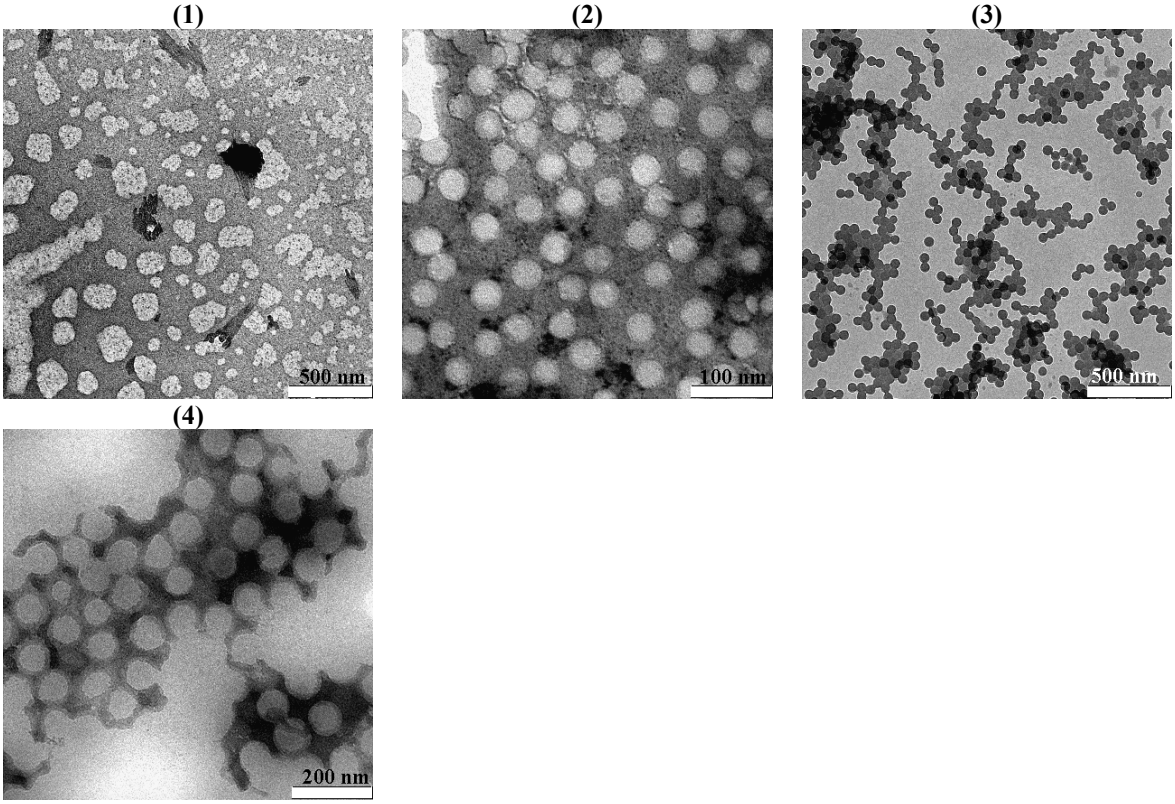

Table 12 Off-line analysis, JAK11: Emulsion polymerization of styrene at 70° C with KPS, with equilibration time, surfactant free, 150 rpm stirring. TEM pictures of samples taken at: (1) 5 min, (2) 10 min, (3) 15 min, (4) 30 min. Time zero is the initiation.

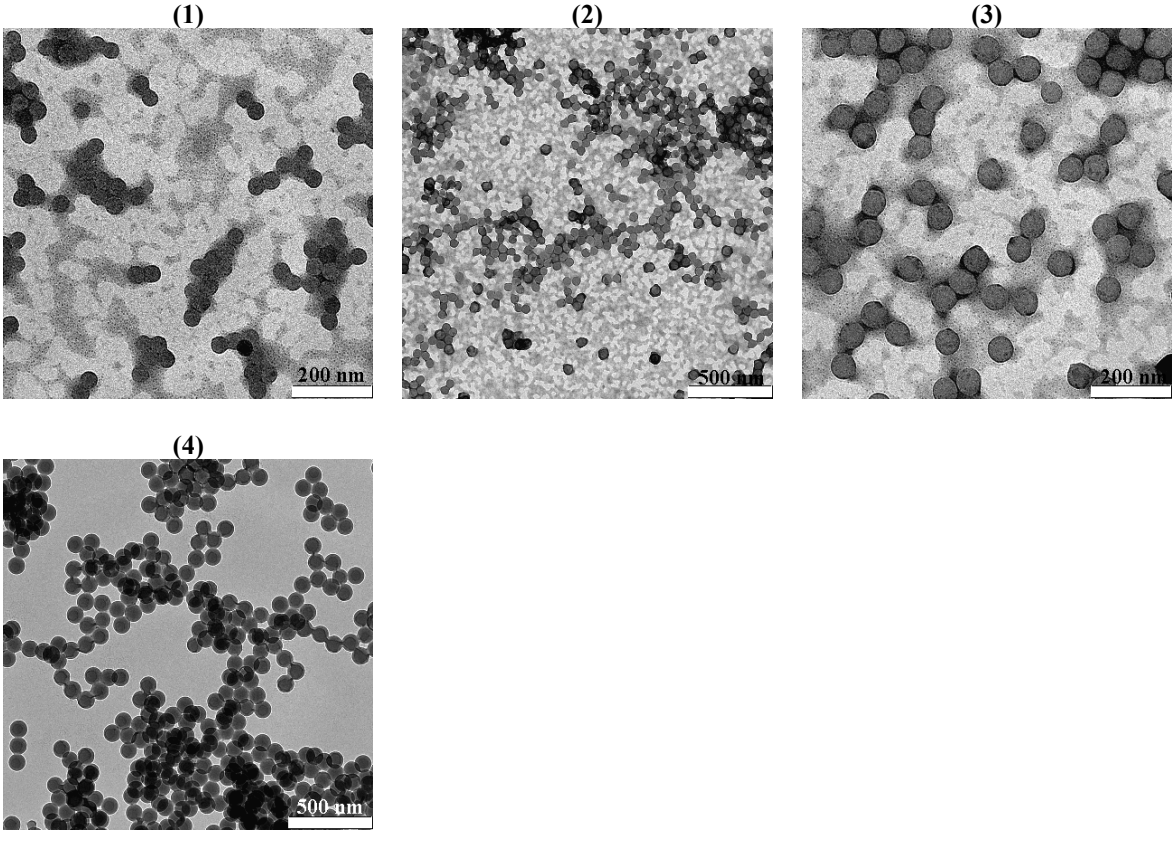

Table 13 Off-line analysis, JAK12: Emulsion polymerization of styrene at 70° C with KPS, with equilibration time, surfactant free, 300 rpm stirring. TEM pictures of samples taken at: (1) 5 min, (2) 10 min, (3) 15 min, (4) 30 min. Time zero is the initiation.

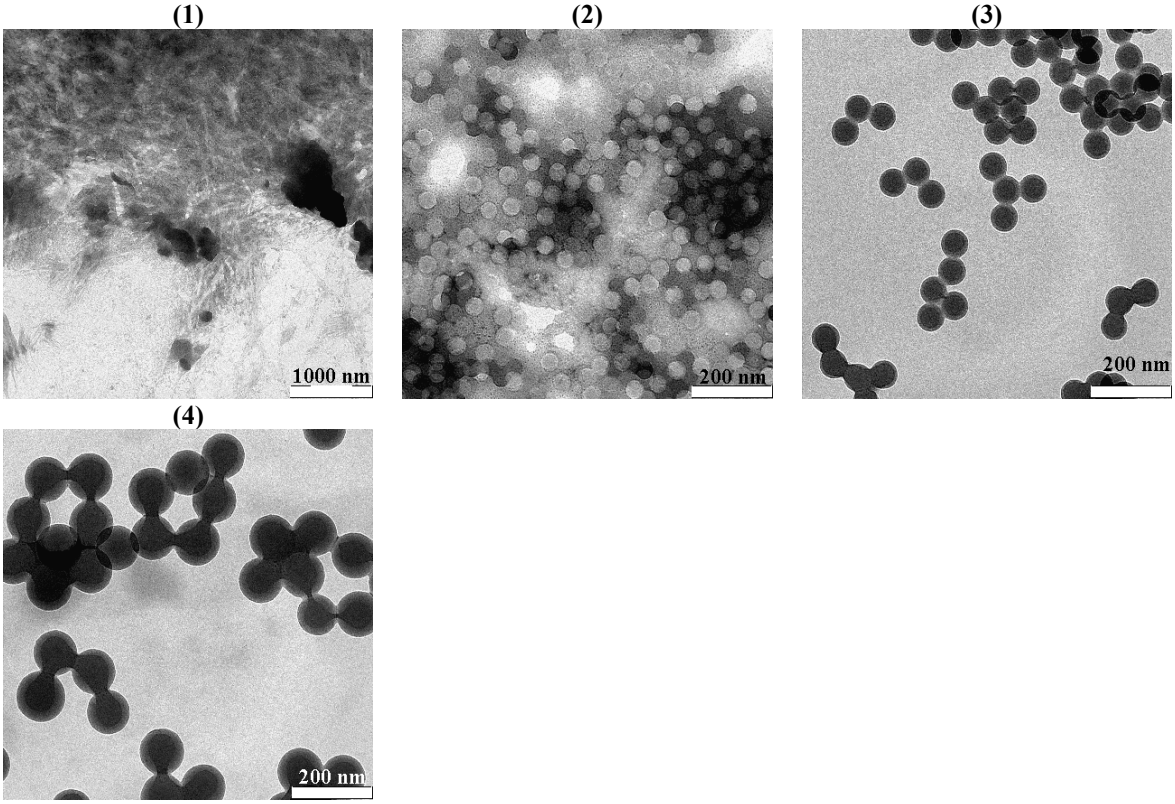

Table 14 Off-line analysis, JAK14: Emulsion polymerization of styrene at 70° C with KPS, No equilibration time, surfactant free, 50 rpm stirring. TEM pictures of samples taken at: (1) -10 min, (2) 5 min, (3) 15 min, (4) 30 min, (5) 60min. Time zero is the initiation.

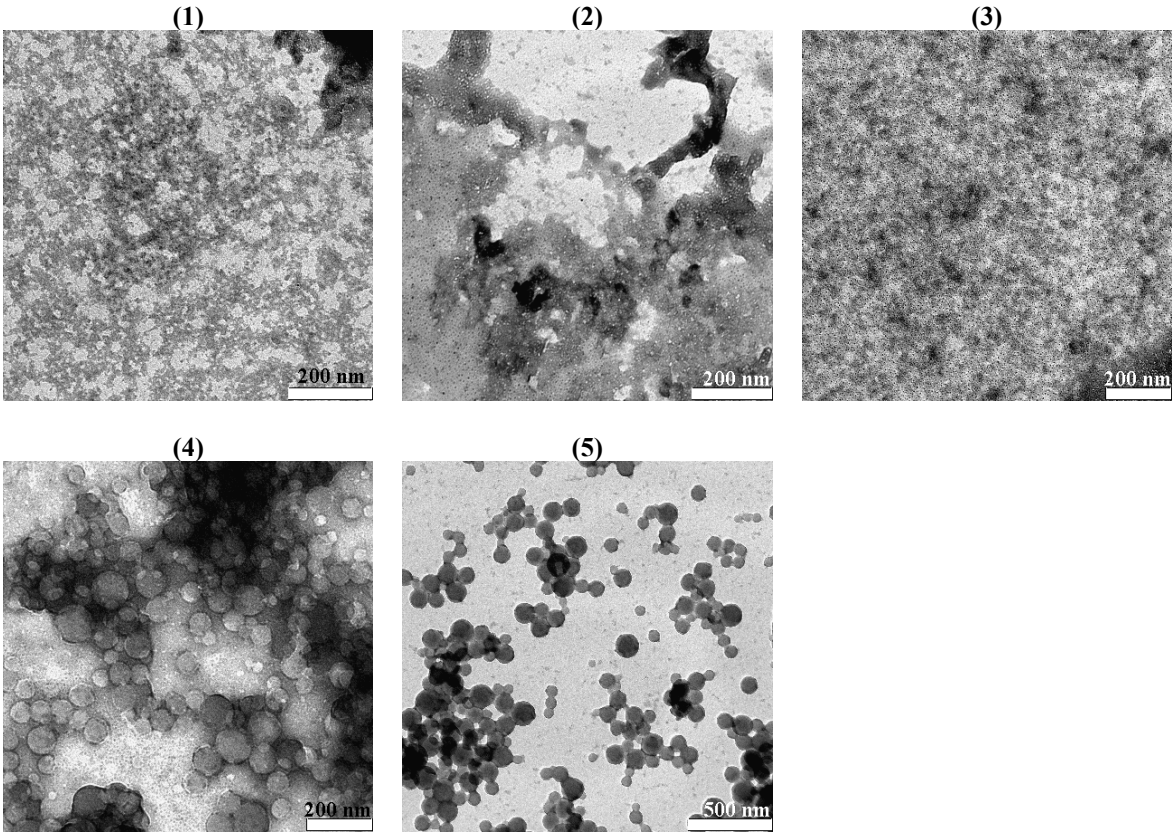

Table 15 Off-line analysis, JAK6: Emulsion polymerization of styrene at 70° C with AIBN, with equilibration time, surfactant free, No stirring. TEM pictures of samples taken at: (1) 5 min, (2) 10 min, (3) 15 min, (4) 30 min, (5) 60 min, (6) 90 min. Time zero is the initiation.

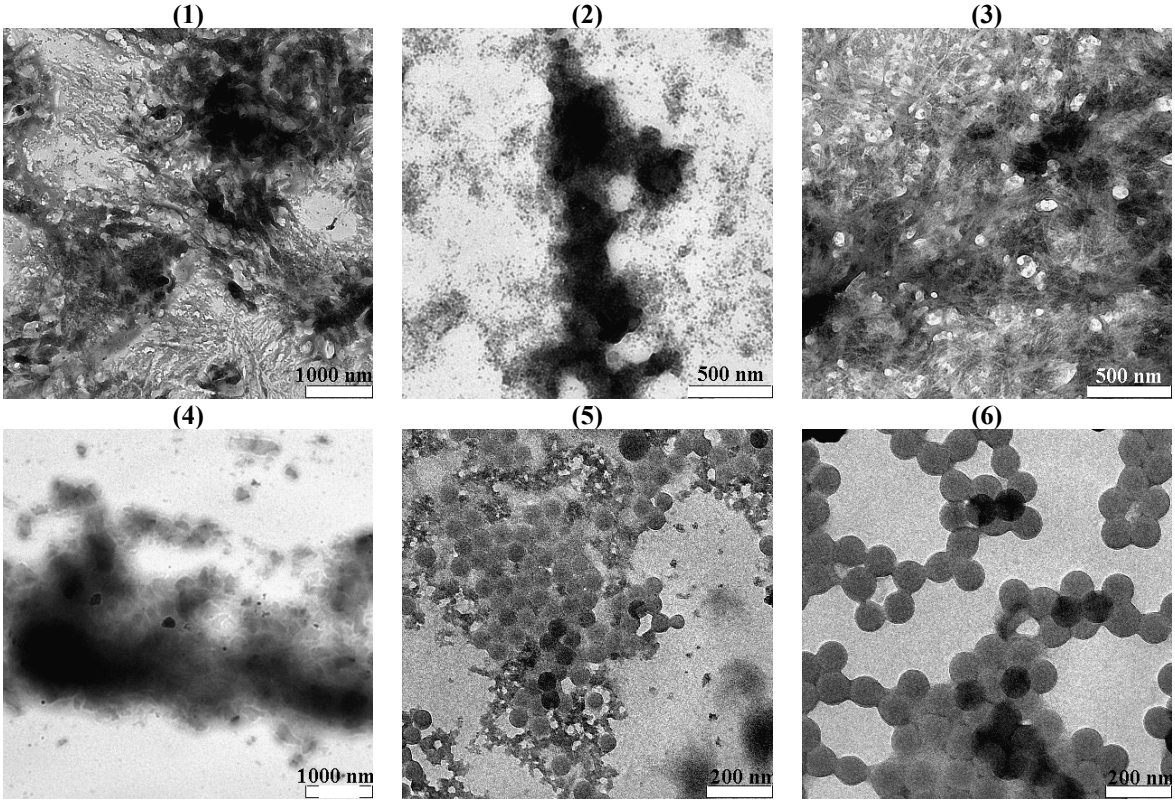

Table 16 Off-line analysis, JAK16: Emulsion polymerization of styrene at 70° C with AIBN, No equilibration time, surfactant free, 50 rpm stirring. TEM pictures of samples taken at: (1) 15 min, (2) 30 min, (3) 60 min, (4) 90 min. Time zero is the initiation.

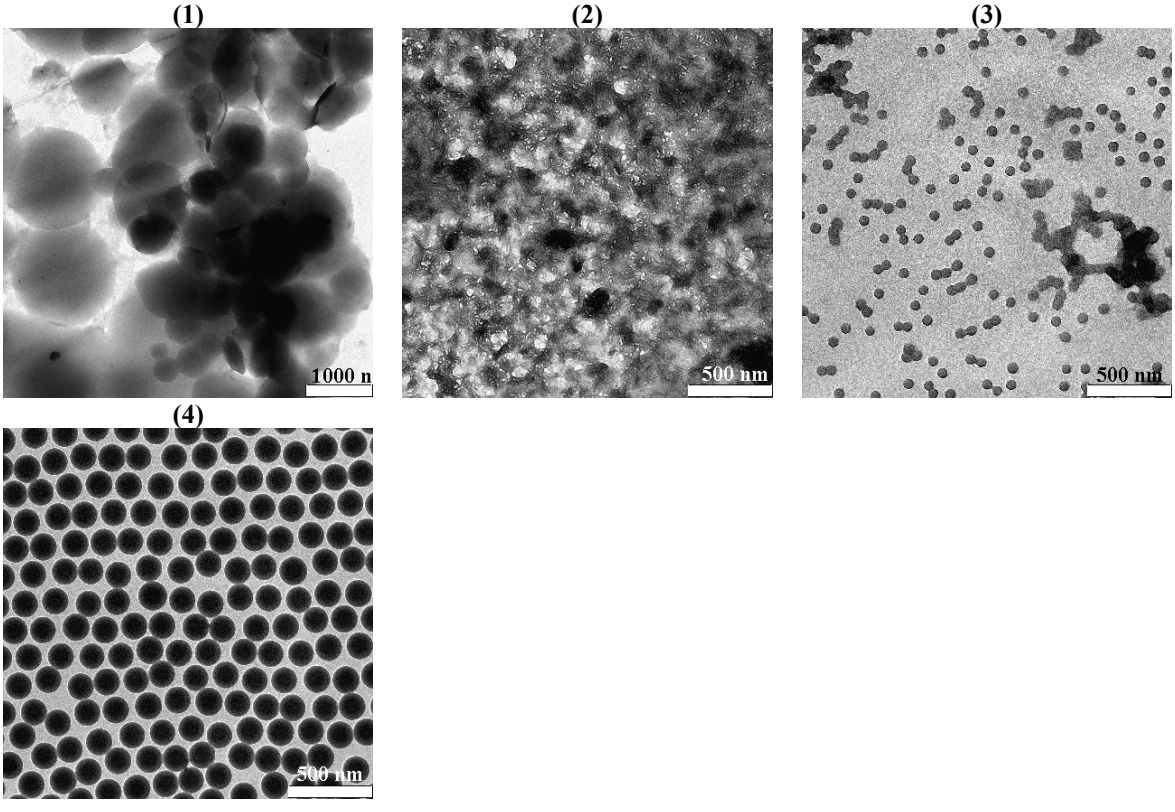

Table 17 Off-line analysis, JAK18: Emulsion polymerization of styrene at 70° C with AIBN, with equilibration time, surfactant free, 50 rpm stirring. TEM pictures of samples taken at: (1) 10 min, (2) 20 min, (3) 30 min, (4) 40 min, (5) 60 min. Time zero is the initiation.

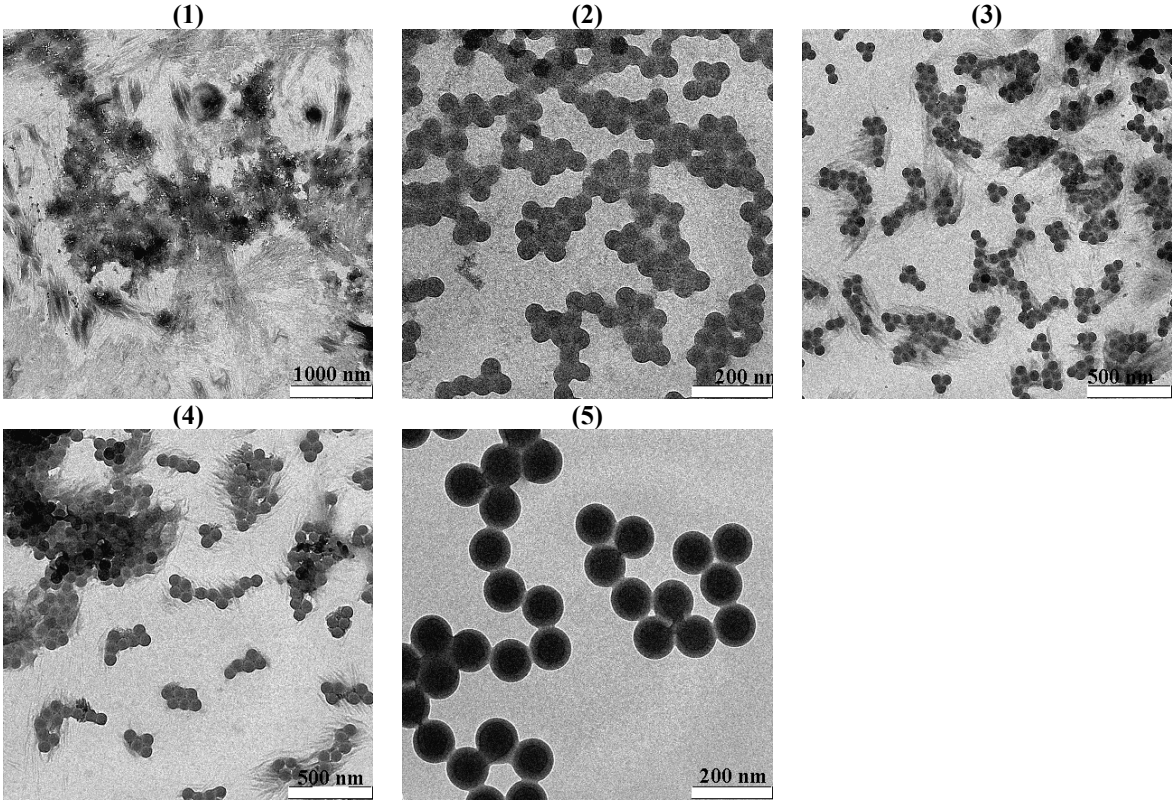

Table 18 Off-line analysis, JAK20: Emulsion polymerization of styrene at 70° C with AIBN, No equilibration time, surfactant free, No stirring. TEM pictures of samples taken at: (1) 30 min, (2) 45 min, (3) 60 min, (4) 90 min, (5) 120 min, (6) 150 min. Time zero is the initiation.

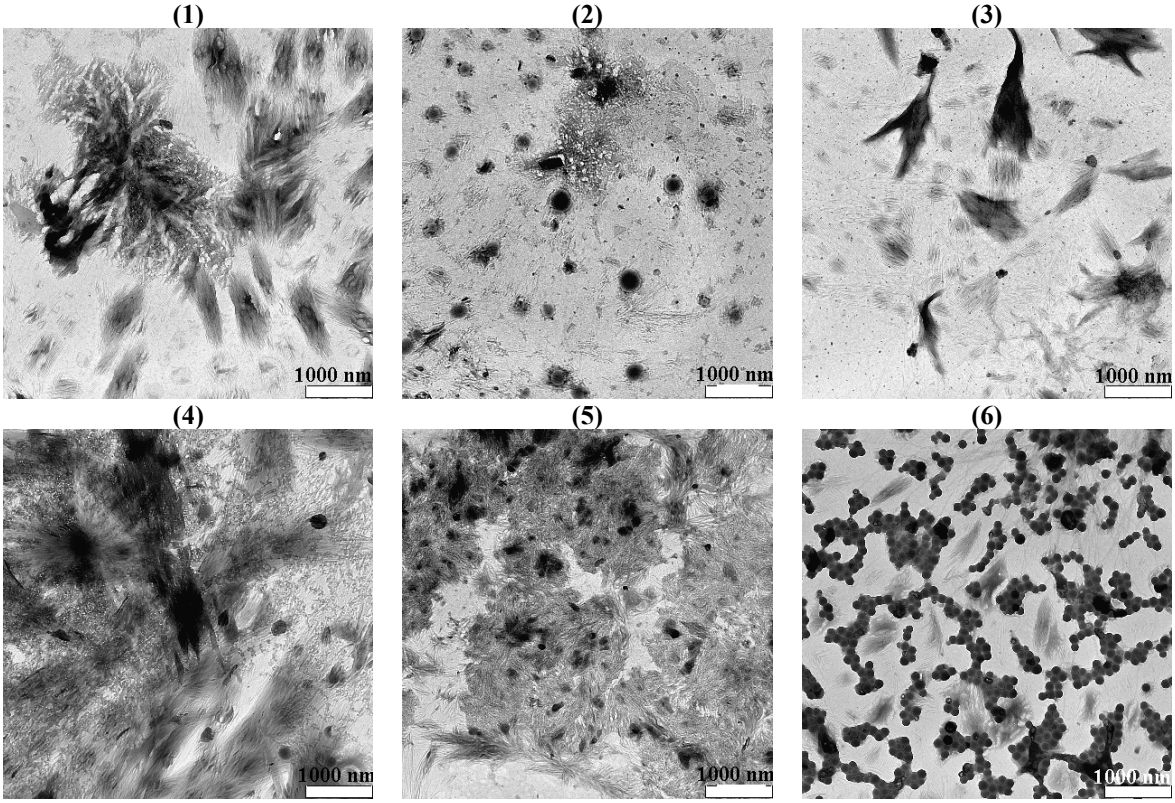

Table 19 Off-line analysis, JAK22: Emulsion polymerization of MMA at 70° C with KPS, with equilibration time, surfactant free, 50 rpm stirring. TEM pictures of samples taken at: (1) -10 min, (2) 2 min, (3) 5 min, (4) 8 min. Time zero is the initiation.

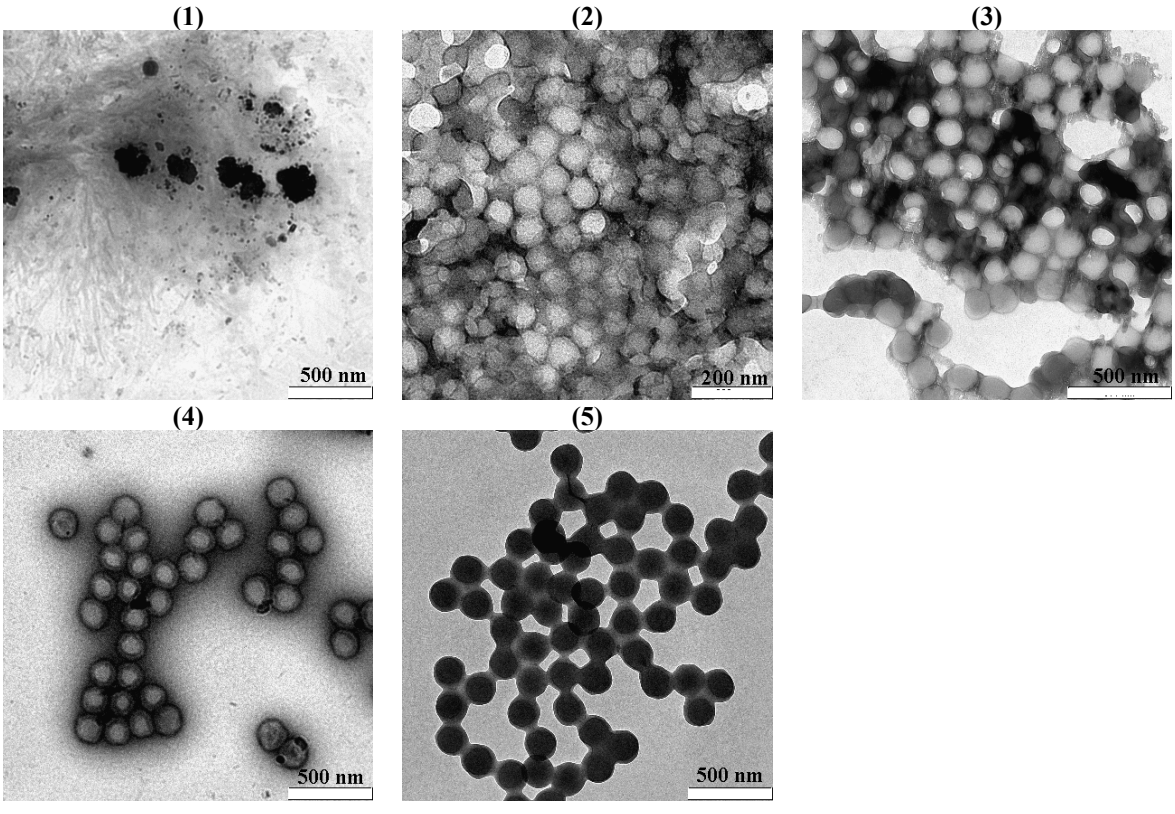

Table 20 Off-line analysis, JAK23: Emulsion polymerization of MMA at 70° C with KPS, ½[I], with equilibration time, surfactant free, 50 rpm stirring. TEM pictures of samples taken at: (1) -10 min, (2) 2 min, (3) 5 min, (4) 8 min, (5) 10 min. Time zero is the initiation.

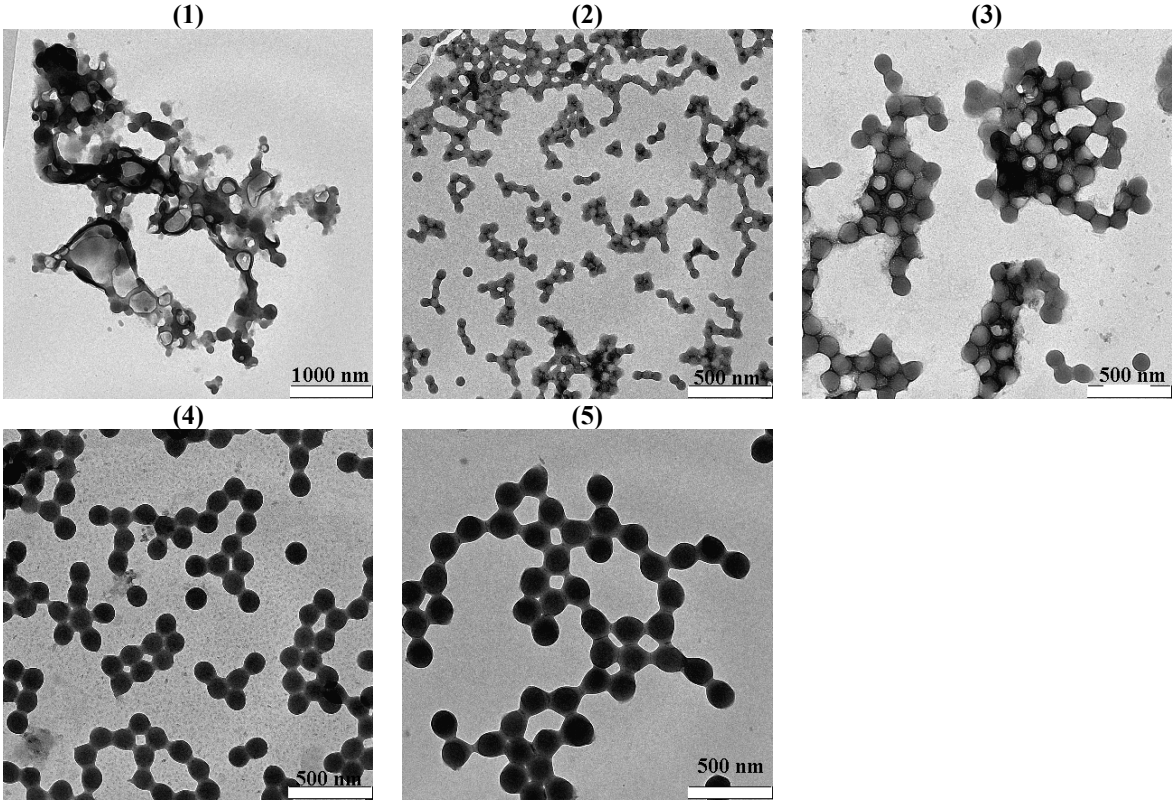

Table 21 Off-line analysis, JAK29: Emulsion polymerization of tBuSty at 70° C with KPS, ½ [I], with equilibration time, surfactant free, 50 rpm stirring. TEM pictures of samples taken at: (1) 5 min, (2) 10 min, (3) 15 min, (4) 20 min, (5) 30 min, (6) 45 min, (7) 60 min, (8) 90 min. Time zero is the initiation.

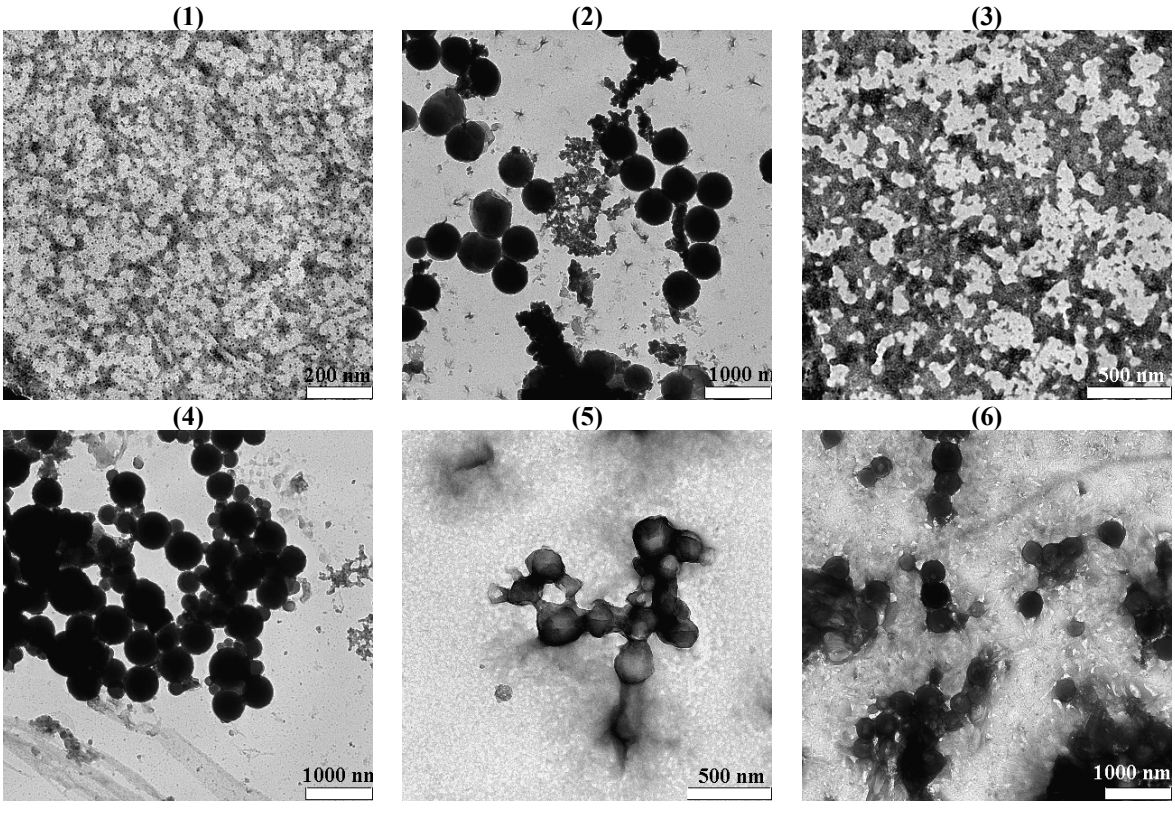

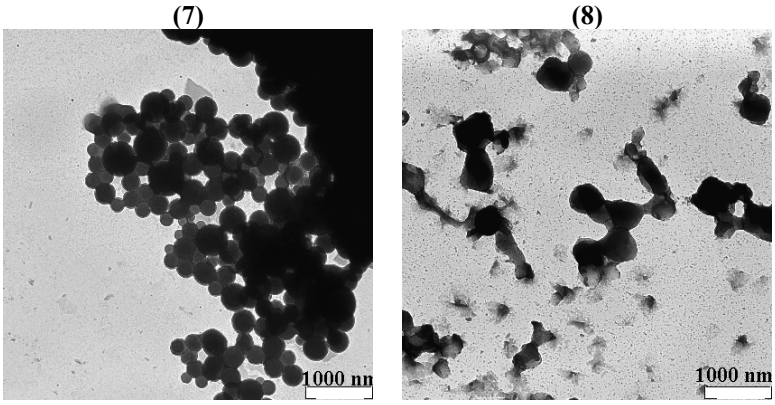

Table 22 Off-line analysis, JAK25: Emulsion polymerization of tBuSty at 70° C with KPS, [I], with equilibration time, surfactant free, 50 rpm stirring. TEM pictures of samples taken at: (1) 5 min, (2) 10 min, (3) 15 min, (4) 20 min, (5) 30 min, (6) 45 min. Time zero is the initiation.

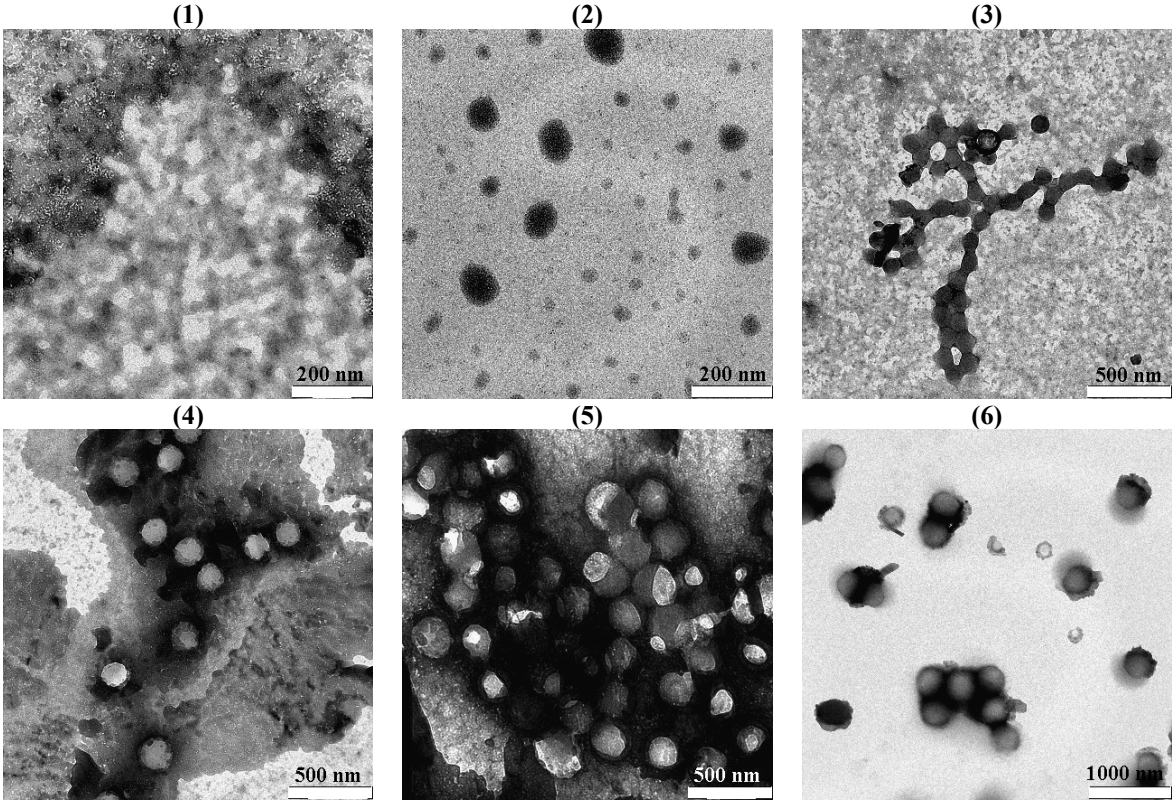

Table 23 Off-line analysis, JAK28: Emulsion polymerization of tBuSty at 70° C with KPS, 2[I], with equilibration time, surfactant free, 50 rpm stirring. TEM pictures of samples taken at: (1) 5 min, (2) 10 min, (3) 15 min, (4) 20 min, (5) 30 min, (6) 45 min, (7) 60 min, (8) 90 min. Time zero is the initiation.

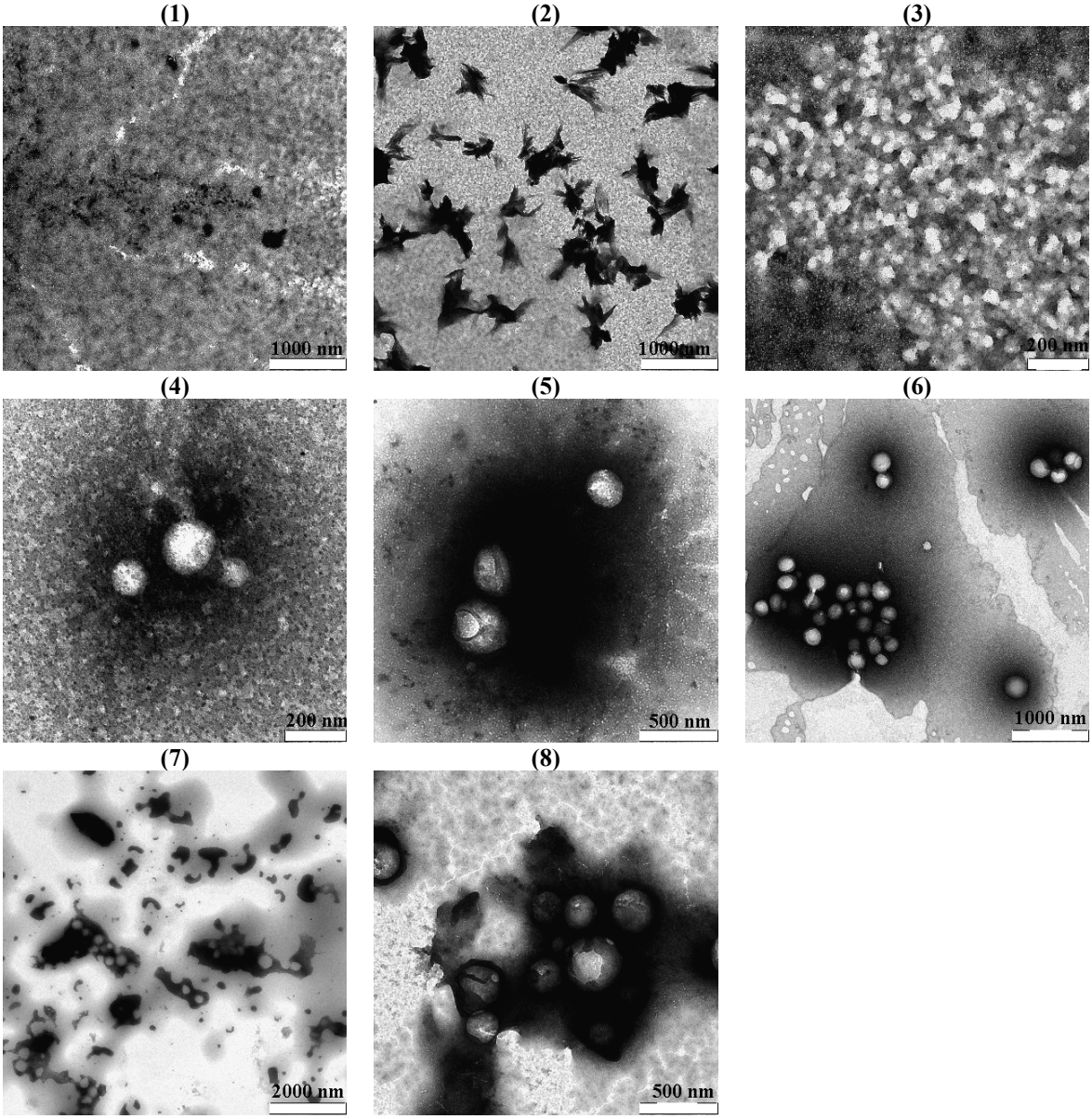

Table 24 Off-line analysis, JAK30: Emulsion polymerization of tBuSty at 70° C with KPS, 5[I], with equilibration time, surfactant free, 50 rpm stirring. TEM pictures of samples taken at: (1) 10 min, (2) 20 min, (3) 40 min, (4) 60 min, (5) 90 min, (6) 120 min, (7) 150 min. Time zero is the initiation.

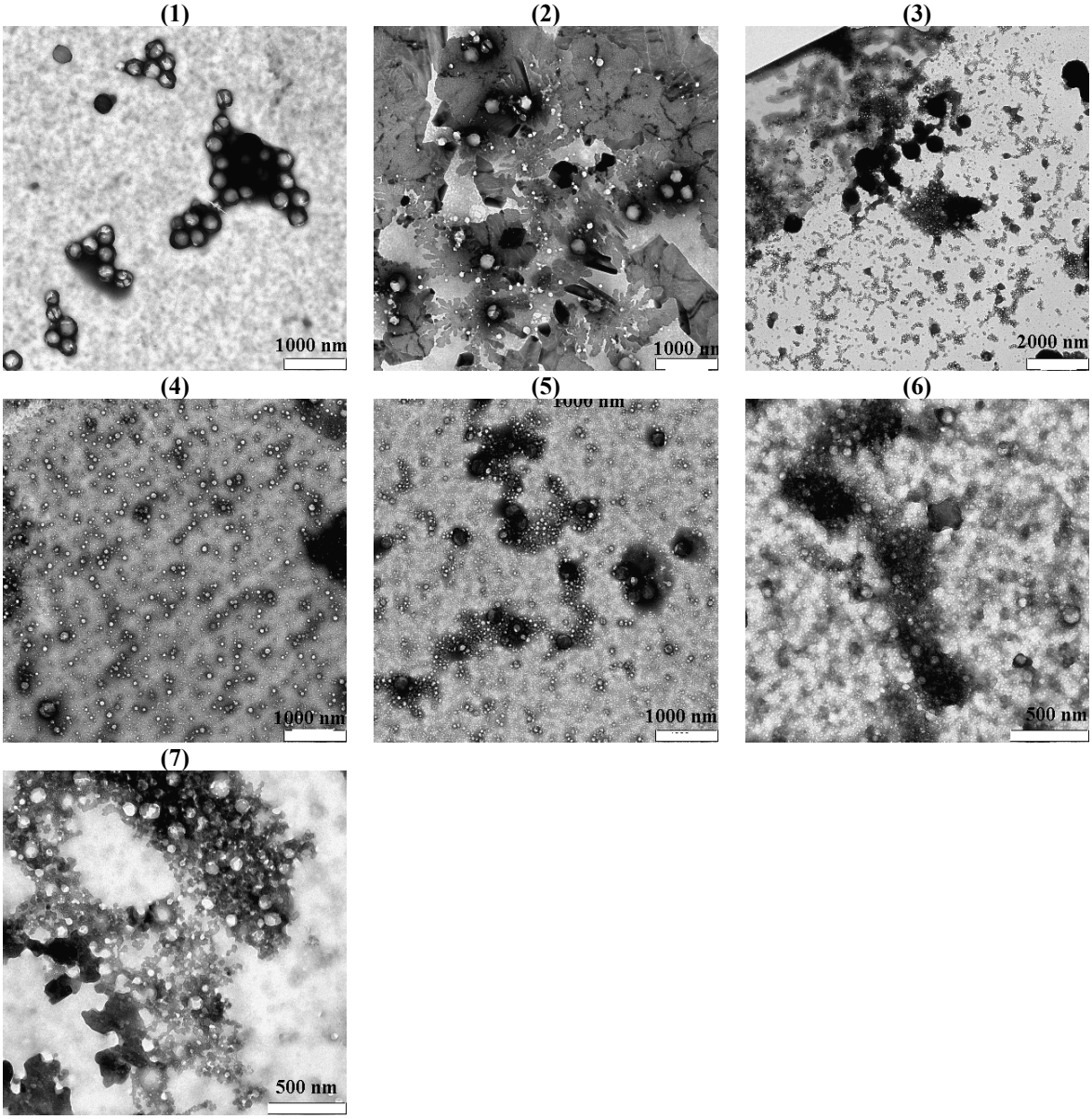

Table 25 Off-line analysis, JAK278: Emulsion polymerization of LMA at 70° C with KPS, with equilibration time, surfactant free, 50 rpm stirring. TEM pictures of samples taken at: (1) -10 min, (2) 5 min, (3) 10 min, (4) 15 min, (5) 20 min, (6) 30 min, (7) 45 min, (8) 60 min, (9) 90 min. Time zero is the initiation.

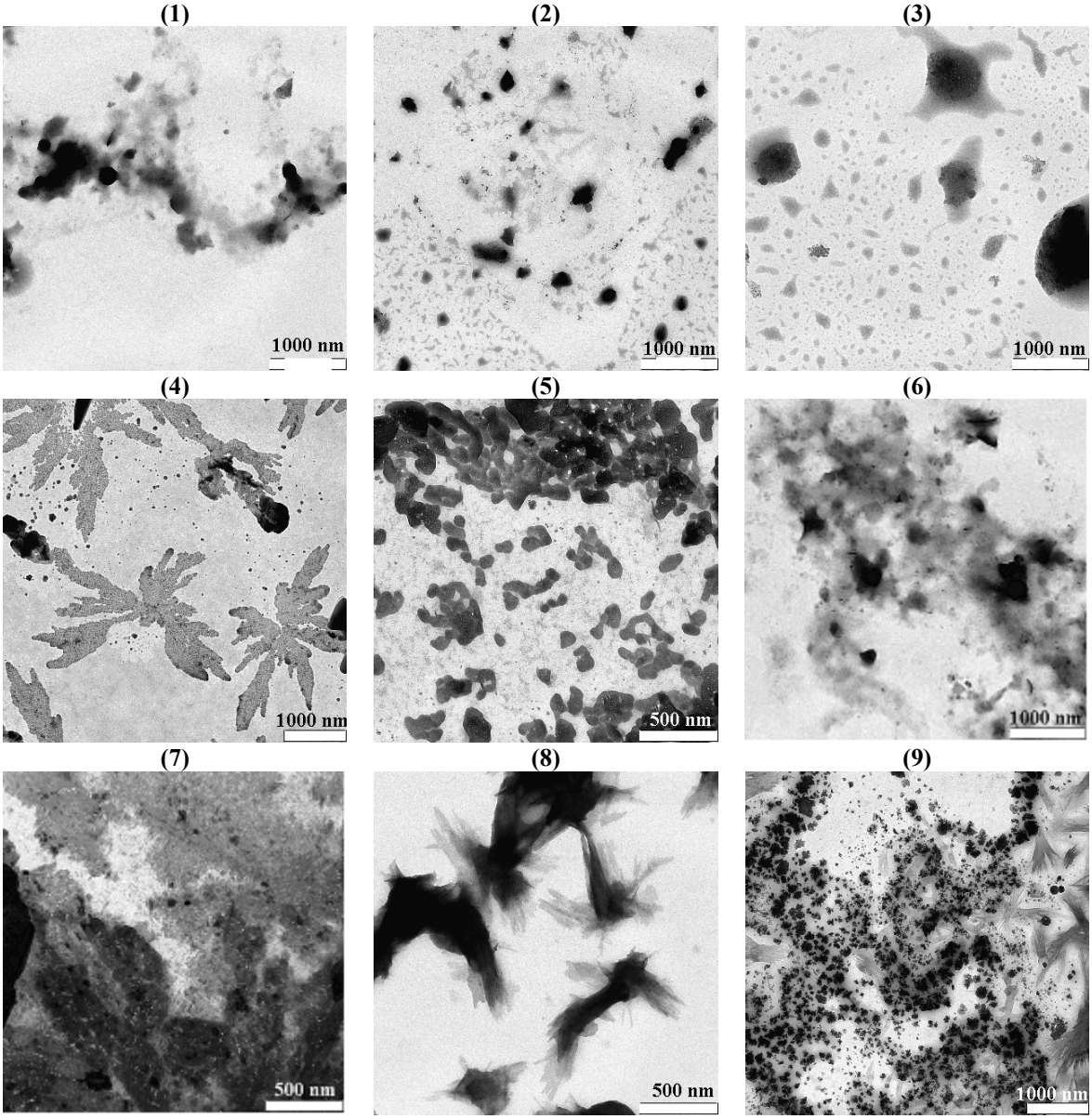

Table 26 Off-line analysis of emulsion polymerizations, the growth in particle size and molecular weight for the polymerization systems mentioned in table 9-25. Each graph corresponds to the table named above. The filled circles show the development of the weight averaged molecular weight, and the squares show the development of the hydrodynamic averaged diameter.

(cf. table 9)

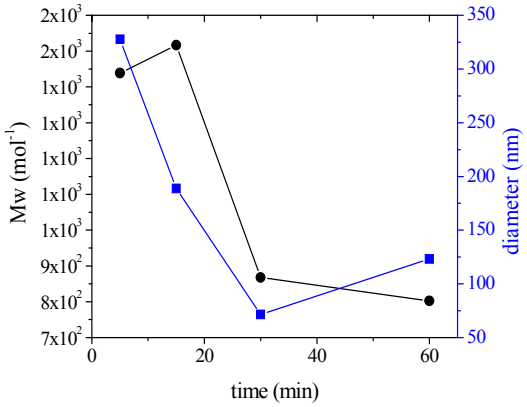

(cf. table 10)

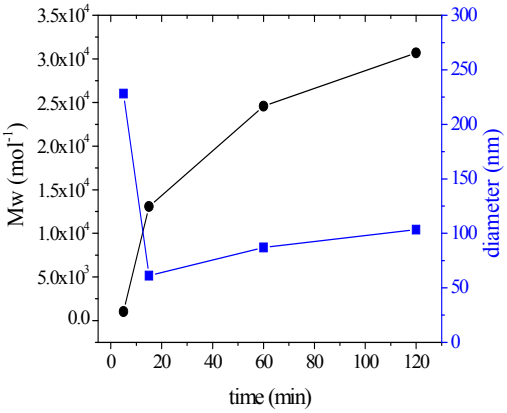

(cf. table 11)

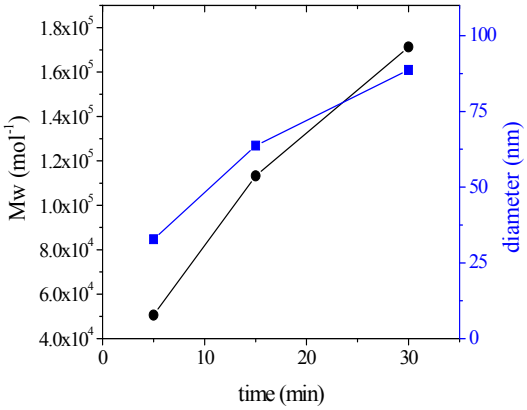

(cf. table 12)

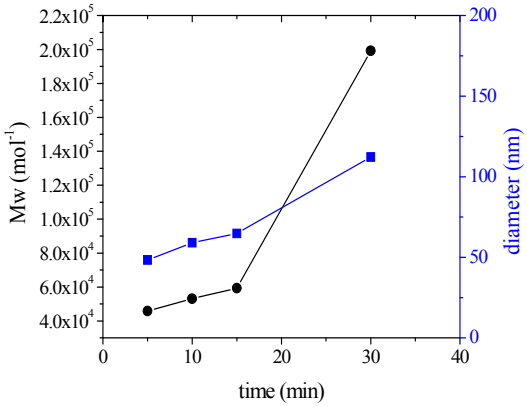

(cf. table 13)

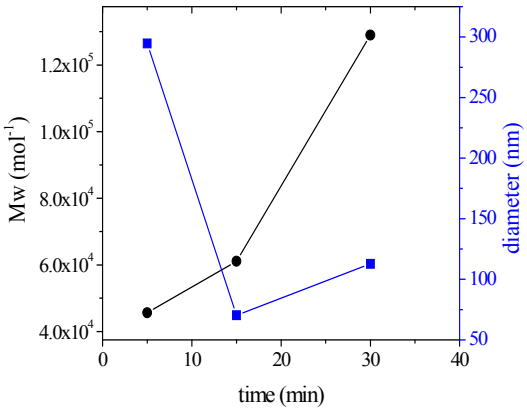

(cf. table 14)

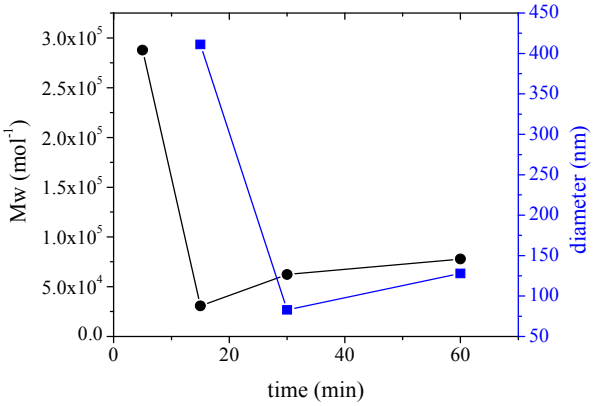

(cf. table 15)

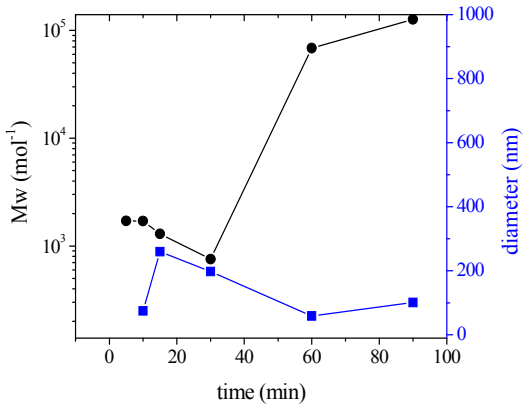

(cf. table 16)

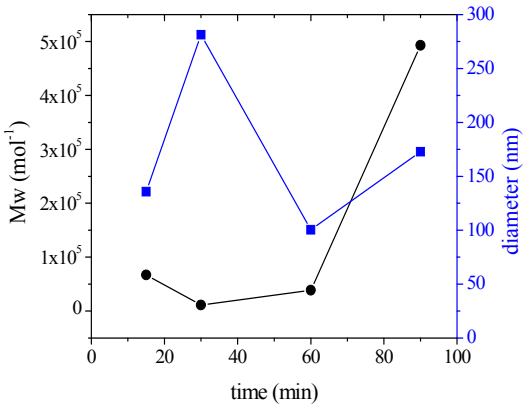

(cf. table 17)

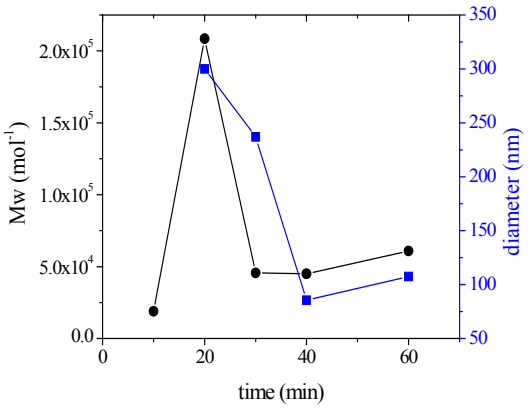

(cf. table 18)

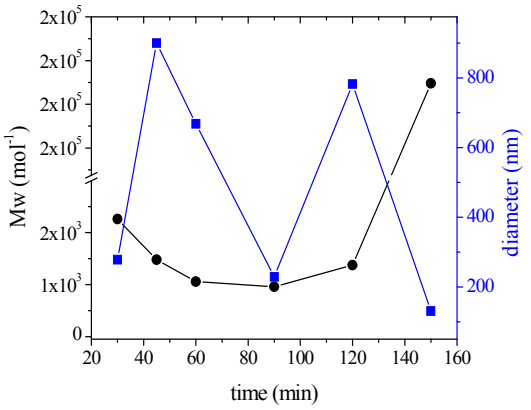

(cf. table 19)

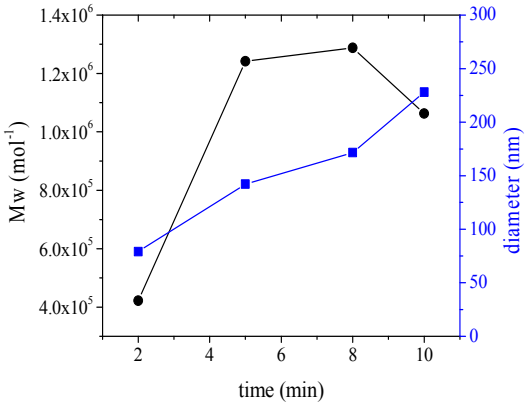

(cf. table20)

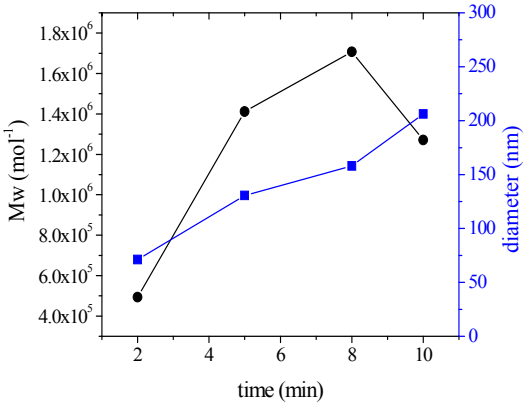

(cf. table 21)

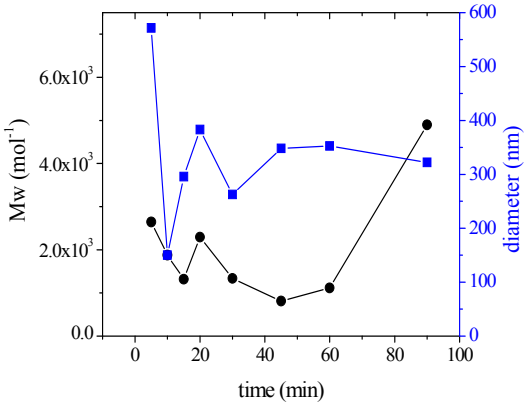

(cf. table22)

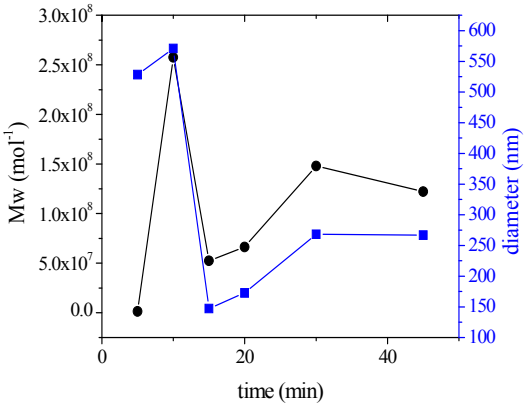

(cf. table 23)

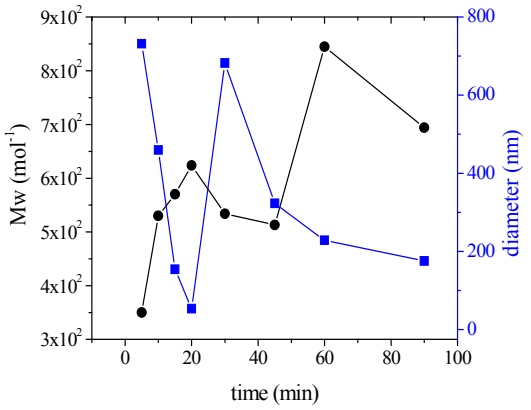

(cf. table 24)

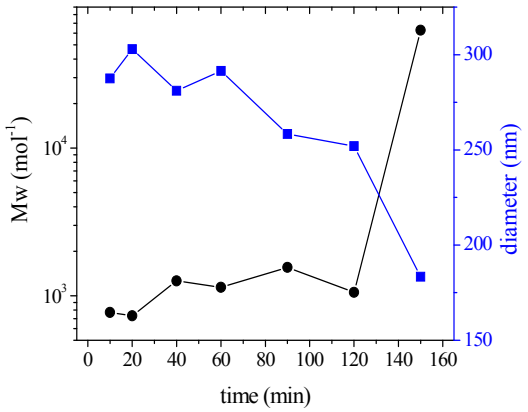

(cf. table 25)

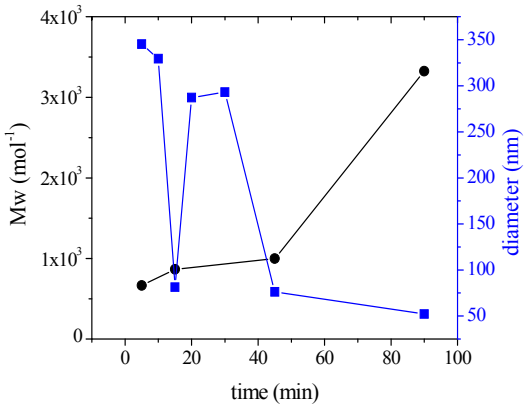

5.4 Symbols and Abbreviation

AAS	2,2´-azobis (N-2´-methylpropanoyl-2-amino-alkyl-1)-sulfonates
AIBN	2,2'-azobis-isobutyronitrile (AIBN)
APG	Allyl phenylpolyol ether sulphate
AUC	Analytical ultracentrifuge
BuMA	butyl methacrylate
$C_{12}E_8$	Octaethylene glycol ether
CMC	critical micellar concentration
CTAB	cetyltrimethyl ammoniumbromide
DAS	2,2´-azobis (N-2´-methylpropanoyl-2-amino-decyl-1)-sulfonates
DLS	Dynamic Light Scattering
FOQELS	Fiber Optical Quasi Elastic Light Scattering
FRP	Free Radical Polymerization
FTIR	Fourier Transform Infrared
HDAS	2,2´-azobis (N-2´-methylpropanoyl-2-amino-hexdecyl-1)-sulfonates
HDC	Hydrodynamic Chromatography
IGEPAL	Ethoxylated nonyl phenyl
KPS	potassium peroxodisulfate
LMA	Lauryl methacrylate
MMA	Methyl methacrylate
MW	Molecular Weight
MWD	Molecular Weight Distribution
NMR	Nuclear Magnetic Resonance
PAA-PS	Polystyrene-block-Polyacrylic acid

PEGA200	poly(ethylene glycol)-azo-initiator
SDS	Sodium dodecyl sulfate
SEC	Size Exclusion Chromatography
Sty	Styrene
t-BuSty	*tert*-butyl styrene
TEM	transmission electron microscopy
UV-Vis	Ultra Violet-Visible
V59	2,2-azobis(2-methylbutyronitrile)
VA-086	2,2-azobis[2-methyl-N-(2-hydroxyethyl)-propionamide]
A (page 33)	surface area
a_h	hydrodynamic radius of the ion
b	correction factor in equation 14.
c_i	concentration
C_{sca}	scattering cross section
C_P	polymer concentration
D	Fickian diffusion coefficient of the particle
D	particle diameter
D_i	intensity averaged diameter
f	factor of initiator efficiency
F	Faraday constant
$G(t)$	autocorrelation function
I	initiator
I_0	incident light intensity,
J	rate of nucleation
j_cr	critical chain length
k_B	Boltzman constant
k_d	decomposition rate coefficient
k_i	Initiation rate coefficient

k_P	propagation rate coefficient
k_t	termination rate coefficient
k_{tc}	termination rate coefficient by combination
k_{td}	termination rate coefficient by disproportionation
M	monomer
m	ratio of the refractive indices of the particles and water
$M\bullet$	growing radicals
M_n	number average molecular weight
M_W	weight average molecular weight
n	degree of polymerization
N_A	Avogadro number
N, N_P	Number of polymer particles
Q	scattering factor
r	radius of particles
r	rate of reaction
$R\bullet$	primary free-radical
R_H	Hydrodynamic radius
R_i	rate of initiation, or generation of free-radicals
R_c	rate of radical capture
R_f	Rate of radical flocculation
R_P	rate of polymerization
RT	thermal energy
R_t	rate of termination
S	surfactant
S	supersaturation
t	time
t_N	Nucleation time (Pre-nucleation period)
T	absolute temperature

T (%)	Transmission
u	mobility of ion
V	volume
X	conversion
z	charge
κ	electrical conductivity
λ	wavelength
Λ_m	molar conductivity
Λ^0_m	limiting molar conductivity
η_0	viscosity
γ_{PW}	interfacial tension between polymer and water
ρ_P	polymer density
σ	interfacial energy
τ	turbidity
v	molar volume
ω	frequency shift

6 References

1. Ebdon, J. R., *New Methods of Polymer Synthesis*. Blackie: New York, **1991**.
2. Tonelli, A. E., Srinivasarao, M., *Polymers from the inside out: an introduction to macromolecules*. Wiley-Interscience: New York, **2001**.
3. El-Aasser, M. S., Sudol, E. D., *Features of Emulsion Polymerization*. In *Emulsion Polymerization and Emulsion Polymers*, Lovell, P. A., El-Aasser, M. S., Eds. J. Wiley & Sons, Inc.: New York, **1997**.
4. Fitch, R. M., *Polymer Colloids: A Comprehensive Introduction*. Academic Press: San Diego, **1997**.
5. Lovell, P. A., *Free-Radical Polymerization*. In *Emulsion Polymerization and Emulsion Polymers*, Lovell, P. A., El-Aasser, M. S., Eds. J. Wiley & Sons, Inc.: New York, **1997**.
6. Harkins, W. D., *A General Theory of the Mechanism of Emulsion Polymerization*. Journal of the American Chemical Society, **1947**, 69, (6), 1428.
7. Smith, W. V., Ewart, R. H., *Kinetics of Emulsion Polymerization*. Journal of Chemical Physics, **1948**, 16, (6), 592.
8. Bartholome, E., Gerrens, H., Herbeck, R., Weitz, H. M., *Uber Die Kinetik Der Emulsionspolymerisation Von Styrol*. Zeitschrift Fur Elektrochemie, **1956**, 60, (3), 334.
9. Hansen, F. K., Ugelstad, J., *Particle Nucleation in Emulsion Polymerization .3. Nucleation in Systems with Anionic Emulsifier Investigated by Seeded and Unseeded Polymerization*. Journal of Polymer Science Part a-Polymer Chemistry, **1979**, 17, (10), 3047.
10. Fitch, R. M., Tsai, C. H., *Polymer colloids: particle formation in nonmicellar systems.* Polymer Letters, **1970**, 8, 703.
11. Fitch, R. M., *Homogeneous nucleation of polymer colloids.* Br. Polym. J., **1973**, 5, 467.
12. Fitch, R. M., Tsai, C. H., In *Polymer Colloids*, Fitch, R. M., Ed. Plenum Press: New York, **1973**; pp 73.
13. Fitch, R. M., Tsai, C. H., *Particle formation in polymer colloids. III. Prediction of the number of particles by a homogeneous nucleation theory*. Polym. Colloids, Proc. Symp., **1971**, 73.
14. Hansen, F. K., *Is There Life Beyond Micelles - Mechanisms of Latex Particle Nucleation*. ACS Symposium Series, **1992**, 492, 12.
15. Hansen, F. K., Ugelstad, J., *Particle Nucleation In Emulsion Polymerization .1. Theory For Homogeneous Nucleation*. Journal of Polymer Science Part a-Polymer Chemistry, **1978**, 16, (8), 1953.
16. Barrett, K. E. J., *Dispersion Polymerization in Organic Media*. J. Wiley: New York, **1975**.
17. Kühn, I., *Untersuchungen zum Mechanismus der Teilchenbildung während der Emulsionspolymerisation*. Universität Potsdam, Teltow, **1996**.
18. Kühn, I., Tauer, K., *Nucleation in Emulsion Polymerization - a New Experimental-Study .1. Surfactant-Free Emulsion Polymerization of Styrene*. Macromolecules, **1995**, 28, (24), 8122.
19. Tauer, K., Kühn, I., *Modeling Particle Formation in Emulsion Polymerization - an Approach by Means of the Classical Nucleation Theory*. Macromolecules, **1995**, 28, (7), 2236.
20. Bovey, F. A., Kolthoff, I. M., Medalia, A. I., Meehan, E. J., *Emulsion Polymerization*. Interscience Pubs.: New York, **1955**.

21. Feeney, P. J., Napper, D. H., Gilbert, R. G., *Coagulative Nucleation and Particle Size Distributions in Emulsion Polymerization*. Macromolecules **1984**, 17, 2520.
22. Feeney, P. J., Napper, D. H., Gilbert, R. G., *Surfactant-Free Emulsion Polymerizations: Predictions of the Coagulative Nucleation Theory*. Macromolecules, **1987**, 20, 2922.
23. Lichti, G., Gilbert, R. G., Napper, D. H., *The Mechanisms of Latex Particle Formation and Growth in the Emulsion Polymerization of Styrene Using the Surfactant Sodium Dodecyl Sulfate*. Journal of Polymer Science: Polymer Chemistry Edition, **1983**, 21, 269.
24. Urban, D., Distler, D., *Introduction*. In *Polymer Dispersions and Their Industrial Applications*, Urban, D., Takamura, K., Eds. Wiley-VCH Verlag GmbH: Weinheim, **2002**; pp 1.
25. Wallach, L. D., Heller, W., Stevenson, A. F., *Theoretical Investigations on the Light Scattering of Colloidal Spheres. XII. The Determination of Size Distribution Curves from Turbidity Spectra* J. Chem. Phys., **1961**, 34, (5), 1796.
26. Zollars, R. L., *Turbidimetric method for on-line determination of latex particle number and particle size distribution*. J. Colloid Interface Sci. , **1980**, 74, (1), 163.
27. Lange, H., *Bestimmung von Teilchengrößen aus Trübung und Brechungsinkrement*. Colloid Polym. Sci. , **1968**, 223, (11), 24.
28. Kerker, M., *The Scattering of Light and other electromagnetic radiation*. Academic Press: New York, **1969**; Vol. 16.
29. Heller, W., *Theoretical Investigations on the Light Scattering of Colloidal Spheres .2. Accurate Interpolations of Theoretical Turbidity-Data*. Journal of Chemical Physics, **1957**, 26, (4), 920.
30. Heller, W., *Theoretical Investigations on the Light Scattering of Colloidal Spheres .3. Analytical Expressions for Turbidity Approximating the Performance of the Mie Equations Prior to the 1st Maximum*. Journal of Chemical Physics, **1957**, 26, (5), 1258.
31. Heller, W., Pangonis, W. J., *Theoretical Investigations on the Light Scattering of Colloidal Spheres .1. Specific Turbidity*. Journal of Chemical Physics, **1957**, 26, (3), 498.
32. Kozempel, S., *Emulgatorfreie Emulsionspolymerisation – Monomerlösungszustand und Teilchenbildung*. University of Potsdam, Potsdam, Germany, **2005**.
33. Kozempel, S., Tauer, K., Rother, G., *Aqueous heterophase polymerization of styrene - a study by means of multi-angle laser light scattering*. Polymer, **2005**, 46, (4), 1169.
34. Tauer, K., Padtberg, K., Dessy, C., *On-Line Monitoring of Emulsion Polymerization*. ACS Symposium Series, Polym. Colloids, **2001**, 93.
35. Tauer, K., Schellenberg, C., Zimmermann, A., *Nucleation in heterophase polymerizations*. Macromolecular Symposia, **2000**, 150, 1.
36. Atkins, P., De Paula, J., *Atkins' Physical Chemistry*. 7th ed.; Oxford University Press Inc.: New York, **2002**.
37. Tauer, K., Deckwer, R., Kuhn, I., Schellenberg, C., *A comprehensive experimental study of surfactant-free emulsion polymerization of styrene*. Colloid and Polymer Science, **1999**, 277, (7), 607.
38. Berne, B. J., Pecora, R., *Dynamic Light Scattering*. John Wiley: New York, **1975**.
39. Azad, A. R. M., Fitch, R. M., Ugelstad, J., *True Emulsion Polymerization of Acrylate Esters Using Mixed Emulsifiers*. Advances in Chemistry Series, **1975**, (9), 135.
40. Ugelstad, J., Hansen, F. K., *Kinetics and mechanism of emulsion polymerization.* . Rubber Chem Technol, **1976**, 49, 536.
41. Goodall, A. R., Wilkinson, M. C., Hearn, J., *Mechanism of Emulsion Polymerization of Styrene in Soap-Free Systems*. Journal of Polymer Science Part a-Polymer Chemistry, **1977**, 15, (9), 2193.

42. Tauer, K., Kühn, I., *Particle nucleation at the beginning of emulsion polymerization*. In *Polymeric Dispersions: Principles and Applications*, Asua, J. M., Ed. Kluwer Academic Publisher: Dordrecht, **1997**; pp 49.
43. Chainey, M., Hearn, J., Wilkinson, M. C., *Kinetics of the surfactant-free emulsion polymerization of styrene: application of quantitative theories to the post nucleation stage.* . J Polym Sci., Polym Chem., **1987**, 25, 505.
44. Chen, S. A., Lee, S. T., Macromolecules, **1992**, 25, 1530.
45. Hearn, J., Wilkinson, M. C., Goodall, A. R., *Polymer Lattices as Model Colloids*. Advances in Colloid and Interface Science, **1981**, 14, (2-3), 173.
46. Song, Z., Poehlein, G. W., *Particle formation in emulsifier-free aqueous-phase polymerization of styrene.* . J Colloid Interface Sci. , **1989**, 128, 501.
47. Kolthoff, I. M., Miller, I. K., *The Chemistry of Persulfate. I. The Kinetics and Mechanism of the Decomposition of the Persulfate Ion in Aqueous Medium*. J.A.C.S., **1951**, 73, 3055.
48. House, D. A., *Kinetics and Mechanism of Oxidations by Peroxodisulfate*. Chem. Reviews, **1962**, 62, 186.
49. Tauer, K., Kozempel, S., Rother, G., *The interface engine: Experimental consequences*. Journal of Colloid and Interface Science, **2007**, 312, 432.
50. Tauer, K., Hernandez, H., Kozempel, S., Lazareva, O., Nazaran, P., *Adoption of the Mechanism of Emulsion Polymerization to New Experimental Results*. Macromolecular Symposia, **2007**, 259, 253.
51. Laaksonen, A., Talanquer, V., Oxtoby, D. W., *Nucleation - Measurements, Theory, and Atmospheric Applications*. Annual Review of Physical Chemistry, **1995**, 46, 489.
52. Tauer, K., Hernandez, H., Kozempel, S., Lazareva, O., Nazaran, P., *Towards a consistent mechanism of emulsion polymerization – new experimental details*. Colloid and Polymer Science, **2007**, In press.
53. Lazareva, O., Lomonosov Moscow State Academy of Fine Chemical Technology, Moscow, to be submitted in **2008**.
54. Tauer, K., Antonietti, M., Rosengarten, L., Müller, H., *Initiators based on poly(ethylene glycol) for starting heterophase polymerizations: generation of block copolymers and new particle morphologies*. Macromolecular Chemistry & Physics, **1998**, 199, 897.
55. *Azo Polymerization Initiator*. In Wako Pure Chemicals Ind. Tokyo Research Laboratories.
56. Holtze, C., Tauer, K., *Surviving Radicals: Promises of a Microwave Effect on Miniemulsion Polymerization for Technical Processes*. Macromol. Rapid Commun. , **2007**, (28), 428.
57. Yalkowsky, S. H., Banerjee, S., *Aqueous solubility - Methods of Estimation for Organic Compounds*. Marcel Dekker Inc.: New York, **1992, 54**.
58. Yalkowsky, S. H., Banerjee, S., *Aqueous solubility - Methods of Estimation for Organic Compounds*. Marcel Dekker Inc.: New York, **1992, 133**.
59. Tauer, K., Mukhamedjanova, M., Holtze, C., Nazaran, P., Lee, J., *Unusual Kinetics in Aqueous Heterophase Polymerizations*. Macromolecular Symposia, **2007**, 248, 227.
60. Smiley, R. A., *Nitriles*. 3rd ed.; Wiley-Interscience: New York, **1981**; Vol. 15.
61. Blachnik, R., Koritnig, S., Steinmeier, D., Wilke, A., Feltz, A., Reuter, H., Stieber, E., *D'ans Lax Taschenbuch fuer Chemiker und Physiker*. Springer: Berlin, **1998**; Vol. 3.
62. Nomura, M., Suzuki, K., *The Kinetic and Mechanistic Role of Oil-Soluble Initiators in Micro- and Macroemulsion Polymerizations*. Industrial & Engineering Chemistry Research, **2005**, 44, 2561.
63. Tauer, K., *Block Copolymers Prepared by Emulsion Polymerization with Poly(ethylene oxide)-azo-initiators*. Polym. Adv. Technol., **1995**, (6), 435.

64. Neelsen, J., Hecht, P., Jaeger, W., Reinisch, G., *Zur Initiierung der Emulsionspolymerisation von Vinylchlorid mit Kaliumperoxidisulfat. 4. Zur Herkunft ionischer Gruppen am Emulsionspolyvinylchlorid*. Acta Polymerica Sinica, **1987**, 38, (10), 555.
65. Carey, F. A., Sundberg, R. J., *Advanced organic chemistry, Part A: structure and Mechanisms*. 4th ed.; Springer: New York, **2000**; p 441.
66. Kenji, Y., Yasukazu, O., Tsuruta, T., *Study on the Modes of Thermal Decomposition of Several Azo-Type Initiators*. Polymer Journal, **1977**, 9, (3), 275.
67. Dunn, A. S., In *Emulsion polymerization*, Piirma, I., Ed. Academic Press: New York, **1982**; p 223.
68. Roe, C. P., *Surface Chemistry Aspects of Emulsion Polymerization*. Industrial and Engineering Chemistry, **1968**, 60, (9), 20.
69. Brodnyan, J. G., Cala, J. A., Konen, T., Kelley, E. L., *The mechanism of emulsion polymerization. I. Studies of the polymerization of methyl methacrylate and n-butyl methacrylate*. J. Colloid Sci. , **1963**, 18, 73.
70. Gardon, J. L., *Emulsion Polymerization .I. Recalculation And Extension Of Smith-Ewart Theory*. Journal Of Polymer Science Part A-1-Polymer Chemistry, **1968**, 6, (3PA1), 623.
71. Brooks, B. W., Makanjuola, B. O., *The Rate Of Persulfate Decomposition In The Presence Of Polymer Lattices*. Makromolekulare Chemie-Rapid Communications, **1981**, 2, (1), 69.
72. Okubo, M., Mori, T., *The Decomposition Of Potassium Persulfate Used As Initiator In Emulsion Polymerization*. Makromolekulare Chemie-Macromolecular Symposia, **1990**, 31, 143.
73. Nozari, S., *Joint nucleation of organic/inorganic nanoparticles*. Universität Potsdam, Potsdam, **2002**.
74. Tauer, K., Kaspar, H., Antonietti, M., *Equilibrium swelling of colloidal polymeric particles with water-insoluble organic solvents*. Colloid and Polymer Science, **2000**, 278, (9), 814.
75. Hernandez, H., *Mechanism of entry of matter into latex particles*. University of Potsdam, Potsdam, to be submitted in **2008**.
76. Hernandez, H. F., Tauer, K., *Brownian Dynamics Simulation of the Capture of Primary Radicals in Dispersions of Colloidal Polymer Particles*. Industrial and Engineering Chemistry Research, **2007**, 46, (13), 4480.
77. Hernandez, H. F., Tauer, K., *Brownian Dynamics Simulation studies on radical capture in emulsion polymerization*. Macromolecular Symposia, **2007**, 259, 274.
78. Harkins, W. D., *A General Theory of the Reaction Loci in Emulsion Polymerization*. Journal of Chemical Physics, **1945**, 13, (9), 381.
79. Harkins, W. D., *A General Theory of the Reaction Loci in Emulsion Polymerization .2*. Journal of Chemical Physics, **1946**, 14, (1), 47.
80. Harkins, W. D., *A General Theory of the Mechanism of Emulsion Polymerization*. Journal of the American Chemical Society, **1947**, 69, (6), 1428.
81. Harkins, W. D., *General Theory of Mechanism of Emulsion Polymerization .2*. Journal of Polymer Science, **1950**, 5, (2), 217.
82. Fuhrhop, J.-H., Köning, J., *Membranes and Molecular Assemblies*. The Royal Society of Chemistry: Cambridge, **1994**.
83. Aslamazova, T., Tauer, K., *On the colloidal stability of polystyrene particles prepared with surface-active initiators*. Advances in Colloid and Interface Science, **2003**, 104, 273.
84. Guyot, A., *Recent progress in reactive surfactants in emulsion polymerisation*. Macromolecular Symposia, **2002**, 179, 105.

85. Sedlak, M., Tauer, K., *Synthesis and Characterization of New Surface Active Azo Initiators for Radical Reactions* Molecules, **2000**, 5, 730.
86. Kusters, J. M. H., Napper, D. H., Gilbert, R. G., German, A. L., *Kinetics of particle growth in emulsion polymerization systems with surface-active initiators*. Macromolecules **1992**, 25, 7043.
87. Vanderhoff, J. W., *Recent advances in the preparation of latexes*. Chemical Engineering Science, **1993**, 48, 203.
88. Walz, R., Bomer, B., Heitz, W., *Monomeric and Polymeric Azoinitiators*. Makromolekulare Chemie-Macromolecular Chemistry and Physics, **1977**, 178, (9), 2527.
89. Schuck, P., *Size-distribution analysis of macromolecules by sedimentation velocity ultracentrifugation and Lamm equation modeling*. Biophysical Journal, **2000**, 78, (3), 1606.

Acknowledgement

First of all, I would like to acknowledge Dr. sc. Klaus Tauer for his supervision and guides all the way during this work. I would like to thank him for his insightful view on the subject, his supports in solving the scientific problems and his motivation for giving very interesting new ideas. Special thanks are for his constructive comments and corrections during writing this thesis.

I would like to thank Prof. Dr. Markus Antonietti for giving me the opportunity to do my PhD thesis in the Max-Planck Institute of Colloids and Interfaces. It was a special pleasure for me working here.

I would like to thank Prof. Dr. Masayoshi Okubo, for the numerous discussions, the useful suggestions during his stay in Golm.

In our group, I would like to thank Mrs. Ursula Lubahn and Mrs. Silvia Pirok for the support in the labs and for improving my German language skill with their patient instruction.

For characterization and analysis of the samples I would like to thank Mrs. Marlies Gräwert for enormous number of GPC measurements; Mrs. Rona Pitschke and Mrs. Heike Runge for (also) enormous number of TEM pictures, Mr. Olaf Niemeyer, Mrs. Antje Völkel, Mrs. Heidi Zastrow, and Mrs. Irina Shekova for NMR, ultracentrifuge, Zeta-potential and tensiometry measurements.

I am indebted to the part-time students who helped me with the experimental parts: Marcel Voigt and specially, I would like to thank Jeongwoo Lee and Jakob Violet for a numerous helpful experimental assistance.

I would like to thank all my colleagues and friends in the MPI not only for their scientific supports and tips, but also for providing a friendly and kind atmosphere which was extremely valuable. Special thanks are due to my colleagues in our group: Dr. Steffen Kozempel for getting me started with the On-line measurements, Hugo Hernandez for the fruitful discussions, Farnoosh Roohi for her friendship and all the nice time we had, Nancy Weber for the language supports, and specially, for helping me to translate the abstract of this thesis in the last minute, Olga Lazareva for the

collaboration on off-line measurements. Moreover, for their help and nice time we spent together in our coffee-corner, I would like to thank Rezan Demir Cakan, Helena Kaper, Zofia Hordyjew-Baran, Emre Yagci, Philipp Adelhelm, Magdalena Titrici, Jelena Buha, and all others.

For the good time we spent together I would like to thank my friends: Dr. Samira Nozari, Fatemeh Ahmadnian, Sara Erfani, Zoya Zarafshan, Sohrab Mokhtari, Raha Roohnia, Samira Ghadimi, Elizabeth L. Paul, Yin Chunhong, Tong Qiong and Rosura F. Suarez, Azadeh Motaghi, Elmira Siroospour, and my family: Parisa and Pouria Nazaran, Dr. Fariba Hatami (particularly for her advises while proof-reading my thesis), Dr. Sadegh Sadeghi pour, Fatemeh and Farzaneh Hatami.

Finally, I want to express my gratitude to Saeed Hatami: his love, support and encouragement have sustained and uplifted me throughout this thesis; and to my parents, who have been the infinites of love, dedication, and patience all over my life.

And of course, the financial support of the Max-Planck Society (MPG) is gratefully acknowledged.